IDŐJÁRÁS

QUARTERLY JOURNAL
OF THE HUNGARIAN METEOROLOGICAL SERVICE

CONTENTS

****

http://www.met.hu/Journal-Idojaras.php

VOL. 113 * NO. 3 * JULY – SEPTEMBER 2009

IDŐJÁRÁS

Quarterly Journal of the Hungarian Meteorological Service

Editorial Office: *Gilice tér 39, H-1182 Budapest, Hungary*
P.O. Box 39, H-1675 Budapest, Hungary
E-mail: bozo.l@met.hu or antal.e@met.hu
Fax: (36-1) 346-4809

Indexed and abstracted in Science Citation Index Expanded™ and Journal Citation Reports/Science Edition
Covered in the abstract and citation database SCOPUS®

Subscription by

mail: IDŐJÁRÁS, P.O. Box 39, H-1675 Budapest, Hungary
E-mail: kenderesy.k@met.hu or antal.e@met.hu

IDŐJÁRÁS

Quarterly Journal of the Hungarian Meteorological Service
Vol. 113, No. 3, July–September 2009, pp. 157–175

Study on the size dependence of complex refractive index of atmospheric aerosol particles over Central Europe

Diana Benkő[1], **Agnes Molnár**[2*], and **Kornelia Imre**[3]

[1]*Department of Earth and Environmental Sciences, University of Pannonia, P.O. Box 158, H-8201 Veszprém, Hungary; E-mail: benkodiana@freemail.hu*

[2]*Air Chemistry Group of Hungarian Academy of Sciences, P.O. Box 158, H-8201 Veszprém, Hungary; E-mail: amolnar@almos.uni-pannon.hu*

[3]*Department of Earth and Environmental Sciences, University of Pannonia, P.O. Box 158, H-8201 Veszprém, Hungary; kornelia@almos.uni-pannon.hu*

(Manuscript received in final form July 15, 2009)

Abstract—The aim of this paper is threefold: (1) to present our results on the complex refractive index regarding Central European background air; (2) to demonstrate the importance of the size dependence of the complex refractive index; (3) to study how the refractive index changes due to the aerosol hygroscopicity. The area of Central Europe is of great importance in modeling anthropogenic climate variations due to its relatively high aerosol burden and to the direct aerosol forcing effect. In this work the complex refractive index of the aerosol is calculated. The calculations are based on the size distribution measured for different aerosols species, as well as on the complex refractive indices of the different components. For this study, ambient aerosol samples were collected at K-puszta, in rural Hungary, by means of electric low pressure (ELPI) and Berner impactors, which make the estimation of the chemical mass closure possible. By using the data measured the complex refractive indices were determined in 8 size ranges (from 31 nm up to 1.7 μm (ELPI) and from 62.5 nm to 16 μm (Berner)), by assuming volume mixing rule. Our results show that the real refractive index of dry aerosol increases with particle size in the optically active range (0.1–1.0 μm) from 1.499 to 1.527. Contrary to the real part, the imaginary refractive index decreases with increasing particle size from 0.025 to 0.008. In a case study we show that the application of a size resolved refractive indices in Mie-calculations instead of a constant value may reduce the uncertainty of the estimation of scattering and absorption (extinction) coefficients and finally – through the single scattering albedo – of the direct aerosol radiation forcing. We found that the overall difference between extinction coefficients estimated by the two approaches varies in the range of –2% and 65%. Further, the absorption coefficient, calculated by applying a constant refractive index, overestimates the value calculated with a varying refractive index by 37%. In the case of the scattering coefficient the corresponding figure is equal to –4%. Finally, the study of hygroscopic mass growth of

* Corresponding author

the aerosol particles indicates that water uptake decreases the real part of the refractive index by 3% (at 86% relative humidity (RH)) compared to the dry aerosol.

Key-words: refractive index, volume mixing rule, size distribution, extinction coefficient, hygroscopic growth

1. Introduction

It is well known that aerosol particles in the atmosphere influence the transfer of solar radiation. For this reason, their effects on the radiative balance of the Earth - atmosphere system have to be considered in climate models. In these models, different physical, chemical, and optical properties of the aerosol should be taken into account. The optical properties of the aerosol are modeled by Mie-theory as a function of particle size distribution and composition determining the refractive index (e.g., *Hatzianastassiou et al.*, 2007). One of the problems arising during such modeling is that the composition and, consequently, the refractive index of the particles are inhomogeneous in space and time. Due to this variability, the direct aerosol radiation effect is also non-uniform as shown by different climate model outputs (e.g., *IPCC*, 2007; *Hatzianastassiou et al.*, 2007; *Kaufman et al.*, 2002; *Seinfeld*, 2008). Information on these parameters (chemical composition, spatial and temporal trends) for different locations and regions is, therefore, needed. More detailed regional input data make the predictions of global models more accurate (e.g., *Kaufman et al.*, 2002; *IPCC*, 2007; *Balkanski et al.*, 2007; *Randles et al.*, 2004; *Hatzianastassiou et al.*, 2007; *Stier et al.*, 2007; *Seinfeld*, 2008; *Ramanathan et al.*, 2007).

Aerosol studies carried out over Central Europe indicate that this area of the continent is characterized by high aerosol loading due to industrial and other anthropogenic sources. Model results show that in Central Europe the aerosol optical depth has significant local maximum with values between 0.1 and 0.2, similar to those found in the eastern US. It follows from the high aerosol burden that in this region both the shortwave atmospheric and the surface radiation forcing are important. As a consequence, the modeled shortwave radiation forcing referring to the total air column shows local minimum, between –1.0 and –2.0 $W m^{-2}$ (*IPCC*, 2007; *Hatzianastassiou et al.*, 2007; *Kaufman et al.*, 2002; *Feczkó et al.*, 2004). These relatively high values indicate that data on the complex refractive index of aerosol particles from this region is of great importance. Unfortunately, only limited information on the complex refractive index is available for Central Europe (e.g., *Ebert et al.*, 2004; *Pesava et al.*, 2001; *Horvath*, 1995). Moreover, these data mainly correspond to urban environments not to regional background air. The main aim of this paper is to present complex refractive index for Central European background air.

As mentioned earlier, optical properties of the aerosol particles depend strongly on the particle size and refractive index. Furthermore, the refractive

index itself is also a function of the size distribution. In spite of this, the dependence of the aerosol refractive index on particle size is generally not considered in climate modeling, due to different reasons, probably one of these is the lack of information on the size resolved complex refractive index. As noted before, only a few papers address the size resolved aerosol refractive index. For urban environments *Horvath* (1995) published data on the imaginary refractive index in the 15 nm–16 μm size range for Vienna, Naples, and Bologna; *Pesava et al.* (2001) reported the aerosol complex refractive index in the size range of 34 nm–15.6 μm for Vienna; *Iinuma et al.* (2000) studied the complex refractive index in Australian cities in the size interval of 0.1–1.0 μm. On the other hand, for rural environments, less information can be found: e.g., *Ebert et al.* (2004) discussed the complex refractive index of aerosol particles at Kleiner Feldberg, in the size range of 0.1–3.0 μm, while *Hand et al.* (2002) summarized the data obtained by different studies carried out in the Great Smoky Mountains National Park (size ranges of 0.12 – 0.28 μm, 0.2 μm, $d < 2.5$ μm). In this paper we also aim to present additional data on the complex refractive index as a function of particle size for Central European rural air, for which no such information can be found in the literature. On the other hand, in a sensitivity study the effect of size resolved complex refractive index on the scattering and absorption coefficient is discussed.

The next problem arises from the hygroscopicity of aerosol particles. As is well known, increasing ambient relative humidity results in water uptake by the particles. The absorbed water changes the size distribution as well as the refractive index of the aerosol. However, in climate forcing estimations, although the hygroscopic growth of the particles is generally considered, the variation of the refractive index due to hygroscopicity is not usually involved. The effect of water uptake on the complex aerosol refractive index is taken into account only in few research studies (*Randles et al.*, 2004; *Iinuma et al.*, 2000). In the present paper the effect of the aerosol hygroscopicity on the aerosol complex refractive index is also discussed.

In summary, the goals of this paper are: (1) to present our results on the complex refractive index over Central European background air; (2) to demonstrate the importance of the size dependence of the complex refractive index; (3) to study changes in refractive index due to the aerosol hygroscopicity.

2. Experimental

2.1. Sampling and analysis

The aerosol sampling was carried out at K-puszta station ($\varphi = 46°58'$, $\lambda = 19°35'$, $h = 125$ m a.s.l.), in rural Hungary. This sampling site belongs to the GAW and EMEP networks, and is located in a forest clearing on the Great

Hungarian Plain. Because of the lack of nearby large emission sources, aerosol characteristics measured at K-puszta represent Central and Eastern European regional air.

In the calculations discussed in this study, the results of 92 aerosol samples overall are used, which were collected during different sampling periods between 1999 and 2002. The details of the sampling periods are given in *Table 1*. One can see from the table that all four seasons are represented. Since aerosol properties may vary significantly during the year, the results from the different sampling periods are distinguished from each other and are presented separately in the following (denoted as ELPI1-5). On the other hand, the results labeled as Berner correspond to the average of more than a whole year.

Table 1. Sampling periods

Sampling period	Date	Number of samples
ELPI1	July 11, 1999 – August 8, 1999	25
ELPI2	July 29, 2000 – August 14, 2000	26
ELPI3	January 31, 2001 – February 3, 2001	8
ELPI4	April 2, 2001 – April 6, 2001	9
ELPI5	October 23, 2001 – October 27, 2001	8
Berner	July 27, 2001 – October 28, 2002	16

76 and 16 aerosol samples were taken on Al-foils by an electric low pressure impactor (ELPI) and a 9-stage Berner impactor, respectively. The large number of ELPI samples is used for characterizing the complex refractive index of fine particles. While the ELPI instrument collects aerosol particles on 13 stages (in the range of 0.031–10.77 μm), in our work only the data of the first 8 stages (0.031–1.7 μm) are considered. This means that our results correspond to the fine particle size range, containing the optically active size interval. On the other hand, Berner impactor samples make it possible to study the size dependence of the refractive index in the 62.5 nm – 16 μm size range. Owing to higher aerosol masses collected, these latter samples were also used to investigate the effect of aerosol hygroscopicity on the refractive index.

The first step of the study is the determination of the mass concentration. In the case of ELPI samples, the mass concentrations in different size ranges are estimated from the conversion algorithm of the device (*ELPI User Manual*, 2003) based on the measured number size distribution; assuming spherical particles of unit density (see details in *Temesi et al.* (2001)). For the Berner samples, the mass is directly measured by weighting, applying a microbalance (the precision of the microbalance (Sartorius) is 10 μg). The dry mass of the samples is determined in an isolated box with low relative humidity (30%), which is adjusted by silica gel. Next, the mass growth of these samples due to their water uptake is measured as a function of increasing relative humidity.

For controlling the relative humidity, saturated solutions of different inorganic salts (NH_4NO_3 (64% RH); NH_4Cl (80% RH); KCl (86% RH)) were applied. Before weighing, the samples are kept at a given relative humidity for more than 48 hours in order to reach equilibrium with their surroundings (for more details see *Imre* and *Molnár*, 2008).

After sampling and weighing, all samples were chemically analyzed in the same way (see *Temesi et al.* (2001) for a detailed description of the analysis). It has to be mentioned, that in the case of Berner samples, the changes in the concentration of the measured inorganic components caused by the exposure to elevated humidities are not significant. This is confirmed by test measurements, which showed negligible differences (around 5%, within the analytical error) between the exposed and non-exposed samples.

The inorganic ion content (NH_4^+, SO_4^{2-}, NO_3^-) of the samples are measured by capillary electrophoresis (detection limit is 70 μg L^{-1}). On the basis of the results of the chemical analysis, the concentrations of the main inorganic compounds in the aerosol ($(NH_4)_2SO_4$, NH_4HSO_4, H_2SO_4, NH_4NO_3) are estimated by applying stoichiometry.

The concentration of the total organic carbon (TC) was measured by a TOC solid analyzer as carbon dioxide by catalytic combustion method with oxygen at 680 °C. The detection limit of carbon measurement is 2 μg (*Temesi et al.*, 2001).

Carbonaceous compounds (especially elemental carbon (EC)) in the particles are mainly responsible for the light absorption (the imaginary part of the refractive index) of the particles. For this reason, from the total carbon data, the concentrations of various carbonaceous species characterized by their different optical and chemical properties are estimated (elemental carbon, slightly absorbing HUmic-LIke Substances (HULIS), and non-absorbing carbon). In our former study (*Molnár et al.*, 1999), the total carbon concentration and absorption coefficient of fine aerosol (PM1) is compared. The results showed that 10% of the total carbon concentration in fine aerosol can be considered as elemental carbon. As mentioned before, direct sources (including traffic) cannot be found in the vicinity of the sampling site. This can be the reason why EC fraction in PM1 is quite low at K-puszta. Besides the lack of direct sources of EC, low EC/TC fraction can be also the result of relatively high organic carbon (OC) concentration due to the abundant biogenic precursors over the site. Significant formation of the secondary OC is followed by decreasing EC/OC ratio as already reported by, e.g., *Turpin* and *Hutzincker* (1995). On the other hand, low EC fraction is not unusual in background monitoring sites, e.g., in Hyytiälä. *Saarikoski et al.* (2005) reported 35 and 5% of OC and EC mass fractions for PM1, respectively. Calculating these fractions to EC/TC ratio, similar value can be obtained.

Not involving the particles smaller than 100 nm, the size distribution of EC and OC(TC) is rather similar (*Cabada et al.*, 2004; *Hitzenberger et al.*, 2006;

Miguel et al., 2004). *Jaffrezo et al.* (2005) stated that both in rural and suburban sites, EC and OC had "very same" distributions in the range of 0.1–1 μm both in winter and summer. Consequently, the OC/EC ratio has only slight size dependence in this size range.

According to the above mentioned reasons, in this work, elemental carbon concentration of all impactor stages is estimated as 10% of the TC concentration. On the other hand, HULIS concentration of the samples is also estimated from the TC data using the results of *Kiss et al.* (2002) and *Gysel et al.* (2004). These authors demonstrated that an average 35% of the TC concentration consists of HULIS in aerosol samples taken at K-puszta. Accordingly, in our calculations we accept this value for HULIS, while the rest of TC concentration is considered as non-absorbing organic carbon. Despite all assumptions, our results on the imaginary refractive index of aerosol particles can have importance, since data on the complex refractive index of aerosol particles are rather scarce. On the other hand, we note that due to the assumptions, these data should be considered as a first estimation of the imaginary part of the refractive index which needs to be confirmed by further studies.

2.2. Mass closure

On the basis of data obtained, the dry mass closure of the aerosol for each sample and impactor stage is estimated. The mass closure data are presented in *Table 2*. For Berner samples, obviously the mass concentrations measured at a relative humidity of 30% are used for this purpose. On the other hand, in the case of ELPI samples, we can assume that the mass concentrations determined relate to dry conditions. This assumption is based on the fact that in the overwhelming majority of cases during the sample collection by ELPI, the ambient relative humidity did not exceed 50%. It goes without saying that this assumption must be considered with caution. However, one can speculate that only a small quantity of water is absorbed by the particles under these conditions.

To establish the mass closure for each sample, the concentrations of $(NH_4)_2SO_4$, NH_4HSO_4, H_2SO_4, NH_4NO_3, EC, HULIS, and non-absorbing carbon are considered (see above). For the conversion of the last three "carbon" concentrations into mass concentrations we assume the following. In the case of EC, a factor of 1 is applied, while for HULIS a mass conversion factor of 1.9 is used. This value is based on the results of elemental composition (molar ratio of C:H:N:O) measurements carried out by UV, fluorescence, Fourier transform, and infrared studies (*Kiss et al.*, 2002; *Gysel et al.*, 2004). For the rest of TC (non-absorbing organic carbon), the conversion factor is adjusted in such a way to obtain a total carbon mass closure. By using this procedure the conversion factor for non-absorbing organic particles varied from sample to sample, but with a maximum value of 1.9.

Table 2. Mass closure of the aerosol samples. Concentrations are given in μg/m^3. *ROM stands for remaining organic material

Sampling period	Cut off (μm)	$(NH_4)_2SO_4$	NH_4HSO_4	H_2SO_4	NH_4NO_3	SiO_2	EC	HULIS	ROM*
ELPI1	0.061	0.007	0.049	0.046	0.011	0.000	0.000	0.000	0.082
	0.11	0.020	0.131	0.188	0.125	0.000	0.003	0.001	0.293
	0.178	0.041	0.274	0.402	0.388	0.043	0.000	0.007	1.010
	0.273	0.053	0.354	0.557	0.835	0.035	0.000	0.022	2.424
	0.419	0.082	0.548	0.849	1.695	0.029	0.000	0.024	6.004
	0.677	0.036	0.239	0.348	0.443	0.048	0.003	0.011	2.900
	1.05	0.015	0.102	0.146	0.039	0.016	0.010	0.009	1.254
ELPI2	0.061	0.021	0.143	0.156	0.014	0.018	0.025	0.004	0.040
	0.11	0.035	0.231	0.356	0.230	0.138	0.021	0.011	0.389
	0.178	0.050	0.335	0.526	0.620	0.357	0.037	0.032	0.985
	0.273	0.063	0.421	0.647	1.126	0.573	0.005	0.031	1.759
	0.419	0.080	0.531	0.835	2.033	1.356	0.000	0.102	4.372
	0.677	0.039	0.262	0.425	0.597	0.638	0.042	0.027	2.688
	1.05	0.029	0.195	0.307	0.061	0.089	0.067	0.014	1.940
ELPI3	0.061	0.015	0.098	0.126	0.004	0.007	0.021	0.018	0.018
	0.11	0.026	0.174	0.274	0.055	0.056	0.010	0.099	0.464
	0.178	0.044	0.291	0.457	0.211	0.042	0.017	0.205	1.383
	0.273	0.059	0.395	0.620	0.295	0.132	0.007	0.307	1.821
	0.419	0.101	0.674	1.059	0.693	0.258	0.000	0.837	5.423
	0.677	0.037	0.245	0.385	0.025	0.145	0.071	0.215	3.280
	1.05	0.017	0.113	0.178	0.005	0.001	0.020	0.023	1.458
ELPI4	0.061	0.016	0.106	0.146	0.035	0.021	0.028	0.024	0.063
	0.11	0.033	0.221	0.347	0.118	0.074	0.022	0.095	0.597
	0.178	0.060	0.402	0.632	0.300	0.159	0.006	0.186	1.578
	0.273	0.078	0.521	0.818	0.535	0.185	0.000	0.255	1.790
	0.419	0.135	0.901	1.415	1.208	0.372	0.000	0.904	8.122
	0.677	0.052	0.345	0.542	0.094	0.248	0.087	0.234	4.260
	1.05	0.020	0.132	0.208	0.013	0.022	0.042	0.037	3.613
ELPI5	0.061	0.018	0.118	0.133	0.014	0.000	0.022	0.013	0.000
	0.11	0.057	0.377	0.584	0.110	0.030	0.021	0.107	0.299
	0.178	0.219	1.458	2.170	0.206	0.133	0.042	0.404	1.763
	0.273	0.215	1.430	2.248	0.347	0.174	0.016	0.461	4.458
	0.419	0.239	1.588	2.495	0.727	0.287	0.096	0.890	8.266
	0.677	0.082	0.545	0.856	0.414	0.146	0.005	0.331	6.454
	1.05	0.051	0.336	0.529	0.147	0.019	0.052	0.166	5.260
Berner	0.0625	0.051	0.340	0.286	0.008	0.093	0.014	0.030	0.507
	0.125	0.067	0.444	0.513	0.179	0.127	0.010	0.065	0.303
	0.25	0.112	0.743	0.935	0.247	0.548	0.093	0.154	0.798
	0.5	0.075	0.502	0.508	0.109	0.639	0.109	0.187	0.942
	1	0.045	0.302	0.275	0.014	0.043	0.030	0.044	0.350
	2	0.060	0.402	0.435	0.003	0.000	0.002	0.053	0.317
	4	0.060	0.398	0.452	0.004	0.000	0.005	0.057	0.345
	8	0.052	0.347	0.335	0.005	0.000	0.000	0.053	0.335

In certain cases, especially for the first two stages of the ELPI and for the first stage of the Berner impactor, the total mass concentrations were lower than the sum of the concentrations of the species obtained from the chemical

analysis. This is probably due to the uncertainty of the determination of low mass concentrations, as well as to the different measurement techniques. *Temesi et al.* (2001) and *Pesava et al.* (2001) already discussed this discrepancy and noted that its reason needs further consideration. Due to this problem, in the following these samples are excluded from calculations of the refractive index. Unfortunately, this step led to the exclusion of the entire first stage of ELPI impactor samples.

It is also to be noted that the sum of the mass concentration of the different species identified chemically is generally found to be lower than the total mass determined, mostly in the coarse size range. Thus, the undetermined aerosol mass fraction increases with the stage number (18–55%), and is likely caused by particles of crustal origin not indentified in this study. Since the soil type around the sampling site is sandy, in further calculations we suppose that this undetermined mass in the coarse mode consist of SiO_2. However, we also found some non-resolved mass in the fine size range. The results of *Mészáros et al.* (1997) show that in Hungary significant concentrations of Al, Fe, and Mn can be measured also in the fine mode. This makes it possible that crustal-like components are present in the fine mode aerosol. For this reason we speculate that even for fine particles the missing fraction is SiO_2 of crustal origin in agreement with the work of *Pesava et al.* (2001).

3. Calculation of the refractive index

After establishing the mass closure for each size selected sample, the complex refractive index is estimated by applying the volume mixing rule. In the calculations we assume that the particles are homogenously, internally mixed. This assumption is the most acceptable in the optically active size range (particles with diameters ranging between 0.1 and 1 μm), where the particles usually arise from the coagulation of smaller particles or from the condensation of low volatility vapors (*Guyon et al.*, 2005). In this way, the average complex refractive index (m) of the total aerosol is given by the following equation (e.g., *Ebert et al.*, 2002):

$$m = \frac{m_1 V_1 + \ldots + m_i V_i}{V_1 + \ldots + V_i} = \frac{n_1 V_1 + \ldots + n_i V_i}{V_1 + \ldots + V_i} - \frac{k_1 V_1 + \ldots + k_i V_i}{V_1 + \ldots + V_i} i, \qquad (1)$$

where m_i, n_i, k_i, and V_i are the complex refractive index, its real and imaginary parts, and the volume of particle group i, respectively.

In order to obtain the volume of the individual aerosol components from the mass measured chemically, their densities should be known. The densities of the inorganic compounds can be easily found in chemical handbooks, while

some information on the density of EC, HULIS, and non-absorbing OC can be taken from recent research papers. *Guyon et al.* (2005) published a value of 1.2 g/cm^3 for EC; *Hoffer et al.* (2005) recommended a density of 1.569 g/cm^3 for HULIS; while according to *Turpin* and *Lim* (2001), for non-absorbing OC the value of 1.2 g/cm^3 can be applied. The summary of the densities considered in our calculations are listed in *Table 3*.

Table 3. Complex refractive indices ($m=n-ki$), $\lambda=589$ nm. [a]*Weast* (1987), [b]*Stelson* (1990), [c]*Seinfeld* and *Pandis* (1998), [d]*Horvath* (1998), [e]*Hoffer et al.* (2005), [f]*Turpin* and *Lim* (2001), [g]*Guyon et al.* (2005)

Compound	n	k	ρ (g/cm^3)
$(NH_4)_2SO_4$	1.521	0 [a]	1.77
NH_4HSO_4	1.473	0 [a]	1.79
H_2SO_4 (97%)	1.426	0 [b]	1.84
NH_4NO_3	1.413	0 [a]	1.725
SiO_2 (550 nm)	1.550	0 [c]	2.2
EC	1.500	0.47000[d]	1.2[g]
HULIS	1.653	0.00187[e]	1.569[e]
Remaining organic material	1.400	0[f]	1.2[f]

As one can see from Eq. (1), for the calculation of refractive indices the knowledge of their real and imaginary parts is necessary. In *Table 3* both the real and imaginary parts of the refractive index are tabulated. The values for inorganic components can be found in appropriate handbooks and papers on the subject. However, for carbonaceous aerosol much less information can be found in the literature. In this work, the refractive indices of carbonaceous aerosol classified into three categories are estimated on the basis of the results published by the following authors: *Horvath* (1998), *Hoffer et al.* (2005), *Turpin* and *Lim* (2001). It has to be noted, that in *Table 3* the refractive indices refer to $\lambda=550$ or 589 nm. Although the refractive index slightly varies in this wavelength range, in the calculation we neglect this unimportant variation.

One has to note that in the case of EC, the refractive index can vary within wide limits due to unknown density differences of black carbon. Besides, soot particles may contain un-burnt, mostly organic material components, which are not light absorbing (*Horvath*, 1995; *Ebert et al.*, 2002). In spite of these problems, we apply the commonly accepted value of $1.50-0.47i$, following the recommendation of *Horvath* (1998).

The complex refractive index of carbonaceous materials is also not well understood. For HULIS, *Table 3* contains the recent estimate of *Hoffer et al.* (2005). In their work, the optical properties of previously isolated HULIS were determined from the fine fraction of biomass burning aerosol during the LBA-SMOCC experiment. Hoffer and his co-workers measured the scattering and

absorption coefficients of HULIS. On the basis of these results, and the size distribution of HULIS particles, the refractive index is derived from closure calculations. Finally, for the remaining, not light absorbing organic material, we consider a complex refractive index of $1.4 - 0i$, as proposed by *Turpin* and *Lim* (2001).

4. *Results and discussion*

4.1. Size distribution of complex refractive index of dry aerosol

The complex refractive index is calculated individually for each aerosol sample. *Figs. 1a* and *1b* show the size distributions of the real and imaginary parts of the refractive index of dry aerosol. It has to be noted again, that the results on the imaginary part of the refractive index are first approximations based on TOC measurements and reasonable estimations (see details in Experimental).

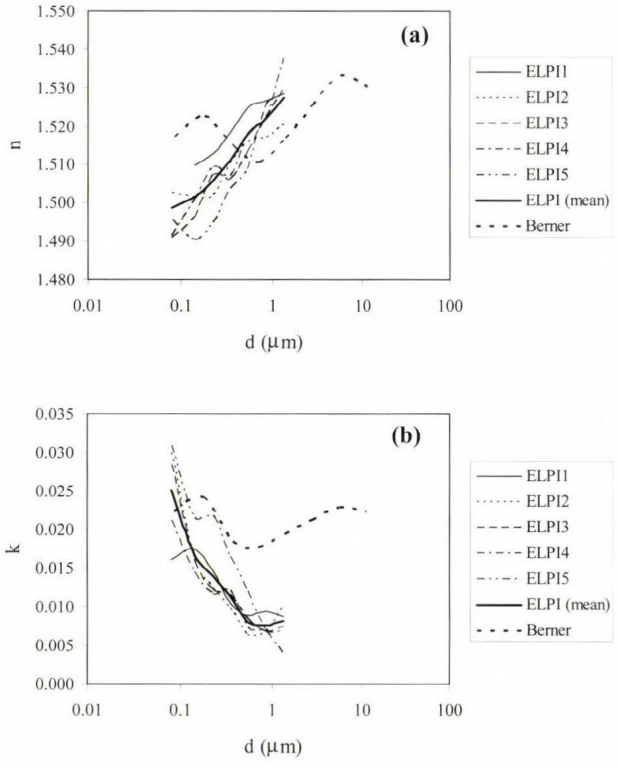

Fig. 1. Size distribution of the real (a) and imaginary (b) refractive index for dry particles.

The curves in these figures represent averages of the sampling periods (ELPI1-5 and Berner, see also in *Table 1*) and the mean distribution of all ELPI samples as ELPImean. The results clearly show that the real part of the refractive index increases, while the imaginary part (calculated from EC and HULIS) decreases with increasing particle size in the range of 0.1 – 1 μm. The data of both the real and imaginary parts in different ELPI campaigns are in good agreement with each other, indicating that seasonal variation is not important. The only exception is the ELPI5 data (referring to fall), when the carbon concentration – consequently, the imaginary part of the refractive index – is higher, probably due to biomass burning in this region. This assumption is confirmed by the aerosol composition (see data in *Table 2*). In ELPI5 samples the concentrations of carbonaceous compounds were the highest and the size distribution of TC was also different compared to the other sampling periods. According to ELPImean data set, the real part of the refractive index changes from 1.499 to 1.527, while in the case of the imaginary part, its value falls from 0.025 to 0.008, and has a local minimum around particle diameter of 1 μm.

On the other hand, the complex refractive index calculated from Berner samples has different size distribution. The real part of the refractive index does not vary as much as the ELPI data, and has a local maximum around 0.2 μm. The values above this size in the fine range are similar to all real refractive indices obtained form the ELPI samples. The imaginary refractive indices of the two different impactors are comparable; however, the values obtained from Berner samples are generally higher than the ELPI data. This discrepancy can be attributed to the different sampling periods of ELPI and Berner samples, different cut-off diameters and size resolution of the impactors (there are 4 and 7 data points in the fine size range in case of Berner impactor and ELPI, respectively), and to the large difference between the sample numbers (76 and 16 for ELPI and Berner impactors, respectively). Despite these facts, Berner samples are included into this work, because the refractive index in the coarse size range is only presented on the basis of these samples (as well as the effect of hygroscopicity, see later). The data in *Figs. 1a* and *1b* show that in the coarse mode, the real refractive index increases with the particles size; the imaginary part starts to increase after the local minimum around 1 μm.

Our results are compared to the refractive indices published by various authors in *Figs. 2a* and *2b*. Considering the value of the real refractive index (*Fig. 2a*), as well as its increasing tendency in the fine size range, our results are in good agreement with that of different authors, especially with the data presented by *Pesava et al.* (2001). Similar to our work, these authors applied the volume mixing rule for the estimation of the refractive indices of atmospheric aerosol from Vienna. The real part ranged between 1.455 and 1.495, with a peak in the 0.33 – 0.55 μm size interval. This difference can be attributed to the different sampling (urban – regional) environments and different analytical

methods applied. Pesava and his co-workers made the chemical analysis by PIXE method. By means of this analysis nitrogen and carbon elements cannot be measured. For this reason, in their refractive index calculation the concentrations of carbonaceous compounds, ammonium, and nitrate ions are estimated. *Hand et al.* (2002) reported similar refractive index to our data, although they calculated and measured it by different methods. Data published by *Guyon et al.* (2005) represent the lowest refractive index, referring to Amazonian rural air. The authors compared the refractive indices derived from different approaches, and concluded that the real part of the refractive index obtained from an iteration procedure and from applying the volume mixing rule agreed well; the difference among them was ± 0.02. The highest refractive index were published by *Ebert et al.* (2004), who determined the size resolved complex refractive index for rural aerosol (Kleiner Feldberg, Germany) from individual particle analysis based on high-resolution scanning electron microscopy and energy-dispersive X-ray microanalysis. The values published by *Rault* and *Chazette* (2007), which were retrieved from a synergy between lidar, sunphotometer, and ground based in situ measurements in Paris, are also higher than our data. The difference in the applied methods may lead to the difference in values of the refractive indices. However, from the data presented in *Fig. 2* it is obvious that the smallest (*Guyon et al.*, 2005) and the largest (*Ebert et al.*, 2004; *Rault* and *Chazette*, 2007) refractive indices differ from our data within – 4 to + 5%, on average.

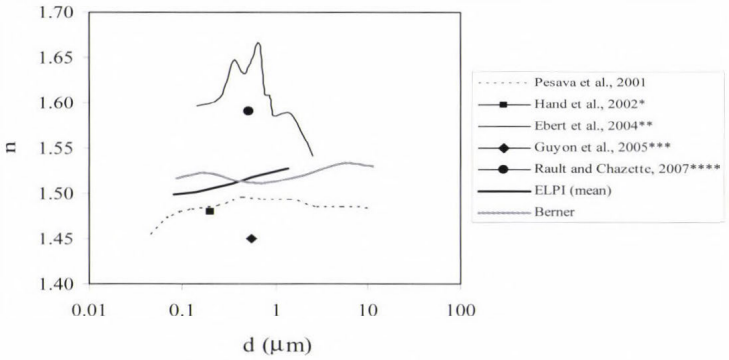

Fig. 2a. Variation of the real part of the refractive index published by different authors. Marking: *mean value; **mean value for rural air masses; ***mean value for background results obtained by applying volume mixing rule, ****$\lambda = 532$ nm.

Fig. 2b shows the variation in the imaginary refractive index published by different authors. In accordance with our results, *Horvath* (1995) found that the imaginary part shows a considerable decrease with increasing particle diameter. However, in the fine size range, *Horvath* (1995), *Pesava et al.* (2001), *Ebert et al.* (2004), *Raut* and *Chazette* (2007) reported higher imaginary refractive

indices than the values presented in this work. This is probably due to the significantly different sampling sites. The results of authors referenced correspond to urban and urban influenced regional air affected by important anthropogenic sources (industrial and traffic), while our sampling site, K-puszta, represents regional background air. The imaginary refractive index published by *Guyon et al.* (2005) for Amazonian background air is also higher than values we found; however, these authors noted that their values might be overestimated.

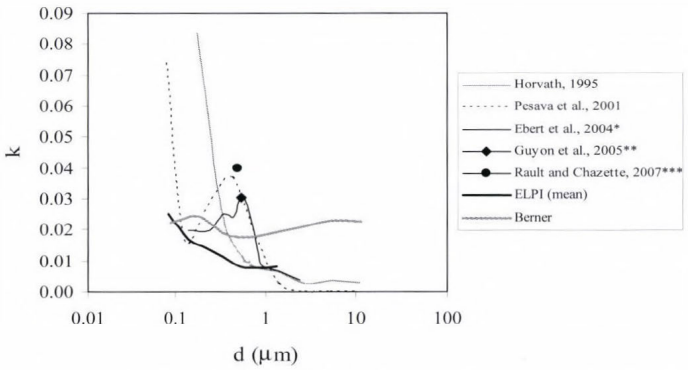

Fig. 2b. Variation of the imaginary part of the refractive index published by different authors. Marking: *mean value for rural air masses; **mean value for background results obtained by applying volume mixing rule, ***$\lambda = 532$ nm.

4.2. Importance of the size resolved refractive index

The importance of using a size resolved refractive index instead of a constant value can be evaluated if the scattering and absorption (extinction) coefficients are calculated by both approaches. In a case study we calculated the optical parameters (at 550 nm) in both ways, by applying the Mie-theory. In the calculations, the ELPI2 data set is used, and the results are tabulated in *Table 4.* In the first columns, the scattering, the absorption (the extinction) coefficients and the single scattering albedos are given which are calculated by means of the averaged (constant) complex refractive index and the mean number size distribution of ELPI2 data. Next, the same parameters are shown determined by considering the size distribution of the complex refractive index.

The results in both cases indicate that particles in the range of 0.273–1.05 μm (this interval is characterized by 0.34–0.84 μm geometric mean cut-off diameters) give the majority of the scattering and extinction coefficients. On the other hand, the contribution of smaller particles (in the 0.061–0.273 μm range) to the absorption coefficient is also important due to the relatively high TC concentration in this size interval. As a result, the difference between the

absorption coefficients calculated by the two approaches is rather high. In the whole size range, the absorption coefficient resulting from constant refractive index overestimates the value calculated with a varying refractive index by 37%. In addition, the difference varies significantly with the particle size (see the last columns in *Table 4*). On the other hand, in this case study the difference between the scattering coefficients is not as high compared to the absorption coefficients; the overall difference is 4%, ranging from –3% to 17%. For the whole size range, the extinction coefficients determined by both approaches give similar values, which is the result of overestimation of the absorption and underestimation of the scattering coefficients. The overall difference is 1%, varying in the range of –2% and 65%. These numbers indicate that the deviation between extinction coefficients with a constant and a size resolved refractive index depends strongly on the particle size. Thus, we can conclude that the application of a constant refractive index instead of size resolved refractive index in Mie-calculations may enhance the uncertainty of the estimation of scattering and absorption (extinction) coefficients.

Table 4. Aerosol extinction coefficient (σ) and single scattering albedo (ω) calculated by applying size resolved and constant (1.510 – 0.01311i) refractive indices. Average of the size selected complex refractive index of ELPI2 data

Mean geometric diameter (μm)	**0.08**	**0.14**	**0.22**	**0.34**	**0.53**	**0.84**	**1.34**	**Σ**
Number concentration (cm^{-3})	**1460**	**983**	**524**	**228**	**118**	**15**	**2**	**3330**
Constant refractive index								
σ_{ext} (Mm^{-1})	0.2	1.9	10.4	36.1	90.1	30.9	5.4	174.9
σ_{scat} (Mm^{-1})	0.1	1.5	9.4	33.7	85.4	28.3	4.2	162.6
σ_{abs} (Mm^{-1})	0.1	0.4	1.1	2.3	4.7	2.5	1.2	12.3
ω	0.46	0.78	0.9	0.94	0.95	0.92	0.78	0.93
Size resolved refractive index								
σ_{ext} (Mm^{-1})	0.3	1.9	10.2	36.3	91.9	31.0	5.7	177.2
σ_{scat} (Mm^{-1})	0.1	1.4	9.2	34.5	89.5	29.7	4.9	169.4
σ_{abs} (Mm^{-1})	0.2	0.5	0.9	1.7	2.4	1.3	0.8	7.8
ω	0.27	0.74	0.91	0.95	0.97	0.96	0.86	0.96
(Constant - Size resolved)/Constant								
$\Delta\sigma_{ext}$ (%)	65	2	-2	1	2	0	6	1
$\Delta\sigma_{scat}$ (%)	-3	-3	-1	2	5	5	17	4
$\Delta\sigma_{abs}$ (%)	123	18	-13	-26	-50	-49	-33	-37
$\Delta\omega$ (%)	41	5	-1	-2	-3	-4	-10	-3

Finally, the effect on the single scattering albedo is evaluated. Single scattering albedo is one of the key parameters which determine the sign of the change in planetary albedo due to the aerosol layer, resulting in negative (cooling) or positive (heating) forcing of the Earth - atmosphere system. The boundary between the heating and cooling effect can be characterized by the critical single scattering albedo (at which the change in planetary albedo is zero). Besides, critical single scattering albedo depends strongly on the local albedo of the underlying surface. The more reflective the surface compared to the aerosol, the higher the critical value. If the single scattering albedo of the aerosol layer is higher than the critical value, the change of the planetary albedo is positive resulting in cooling effect, and *vice versa* (*Seinfeld* and *Pandis*, 1998; *IPCC*, 2007; *Seinfeld*, 2008; *Ramanathan et al.*, 2007; *Stier et al.*, 2007; *Randles et al.*, 2004).

The regions, where the single scattering albedo is close to the critical value, are sensitive to changes in the single scattering albedo. Small increase or decrease in this parameter (few %) can lead to change in the sign of the aerosol radiative forcing. Our results (last columns in *Table 4*) make it clear that the consideration of the size dependence of the complex refractive index instead of constant values may yield important variations in the single scattering albedo, which even can lead to change in the sign of radiative forcing of the Earth-atmosphere system. For this reason, mainly over the sensitive regions, the implication of the size distribution of the complex refractive index can decrease the uncertainty of the estimation of the aerosol direct radiative forcing.

4.3. Effect of hygroscopic mass growth on the refractive index

Increasing relative humidity results in water uptake by the aerosol particles. The water uptake of the particles changes their size as well as the chemical composition of the aerosol. Even, above the deliquescence relative humidity, water can be the most abundant compound in hygroscopic particles (e.g., *Randles et al.*, 2004). Taking into account the amount of the absorbed water measured (see paragraph 2.1), the complex refractive index of the wet aerosol was recalculated ($m_{\text{water}}=1.33-0i$) by using the volume mixing rule. In *Fig. 3a*, the effect of hygroscopic mass growth on the real refractive index is plotted. One can see that the water uptake decreases the refractive index of the particles compared to the dry aerosol. Moreover, with increasing relative humidity, the size distribution of the refractive index changes, which is also shown in *Fig 3a*. Local minimum and maxima of the 'dry' curve become more significant with increasing relative humidity, due to the various hygroscopic mass growths in different size ranges caused by differences in the chemical composition. These results are in agreement with the data by *Iinuma et al.* (2000) who studied the effect of aerosol hygroscopicity in the air over Australian cities. At 80% RH, they reported –1% to –5% decreases in the real part in Canberra, while our

results show a reduction between –3 and – 6%, probably due to the difference in the hygroscopic properties of the aerosol. We also have to note that water uptake decreases the imaginary part of the refractive index as shown in *Fig. 3b*, in accordance with the data of *Iinuma et al.* (2000). This decrease is obviously caused by the mass increase of the particles, as water is not light absorbing in the visible radiation range.

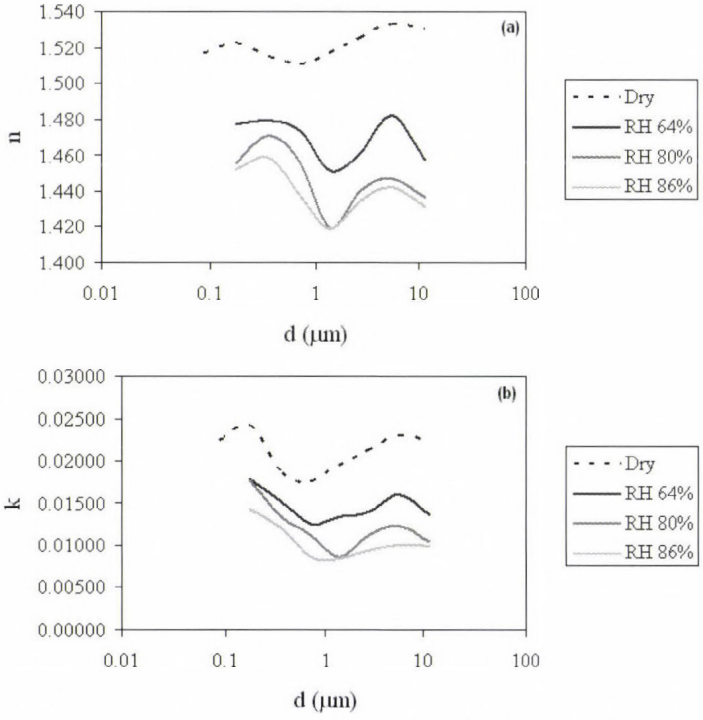

Fig. 3. The effect of hygroscopic mass growth on the real (a) and imaginary (b) refractive indices.

5. Summary and conclusions

The size dependent complex refractive index of dry ambient aerosol is estimated on the basis of the mass closure of the aerosol, as well as on the refractive indices and densities of different aerosol constituents. In the calculation, the approach of the volume mixing rule was applied. Calculations made by the Mie-theory indicate that the extinction coefficient and the single scattering albedo are different if the size resolved refractive index is used instead of a size-independent constant value. The study carried out also show that hygroscopic mass growth of the particles influence the refractive index. The main results obtained can be summarized as follows.

(i) In agreement with results published by different authors, in the optically active size range (0.1–1μm) the real part of the refractive index of dry aerosol increases with particle size, while, at the same time, a significant decrease can be found in the imaginary refractive index. This latter parameter has a local minimum around particle diameter of 1μm. Its size distribution is in close connection with the size dependent variation of EC concentrations.

(ii) No significant seasonal variation was found in the real or imaginary parts of the aerosol refractive index. However, during the fall, the imaginary part was found to be somewhat higher than in other seasons, probably due to some biomass burning in the region.

(iii) The absorption coefficient, calculated by applying a constant refractive index, overestimates the value calculated with changing refractive index by 37%. Further, an overall underestimation of 4% occurs in the case of the scattering coefficient, ranging from –3% to 17%. As the result of the overestimation of the absorption coefficient and underestimation of the scattering coefficient, the overall difference between the extinction coefficients is 1%, varying in the range of –2% and 65%. These numbers indicate that the deviation between extinction coefficients with a constant and a size resolved refractive index varies strongly with the particle size. We concluded that the application of a constant refractive index instead of size resolved values may enhance the uncertainty of the estimation of scattering and absorption coefficients.

(iv) It follows from our results that the consideration of the size dependence of the complex refractive index instead of constant values may yield changes (some %) in the single scattering albedo. Even this can lead to change in the sign of radiative forcing of the Earth-atmosphere system, mainly over sensitive regions, where the single scattering albedo is close to the critical value.

(v) Finally, our results show that water uptake by particles decreases the real part of their refractive index (by 5% at 86% relative humidity compared to the dry aerosol). Water uptake also decreases the imaginary part of the refractive index, which is obviously caused by the aerosol mass increase.

It goes without saying that our results on the size variation of dry complex refractive index should be confirmed by further similar studies. Moreover, more research is needed to clarify the effect of the hygroscopicity of aerosol particles on the refractive index.

Acknowledgements—The authors are indebted to the Hungarian Science Foundation (OTKA) for the financial support of this work (project numbers: T 047222 and TS 049845). The authors are grateful for the beneficial help from *Ernő Mészáros*.

References

Balkanski, Y., Schulz, M., Claquin, T., and *Guibert, S.*, 2007: Reevaluation of Mineral aerosol radiative forcings suggests a better agreement with satellite and AERONET data. *Atmos. Chem. Phys. 7,* 81–95.

Cabada, J.C., Rees, S., Takahama, S., Khlystov, A., Pandis, S.N., Davidson, C.I., Robinson, A.L., 2004: Mass size distributions and size resolved chemical composition offine particulate matter at the Pittsburgh supersite. *Atmos.Environ. 38,* 3127–3141.

Ebert, M., Weinbruch, S., Rausch, A., Gorzawski, G., Hoffmann, P., Wex, H., Helas, G., 2002: Complex refractive index of aerosols during LACE 98 as derived from the analysis of individual particles. *J. Geophys. Res. 107,* No. D21, 8121, doi:10.1029/2000JD000195.

Ebert, M., Weinbruch, S., Hoffmann, P., Ortner, H.M., 2004: The chemical composition and complex refractive index of rural and urban influenced aerosols determined by individual particle analysis. *Atmos. Environ. 38,* 6531-6545.

ELPI (Electric Low Pressure Impactor) *User Manual,* 2003, Dekati Ltd.

Feczkó, T., Mészáros, E., and *Molnár, A.,* 2004: Radiative forcing tendency due to anthropogenic aerosol particles and greenhouse gases in Hungary. *Időjárás 108,* 1-10.

Guyon, P., Boucher, O., Graham, B., Beck, J., Mayol-Bracero, O.L., Roberts, G.C., Maenhaut W., Artaxo, P., Andreae, M.O., 2005: Refractive index of aerosol particles over the Amazon tropical forest during LBA-EUSTACH 1999. *J. Aerosol Sci. 34,* 883-907.

Gysel, M., Weingartner, E., Nyeki, S., Paulsen, D., Baltensperger, U., Galambos, I., Kiss, G., 2004: Hygroscopic properties of water-soluble matter and humic-like organics in atmospheric fine aerosol. *Atmos. Chem. Phys. 4,* 35-50.

Hand, J.L., Kreidenweis, S.M., Kreisberg, N., Hering, S., Stolzenburg, M., Dick, W., McMurry, P.H., 2002: Comparison of aerosol properties measured by impactors and light scattering from individual particles: refractive index, number and volume concentrations, and size distributions. *Atmos. Environ. 36,* 1853-1861.

Hatzianastassiou, N., Matsoukas, C., Drakakis, E., Stackhouse Jr., P.W., Koepke, P., Fotiadi, A., Pavlakis, K.G., and *Vardavas, I.,* 2007: The direct effect of aerosols on solar radiation based on satellite observations, reanalysis datasets, and spectral aerosol optical properties from Global Aerosol Data Set (GADS). *Atmos. Chem. Phys. 7,* 2585–2599.

Hitzenberger, R., Ctyroky, P., Berner, A., Turšič, J., Podkrajšek, B., Grgić, I., 2006: Size distribution of black (BC) and total carbon (TC) in Vienna and Ljubljana. *Chemosphere 65,* 2106–2113.

Hoffer, A., Gelencsér, A., Guyon, P., Kiss, G., Schmid, O., Frank, G., Artaxo, P., Andreae, M.O., 2005: Optical properties of humic-like substances (HULIS) in biomass-burning aerosols. *Atmos. Chem. Phys. Discussions 5,* 7341-7360.

Horvath, H., 1995: *Size segregated light absorption coefficient of the atmospheric aerosol. Atmos. Environ. 29,* 875-883.

Horvath, H., 1998: Influence of atmospheric aerosols upon the global radiation balance. In *Atmospheric Particles IUPAC Series on Analytical and Physical Chemistry of Environmental Systems*. John Wiley, New York, Vol. 5, 543-596.

Iinuma, Y., Box, G.P., Gras, J.L., Keywood, M., & Ayers, G., 2000: Comparison of predicted and measured aerosol optical and physical properties in Australian cities. *Proc. 15th International Clean Air Conference.* Sydney, 2000. Clean Air Society of Australia & New Zealand, Mitcham, Vic., Australia, 227-231.

Imre, K. and *Molnár, A.,* 2008: Hygroscopic behaviour of Central European atmospheric background aerosol particles in summer. *Időjárás 112,* 63-82.

IPCC, 2007. *Forster, P., V. Ramaswamy, P. Artaxo, T. Berntsen, R. Betts, D.W. Fahey, J. Haywood, J. Lean, D.C. Lowe, G. Myhre, J. Nganga, R. Prinn, G. Raga, M. Schulz* and *R. Van Dorland,* 2007: *Changes in Atmospheric Constituents and in Radiative Forcing.* In *Climate Change 2007: The Physical Science Basis.* Contribution of Working Group I to the Fourth Assessment Report of the Intergovernmental Panel on Climate Change [*Solomon, S., D. Qin, M. Manning, Z. Chen,*

M. Marquis, K.B. Averyt, M. Tignor and *H.L. Miller* (eds.)]. Cambridge University Press, Cambridge, United Kingdom and New York, NY, USA.

Jaffrezo, J.-L., Aymoz, G., and *Cozic, J.,* 2005: Size distribution of EC and OC in the aerosol of Alpine valleys during summer and winter. *Atmos. Chem. Phys. 5,* 2915–2925.

Kaufman, Y.J., Tanré, D., Boucher, O., 2002: A satellite view of aerosols in the climate system. *Nature 419,* 215-223.

Kiss, Gy., Varga, B., Galambos, I., Ganszky, I., 2002: Characterization of water soluble organic matter isolated from atmospheric fine aerosol. *J. Geophys. Res. 107,* No. D21, 8339, doi:10.1029/2001JD000603.

Mészáros, E., Barcza, T., Gelencsér, A., Hlavay, J., Kiss, Gy., Krivácsy, Z., Molnár, A., Polyák, K., 1997: Size distributions of inorganic and organic species in the atmospheric aerosol in Hungary. *J. Aerosol Sci. 28,* 1163-1175.

Miguel, A.H., Eiguren-Fernandez, A., Jaques, P.A., John R. Froines, J.R., Grant, B.L., Mayo, P.R., Sioutas, C., 2004: Seasonal variation of the particle size distribution of polycyclic aromatic hydrocarbons and of major aerosol species in Claremont, California. *Atmos. Environ. 38*, 3241–3251.

Molnár, A., Mészáros, E., Hansson, H.C., Karlsson, H., Gelencsér, A., Kiss, Gy., Krivácsy, Z., 1999: The importance of organic and elemental carbon int he fine atmospheric aerosol particles. *Atmos. Environ. 33,* 2745-2750.

Pesava, P., Horvath, H., Kasahara, M., 2001: A local optical closure experiment in Vienna. *J. Aerosol Sci. 32,* 1249-1267.

Ramanathan, V., Li, F., Ramana, M.V., Praveen, P.S., Kim, D., Corrigan, C.E., Nguyen, H., Stone, E. A., Schauer, J.J., Carmichael, G.R., Adhikary, B., Yoon, S.C., 2007: Atmospheric brown clouds: Hemispherical and regional variations in long-range transport, absorption, and radiative forcing. *J. Geophys. Res. 112,* D22S21, doi:10.1029/2006JD008124.

Randles, C.A., Russell, L.M., Ramaswamy, V., 2004: Hygroscopic and optical properties of organic sea salt aerosol and consequences for climate forcing. *Geophys. Res. Lett. 31,* L16108, doi:10.1029/2004GL020628.

Raut, J.C. and *Chazette, P.,* 2007: Retrieval of aerosol complex refractive index from a synergy between lidar, sunphotometer and in situ measurements during LISAIR experiment. *Atmos. Chem. Phys. 7,* 2797-2815.

Saarikoski, S., Mäkelä, T., Hillamo, R., Aalto, P.P., Kerminen, V.-M., Kulmala, M., 2005: Physico-chemical characterization and mass closure of size segregated atmospheric aerosols in Hyytiälä, Finland. *Boreal Environ. Res. 10,* 385–400.

Seinfeld, J.H. and *Pandis, S.N.,* 1998: *Atmospheric Chemistry and Physics.* John Wiley & Sons.

Seinfeld, J., 2008: Atmospheric science: Black carbon and brown clouds. *Nature Geoscience 1,* 15-16, doi:10.1038/ngeo.2007.62.

Stelson, A.W., 1990: Urban aerosol refractive index prediction by partial molar refraction approach. *Environ. Sci. Technol. 24,* 1676-1679.

Stier, P., Seinfeld, J.H., Kinne, S., and *Boucher, O.,* 2007: Aerosol absorption and radiative forcing. *Atmos. Chem. Phys. 7,* 5237–5261.

Temesi, D., Molnár, A., Mészáros, E., Feczkó, T., Gelencsér, A., Kiss, G., Krivácsy, Z., 2001: Size resolved chemical mass balance of aerosol particles over rural Hungary. *Atmos. Environ. 35,* 4347-4355.

Turpin, B.J., Hutzincker, J.J., 1995: Identification of secondary organic aerosol episodes and quantization of primary and secondary organic aerosol concentrations during SCAQS. *Atmos. Environ. 29,* 3527–3544.

Turpin, B.J., Lim, H.J., 2001: Species contributions to PM2.5 mass concentrations: Revisiting common assumptions for estimating organic mass. *Aerosol Sci. Technol. 35,* 602-610.

Weast, R.C., 1987: Physical constants of organic compounds. *CRC Handbook of Chemistry and Physics*, 68th Edition (ed.: *R.C. Weast*). CRC Press, Boca Raton, FL, B67-B146.

IDŐJÁRÁS

Quarterly Journal of the Hungarian Meteorological Service
Vol. 113, No. 3, July–September 2009, pp. 177–187

Determination of ambient air pollution: Tasks, methods, approaches

Krisztina Labancz[1*] and **István Matyasovszky**[2]

[1]*Hungarian Meteorological Service,*
P.O. Box 39, H-1675 Budapest, Hungary; E-mail: labancz.k@met.hu

[2]*Department of Meteorology, Eötvös Loránd University,*
P.O. Box 32, H-1518 Budapest, Hungary; E-mail: matya@ludens.elte.hu

(Manuscript received in final form June 20, 2009)

Abstract—Estimation of the level of ambient air pollution is a complicated task, which includes concentration measurements, modeling of dispersion and transport of air pollutants, and estimation of possible effects of a large number of different local sources. In this paper, a detailed description of the European ambient air quality legislation is presented indicating the tools for air quality control (monitoring, modeling, other methods) which should be applied by the member states. Hungarian regulation and the corresponding measurement and modeling activities are also described. Finally, a newly developed statistical method is presented, which can be a useful tool in planning an aimed measurement campaign to estimate the local ambient air quality around a new source. By the aid of this method the necessary time length and the best starting date of the measurement campaign can be estimated.

Key-words: ambient air quality, EU directives, legislation, assessment techniques, statistical model

1. Introduction

Ambient air quality is still a major problem in Europe, where long term exposure to air pollutants can cause damages to ecosystems, human health, and materials. Because of the health risks, the EU 2008 directive (*EU*, 2008) recommends member states to ensure that information about the level of ambient air pollution obtained by either measurements or other methods (e.g., modeling or objective estimation) are provided to the public. In order to follow these guidelines, a system of monitoring networks, air pollution transport and dispersion modeling activities, and studies of suitable objective estimation methods has to be set up.

* Corresponding author

In this paper, a description of the European ambient air quality legislation is presented indicating the tools for air quality control (monitoring, modeling, and other methods) which should be applied by the member states.

As the continental regional background air pollution is suitably calculated by long-range transport models run at the Europeans scientific centers, this paper focuses on the effect of the local sources on local scales. In urban areas, the total description of local ambient air quality by measurements requires many monitoring stations. Moreover, many suitable models exist for the calculation of air pollution dispersion and for chemical reactions, and the system of monitoring stations, modeling tools and available meteorological parameters provides relevant urban background air quality estimations (*Berkovicz et al.,* 1994). However, improved understanding of spatiotemporal variability in ambient air pollutant concentrations in urban areas is useful in many contexts and needs additional, mainly statistical estimation tools (*Morel et al.*, 1998; *Marshall et al.*, 2007; *Singh et al.*, 2009).

Statistical estimation methods play an important role in calculating air pollution around industrial site. Air quality around point sources and possible exceedances of short term limit values are not possible to determine without a large number of monitoring stations. The best way is to combine measurements and statistical estimation methods (*Rumburg et al.*, 2000; *McMillan et al.*, 2004). This paper presents a new statistical method for calculating the necessary time length of a measurement campaign to be carried out to estimate the local ambient air concentrations around a source.

2. Legislation

2.1. Regulation in the European Union

There are a number of EU laws that regulate air pollution. The Air Quality Framework Directive (*EU*, 1996) and its four daughter directives describe the basic principles as to how air quality should be assessed and managed, and list the pollutants for which air quality standards and objectives will be developed and specified in legislation. Other laws (the National Emission Ceilings Directive, sectoral emission laws) set national emission ceilings which must be achieved by 2010 through EU wide and national measures. Also, EU member states systematically exchange information on most effective abatement measures and coordinate their efforts in tackling transboundary air pollution.

The Air Quality Framework Directive sets concentration limit values or target values for a range of air pollutants. It defines minimum requirements for air quality assessments – through monitoring and modeling – that provide a good indication of air quality concentrations throughout the member states' territory. Where thresholds are exceeded, member states are expected to act.

Daughter directives complete the list of pollutants in details. For example, the First Daughter Directive (*EU*, 1999) sets the limit values for SO_2, NO_2 and NO_x, PM, and Pb in ambient air. The directive lists the limit values set in the member states' own legislation like the joint decree of the Minister of Environment and Water and the Minister of Health on the Hungarian limit values (*HU*, 2001a).

When the limit values are set, the ambient air quality shall be assessed in each member state. The directive sets the tools for air quality control which should be applied. Measurement is mandatory in zones with a population of more than 250,000 inhabitants, with high population concentration (agglomerations), and where the concentrations are near to or exceed the limit value. In zones with lower concentrations, member states can apply additional tools for quality control and the assessment of exceedances in addition to measurement data, e.g., air quality models and statistical methods. Based on the number of inhabitants and the limit value exceedances, the directive sets two limit values: a higher assessment level (tolerance limit), X, and a lower assessment level (acceptable limit), *Y*. The value of *X* and *Y* were determined by an expert group of the European Commission. *Table 1* shows the summary of recommended assessment techniques.

Table 1. Summary of requirements for measurements and other assessment methods

Type of zone	**Assessment technique**
Agglomeration, >250,000 inhabitants	Monitoring is mandatory even if levels are <X% of limit value
Zones with levels >*X* % of limit value	Monitoring is mandatory
Zones with levels <*X* % but >*Y*% of limit value	A combination of measurements and modeling may be used
Zones with levels <*Y* % of limit value	Modeling or objective estimation is sufficient

Determination of *X* and *Y* is based on the inter-annual variations and normalized standard deviation of data at monitoring stations. For NO_2 it is estimated, that there is a slight variation between stations, but the standard deviation is generally consistent for NO_2 throughout the European Union. The recommended values for *X* are 80% of the annual limit value and 60% of the hourly limit value, while for *Y* the values are 75% of the annual and 50% of the hourly limit values.

2.2. Measurements and modeling in Hungary

In Europe, there is a scientifically based and policy driven program, the EMEP (Co-operative Programme for Monitoring and Evaluation of the Long-range Transmission of Air Pollutants in Europe), which has a monitoring network for continuously measuring the regional background air pollution level. In Hungary,

there is a background air pollution monitoring network of four stations, where air and precipitation samples and monitored values of about 20 elements are collected. The samples are analyzed in the laboratory of the Hungarian Meteorological Service. The urban ambient air pollution is monitored by an other network, the National Urban Air Quality Network carried out by the local environmental protection agencies. The network consists of 52 automatic stations measuring concentrations of 12 pollutants and 5 meteorological parameters. In addition to the monitoring of background values, there are aimed scientific measurements, as well as the Hungarian legislation ordains measurement campaigns in case of building a new source of air pollutants (an industrial unit, factory, or stack). In case of an aimed campaign, two important practical points are emerged: one is to determine the range area where the pollution emitted by the source has measurable effect on the surroundings and mark the places of sampling inside the range, and the other is to determine the optimal length of the measurement campaign.

Measurements are accurate and continuous in time, but point-wise in space, therefore, they operability is limited in space. The directives stimulate the use of models, which are less accurate but have better opportunities for spatial coverage. Depending on the size of the modeled area, there are different air pollution transport and dispersion models with global, regional, and local scales. The long-range transport of emitted air pollutants are modeled in the main European centers, like the EMEP, to regularly provide governments with qualified scientific information to support the development and further evaluation of the international protocols on emission reductions. On urban and local scales, every member states has its own air quality models. The Hungarian Meteorological Service runs models both on urban and local scales.

2.3. Regulation in Hungary

In Hungary, a governmental regulation (*HU*, 2001b) defines the ambient level of air pollution as "the average air pollution caused by other sources in given distance and time length around a given source". To calculate the effect of a new source, the concentration of air pollutants caused by the emission of the new source should be added to the above defined ambient level. The ambient air pollution consists of two components: one is the regional background concentration of pollutants calculated by global or regional long-range transport models; the other is the so-called supplementary pollution, the local effect of pollution sources in the vicinity of the examined source.

The total pollution in the surroundings of a given source is calculated by the sum of the ambient air pollution and the so-called excess pollution, which is also defined by the above mentioned regulation. By definition it is "the pollution near the given source caused by the emission of the source itself, the emission of the increased traffic, and the effect of the possibly modified air flow around the source".

3. Tasks

As a result of the above described regulations, estimating the level of ambient air pollution is a different kind of task than calculating the effect of a given source or modeling the transport of air pollutants. The task is to estimate the level of the permanently existing ambient concentrations which is made up of the emissions of local point-, line-, area-, or mobile sources, regional concentration levels, and long-range transport. Finally, the effect of a given source may be added to the estimated or calculated ambient level. Therefore, three types of the tasks can be formed:

- Evaluation of urban air quality on the base of the data measured by the urban monitoring network; analysis of characteristic weather situations.
- Urban air quality forecast calculated by an urban dispersion model using numerical weather prediction outputs and emission data.
- Calculating/estimating the effects of new local sources.

Let us take a close look at the third task! There is a village or smaller town, where no measurements were carried out in the past. A new industrial unit, factory or stack with significant pollution is planned to be built here. A study should be made on evaluation the effects of the new source and estimating the new air pollution level, which cause damage to the ecosystem and the human health in the town and its vicinity. The study should estimate if the sum of the original ambient air pollution and the effect of the new source would exceed the official limit values. The task has two parts: one is to estimate the original local ambient air pollution, the other is to calculate the effect of the new source. The later objective can be solved by the aid of a local scale dispersion model developed for regulatory purposes.

Based on the above described official definitions, the ambient level of air pollutants is composed of the regional background pollution and the effect of the local sources. Yearly average concentration values calculated for grid points over Hungary by the global or regional long-range transport models of European centers (like EMEP) are taken as regional background values. The real challenge of the task is to estimate the air pollution level caused by the local sources, as the emission of the sources, moreover, the local sources themselves are not known in most cases. The most one can do is relying on estimations. There are two ways of estimating the effect of local sources:

- The background concentrations of air pollutants calculated and reported yearly by the EMEP center is accepted as local ambient air pollution level. This choice is reasonable as the EMEP model uses the official emission data reported yearly by the member states, therefore, the local sources are taken into account indirectly. Moreover, long-range transport models give good spatial coverage of transboundary air

pollution. The problem of this choice is that it does not give acceptable estimation for the possible limit value exceedances caused by the joint effect of the original and new local sources.

- The local air pollution level is estimated by an aimed measurement campaign. If the volume of the investment is big enough, the builder must carry on a measurement campaign at the place of the new source. Statistical methods can be useful tools in optimizing the time length and the starting date of the compulsory measurements, making it cost-effective and suitable.

4. Statistical modeling

To calculate the effect of a new pollutant source on its surroundings, the degree of the existing background pollution has to be estimated. There are two practical problems which make the estimation difficult: one is that often there are no measurements previously performed at the area nearby the new source, the other is that the time disposable for performing necessary measurements is highly restricted, no more than a few months. Therefore, the length of measuring period should be optimized. 14-year long time series of three pollutants were used for estimating the optimal length of measurements, assuming that the series of the two tasks have similar statistical features.

4.1. Data

A suitable dataset to conduct the statistical modeling was obtained from the National Urban Air Quality Monitoring Network carried out by the local environmental protection agencies. This ambient air monitoring program continuously observes the hourly and daily means of concentrations of 12 pollutants and 5 meteorological parameters. Data of 8 monitoring stations located in downtown and suburban areas of Budapest were available for the period of 1991–2005. In 2003, the structure of monitored data was changed to a certain extent: some stations were transferred, a new station started to work, and new elements (e.g., aromatic hydrocarbons) were taken into the monitoring program.

Time series of hourly NO_2, SO_2, and CO concentrations were chosen for the period of 1992–2005 measured at a downtown station (Baross Square, see *Fig. 1*). Time series observed at this station are the longest, most complete series. Unfortunately, the place of the station was changed in the beginning of 2006 because of street reconstruction works. Concentration of NO_2 describes the degree of air pollution caused by traffic, while SO_2 and CO indicate the urban background pollution and the pollution of industrial origin. This study is based on daily mean values of the three pollutants derived from the hourly data.

Figures show the results calculated for SO_2 as this pollutant best indicates the background pollution. Calculations for NO_2 and CO gave similar results.

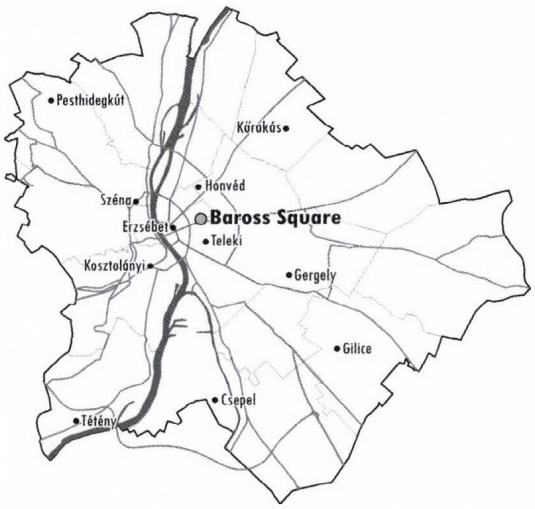

Fig. 1. Urban air pollution monitoring stations in Budapest.

To estimate the optimal length of a measuring campaign, two important concentration measures – daily mean and limit value exceedance – were examined. This study presents the results for the reliable estimation of daily mean background concentration.

4.2. Estimation of necessary time length of measurements – mean concentration method 1

The first question addressed is how many daily measurements (n) are needed to ensure that the mean of these daily mean measured values lies within a specified interval (h) of the expected value with a large probability ($1-\varepsilon$)? Supposing that the time series of measured data comes from a first order autoregressive process, the solution is

$$n = \frac{1+a}{1-a}\left(\hat{s}\, y_\varepsilon / h\right)^2, \tag{1}$$

where $y_\varepsilon = 1.64,\ 1.96,\ 2.58$ at $\varepsilon = 0.1,\ 0.05,\ 0.01$, respectively, furthermore, a is the one day lag autocorrelation and $\hat{s}$ is the adjusted empirical standard deviation. These latter two parameters can be estimated from data, while h is chosen as a specific portion of the standard deviation. Eq. (1) is based on the classical one-sample t-test (*Dévényi* and *Gulyás*, 1988) but taking into account

autocorrelations of data. *Fig. 2* shows necessary measurement lengths (n) for $(1-\varepsilon)100\% = 90$, 95, and 99%.

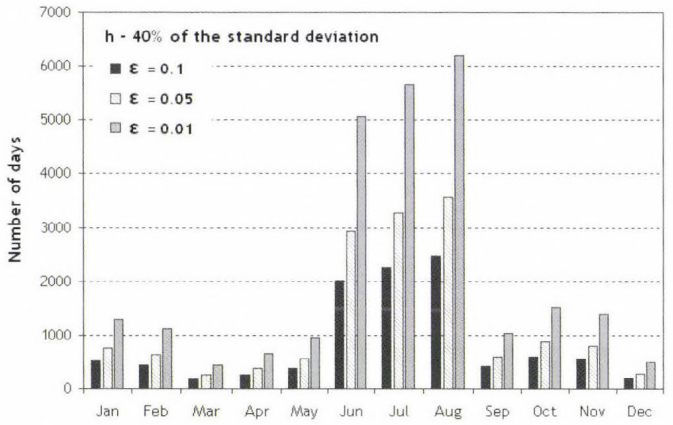

Fig. 2. Necessary measurement length in days for estimating daily average concentration of SO_2 using method 1.

Although quite high h values are chosen (20, 40, and 80% of the standard deviation), results obtained are not practically useful as the necessary measurement lengths are extremely large (from several hundred days to 6000 days when starting the measuring campaign in summer). Similar conclusions can be drawn for daily maximum concentrations, too.

The summer maximum is not surprising. Eq. (1) shows that the number of measurements n depends only on the autocorrelation a when h is chosen as a specific portion of the standard deviation. Since the main source of sulfur dioxide is the heating, the concentration of SO_2 in the air is steadily low in summer; therefore, the concentration series has high autocorrelation. On the other hand, in the heating season the volume of combustion is changing with the altering weather conditions, thus, the autocorrelation is low.

4.3. Estimation of necessary time length of measurements – mean concentration method 2

A much simpler and practically useful approach is to take the background concentration as the average concentration of a given particular year. The question is how long measuring period shorter than one year is necessary to form an average (within-year average) enough close to the annual average. The term "enough close" means that the null-hypothesis of having no systematic difference between the two averages is not rejected at a significance level $(1-\varepsilon)100\%$. The larger the value of ε the larger the certainty of having no systematic difference is. However, higher certainties require longer measuring

periods. The answer depends on the starting date of measurements due to the annual course of pollutants concentrations. The test statistic z_i is used for the purpose as follows:

$$z_i = \frac{\bar{x}_i - \bar{x}_n}{\sqrt{\frac{1+a_i}{1-a_i} s_i^2 \frac{(n-i)^2}{in^2} + \frac{1+a_{n-i}}{1-a_{n-i}} s_{n-i}^2 \frac{n-1}{n^2}}}, \tag{2}$$

where $\bar{x}_i$ and $\bar{x}_n$ are the two means to be compared, n is the number of days of a year ($n=365$), a is the one day lag autocorrelation, and s is the standard deviation, while the subscripts refer to the number of days used to estimate the corresponding quantities. Eq. (2) is based on the Welsh test (*Dévényi* and *Gulyás*, 1988) considering autocorrelations of data. When i is not too small, the test statistic approximately follows the standard normal distribution under the null-hypothesis that the expectation of the difference between the annual and actual within-year average is zero (there is no systematic difference between averages). Significance levels chosen are 80, 90, and 95%. The analysis is performed again with data of Baross Square but using only the last two years.

Fig. 3 shows the minimum necessary measurement lengths for daily mean SO_2 concentrations. Months in the horizontal axis refer to the starting date of the measurements. Minimum necessary measurement lengths mean the shortest measuring period ensuring the acceptance of the null-hypothesis. The most appropriate start of the measurement campaign is in August (40 days) and July (85 days), or in February (120 days) in case of a winter starting. These measuring periods satisfy practical possibilities.

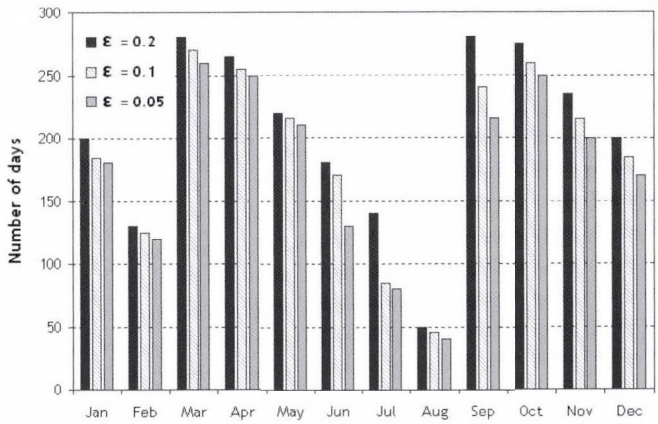

Fig. 3. Necessary measurement length in days for estimating daily average concentration of SO_2 using method 2.

Two local minimum appear in *Fig. 3,* at the end of winter and summer. Since the main source of sulfur dioxide is the heating, the measured concentrations of SO_2 are continuously above the mean value in winter; therefore, the mean concentration of the measuring period will approximate the yearly mean value after a relatively longer time period without heating. For estimating the yearly mean value, a good measuring period starts at the end of winter, when the volume of heating is quickly decreasing, thus the mean of measured values tends to the yearly mean value. Similarly, the measured concentrations are well below the mean value in summer, which again needs a longer averaging time period to tend to the yearly mean value. Hence, the beginning of autumn is the best period to reach the yearly mean by averaging values over a short period.

In addition to the average concentrations, the limit value exceedance should be examined in the prevailing measurement campaign. The builder of a new source should prove that the probability of limit value exceedance is very low. New statistical formulae developed for this purpose are being tested currently. The core of the method is to join typical meteorological conditions accompanied by possible limit value exceedances.

5. Conclusions and future plans

Description of the European ambient air quality legislation was presented in this study, indicating the tools for air quality control (monitoring, modeling, and other methods) which should be applied by the member states. Hungarian regulation and the corresponding measurement and modeling activities were also described. Measurements and modeling are the most important tools in the ambient air quality control, but other estimation methods are also recommended as assessment techniques in background areas and around industrial sources. A newly developed statistical method was presented in the paper which can be a useful tool in planning an aimed measurement campaign to estimate the local ambient air quality around a new source. By the aid of this method the necessary time length and the best starting date of the measurement campaign can be estimated on the base of daily mean concentration measurements carried out at another site. In the future, the method will be extended to limit value exceedances.

References

Berkowicz, R., Hertel, O., Sørensen, N.N., and *Michelsen, J.A.*,1994: Modelling air pollution from traffic in urban areas. In *Flow and Dispersion Through Obstacles* (eds.: *R.J. Perkins* and *S.E. Belcher*). Cambridge, UK, 28–30 March 1994, 121–142.

Dévényi, D. and *Gulyás, O.,* 1988: *Mathematical Statistics for Meteorologists* (in Hungarian). Tankönyvkiadó, Budapest, 443 pp.

Marshall, J.D., Nethery, E., and *Brauer, M.*, 2007: Within-urban variability in ambient air pollution: Comparison of estimation methods. *Atmos. Environ. 42,* 1359-1369.

McMillan, N., Bortnick, S.M., Irwin, M.E., and *Berliner, L.M.,* 2004: A hierarchical Bayesian model to estimate and forecast ozone through space and time. *Atmos. Environ. 39,* 1373-1383.

Morel, B., Yeh, S., and *Cifuentes, L.,* 1998: Statistical distributions for air pollution applied to the study of the particulate problem in Santiago. *Atmos. Environ. 33,* 2575-2585.

Rumburg, B., Alldredge, R., and *Claiborn, C.,* 2000: Statistical distributions of particulate matter and the error associated with sampling frequency. *Atmos. Environ. 35,* 2907-2920.

Singh, B., Carnevale, C., Pisoni, E., Volta, M., 2009: A comprehensive stochastic methodology to forecast ozone and PM10 in a metropolitan area. In *7th International Conference on Air Quality – Science and Application* (ed.: *R.R. Sokhi*). Istanbul, Turkey, 24 –27 March 2009 (in press).

EU, 1996: Council directive on ambient air quality assessment and management. Council Directive 1996/62/EC.

EU, 1999: Council directive relating to limit values for sulphur dioxide, nitrogen dioxide and oxides of nitrogen, particulate matter and lead in ambient air. Council Directive 1999/30/EC.

EU, 2008: Directive of the European Parliament and of the Council on ambient air quality and cleaner air for Europe. Council Directive 2008/50/EC, May 21.

HU, 2001a: Joint order of the Minister of Environment and Water and Minister of Health on air pollution limit values and limit values for emission of point sources (in Hungarian). 14/2001(V.9), KöM-EüM rend.

HU, 2001b: Decree of Government on some regulations on air quality protection (in Hungarian). 21/2001(II.14) Korm. rend.

IDŐJÁRÁS

Quarterly Journal of the Hungarian Meteorological Service
Vol. 113, No. 3, July–September 2009, pp. 189–202

Operator splitting in the Lagrangian air pollution transport model FLEXPART

Zsófia Kocsis[1*], **Zita Ferenczi**[1], **Ágnes Havasi**[2], and **István Faragó**[3]

[1]*Hungarian Meteorological Service,*
P.O. Box 38, H-1525 Budapest, Hungary; E-mails: kocsis.zs@met.hu; ferenczi.z@met.hu

[2]*Department of Meteorology, Eötvös Loránd University,*
P.O. Box 32, H-1518 Budapest, Hungary; E-mail: hagi@nimbus.elte.hu

[3]*Department of Applied Analysis and Computational Mathematics, Eötvös Loránd University,*
P.O. Box 32, H-1518 Budapest, Hungary; E-mail: faragois@cs.elte.hu

(Manuscript received in final form February 18, 2009)

Abstract—Operator splitting is a widely applied computational procedure in the numerical integration of long-range air pollution transport models. It is based on a decomposition of the model problem into smaller sub-problems, which are connected through their initial conditions. In this paper we apply four different splitting techniques in the Lagrangian FLEXPART model. The results are compared with measurement data collected during the ETEX experiment.

Key-words: splitting methods, particle model, Langevin equation, ETEX experiment

1. Introduction

In the past few decades, special emphasis has been laid on the investigation of the mechanisms and effects of atmospheric pollution. Several by-products of industry, agriculture, and traffic are emitted directly into the air, where these pollutants go through further processes: they are transported by the wind and dispersed by turbulent eddies, undergo chemical transformations, and, finally, are removed from the air by some form of deposition. Thus, the air pollution process is a very complicated one, consisting of several simultaneous interrelated sub-processes. Our major tools for the description of changes in the pollutant concentrations are mathematical models.

The mathematical modeling of air pollution phenomena, especially long-range air pollution transport, is usually based on a highly complicated system of

* Correspondig author

differential equations. The high complexity of this system requires the application of numerical solution techniques. Since our natural expectation is real-time simulation, therefore, in addition to the accuracy of the results, the efficiency of the computations is a crucial requirement as well. If some "off-the-shelf" solver is applied directly to the system, then these two requirements can hardly be met at the same time. Therefore, procedures, that allow us to lead the solution of the system back to the solution of simpler systems for which sufficiently accurate as well as efficient methods exist, are of great significance. This is exactly what operator splitting attains.

The aim of the paper is to present different kinds of operator splitting methods and demonstrate their applicability in air pollution transport modeling. The experiments were performed with the FLEXPART model, developed by Andreas Stohl and adapted by the Hungarian Meteorological Service. Certain parts of the program package were modified for the inclusion of splitting. The effects of different splitting methods were investigated in computer experiments where the model results were compared with measurement data.

2. The FLEXPART model

The FLEXPART model has been developed for approximately ten years for the computation of long and medium range transport of air pollutants emitted by point sources, and has continuously been under development. Nowadays line, area, and volume sources can also be investigated by the model. The model computes the trajectories of the emitted pollutant particles, and their concentration changes along the trajectories as an effect of diffusion, dry and wet deposition, and radioactive decay. It can be used for operational runs as well as for research purposes. The source code of the model can be freely downloaded from the site http://transport.nilu.no/flexpart.

FLEXPART can be applied in two different modes, namely, in forward and backward mode. In the first case the path of the emitted pollutant is followed forward in time, while in the second case the trajectories are followed backward in time, and so the source of the pollutant can be found.

The input data for the model, i.e., the meteorological (analysis and forecast) fields are provided by the ECMWF numerical weather prediction model in gridded binary (GRIB) format (*ECMWF*, 1995). The interpretation of the data necessitates the use of a GRIB decoding software, which can also be accessed freely in the internet. FLEXPART uses five three-dimensional scalar fields, namely, the horizontal and vertical wind components, temperature, and specific humidity. The vertical layers of the input data should coincide with those of the ECMWF model, which are given in hybrid coordinate system. The model transforms the hybrid coordinates into pressure coordinates. Moreover, the model needs the following two-dimensional fields: surface pressure, total cloud

cover, 10-meter horizontal wind components, 2-meter temperature and dewpoint, large-scale and convective precipitation, sensible heat flux, topography, surface cover, etc. The planetary boundary layer is parameterized by means of the Monin-Obukhov similarity theory.

The motion of the particles is composed of two components: the random wind velocities and an evolution part, which is supposed to be a Markov process. These two processes are described by the Langevin equation. The equation for the vertical wind component w can be given as

$$dw = -w\frac{dt}{\tau_{L_w}} + \frac{\partial \sigma_w^2}{\partial z}dt + \frac{\sigma_w^2}{\rho}\frac{\partial \rho}{\partial z} + \left(\frac{2}{\tau_{L_w}}\right)^{1/2}\sigma_w dW\,, \tag{1}$$

where w is the turbulent vertical wind component, σ_w is its standard distribution, τ_{L_w} is the Lagrangian time scale of the autocorrelation of the vertical wind, ρ is the air density, and dW is an increment. This kind of description of the turbulent motion has the advantage that it is simple, flexible, and able to combine the spatial and temporal changes of the turbulent properties (*Carvalho et al.*, 2007).

3. Operator splitting methods and their application in the FLEXPART model

Operator splitting is based on an appropriate decomposition of the right-hand side of an evolution equation. In the traditional formulation of these equations, the time derivative is on the left-hand side, and the right-hand side contains terms with no time derivative that describe the effects of different physical/-chemical sub-processes. The different sub-processes are treated separately, by coupling the corresponding mathematical problems through their initial conditions. This procedure has been widely used in various fields of applied mathematics, including air pollution meteorology (*Zlatev*, 1995) and circulation models (*Lanser* et al., 2001; *Havasi*, 2007).

Hereinafter we give a brief description of the operator splitting approach. For more details we refer to *Havasi et al.* (2001) and *Faragó* (2006). It is worthwhile to formulate the splitting procedure in general terms. Let **X** denote some normed space, and consider the abstract initial value problem

$$\left.\begin{aligned} &\frac{dy}{dt}(t) = Ay(t), \\ &y(0) = y_0, \end{aligned}\right\} \tag{2}$$

on $[0,T]$, where w: $[0,T] \rightarrow \mathbf{X}$ is the unknown function, and A is an operator $\mathbf{X} \rightarrow \mathbf{X}$. This abstract initial value problem can stand for a partial differential

equation as well as for a system of ordinary differential equations, obtained, e.g., after spatial discretization of a partial differential equation. Assume that the operator A can be decomposed into a sum of two sub-operators, A_1 and A_2, such that a problem with only operator A_1 on the right-hand side and a problem with only operator A_2 on the right-hand side are easier to integrate than the original problem. We divide the time interval $[0,T]$ of the problem into n smaller sub-intervals of length $\tau = T/n$, called splitting time step.

The simplest and most natural splitting method is the sequential splitting, where – at each time step – we first solve a problem that contains only the operator A_1 on the right-hand side and then a problem with only A_2. The initial condition is always the solution of the previous sub-problem. (During the solution of the first sub-problem in the first time step, the initial condition specified for the original problem is used.)

To formulate the sequential splitting mathematically, denote by $S_1(t_n, \tau)$ the solution operator belonging to the sub-problem defined by A_1 on $[t_n, t_n+\tau]$, and by $S_2(t_n, \tau)$ that defined by A_2 on $[t_n, t_n+\tau]$. (We call solution operator the operator which assigns the solution at the end of the time step to that at the beginning of the time step. In our case $S_1(t_n, \tau)$ and $S_2(t_n, \tau)$ are the numerical solution operators of the sub-problems, however, they could be the exact solution operators as well, if the sub-problems were solved exactly.) If $y_{seq}(t_n)$ denotes the solution obtained by the sequential splitting at time level t_n, then the solution at time t_{n+1} reads

$$y_{seq}(t_{n+1}) = S_2(t_n,\tau)\, S_1(t_n,\tau) y_{seq}(t_n). \tag{3}$$

A more accurate splitting scheme is the Marchuk-Strang splitting (*Marchuk*, 1968, *Strang*, 1968), where at each time step we first solve a problem with A_1 over half a splitting time step, then a problem with A_2 over the whole time step, and, finally, a problem with A_1 again over half a time step:

$$y_{MS}(t_{n+1}) = S_1\left(t_n + \frac{\tau}{2}, \frac{\tau}{2}\right) S_2(t_n,\tau)\, S_1\left(t_n, \frac{\tau}{2}\right) y_{MS}(t_n). \tag{4}$$

A newly developed splitting scheme is the additive splitting (*Faragó et al.*, 2008), where both sub-problems use the same initial condition (the solution of the previous time step), which is subtracted from the sum of the two solutions:

$$y_a(t_{n+1}) = \big(S_1(t_n,\tau) + S_2(t_n,\tau)\big) y_a(t_n) - y_a(t_n). \tag{5}$$

The fourth method that we will study is called modified additive splitting (*Kocsis*, 2008), which has the algorithm

$$y_{ma}(t_{n+1}) = 0.5\left(S_1(t_n, 2\tau) + S_2(t_n, 2\tau)\right) y_{ma}(t_n). \tag{6}$$

Here the sub-problems are solved over time steps of length 2τ by using the same initial condition, and then the two solutions, obtained in this way, are symmetrically averaged. This modified method has better stability properties than the ordinary additive splitting, because the negative weights, which usually cause problems in proving the stability, are avoided in the time-stepping operator. Here and further on, by stability we mean the usual stability notion in numerical mathematics, namely, the continuous dependence of the numerical solution on the input data.

Originally, no operator splitting was used in the FLEXPART model, therefore, the source code had to be modified for the inclusion of operator splitting. The splitting procedure was applied to the Langevin equation describing both horizontal wind components

$$du = -u\frac{dt}{\tau_{L_u}} + \left(\frac{2}{\tau_{L_u}}\right)^{1/2} \sigma_u dU, \tag{7}$$

$$dv = -v\frac{dt}{\tau_{L_v}} + \left(\frac{2}{\tau_{L_v}}\right)^{1/2} \sigma_v dV, \tag{8}$$

where u and v are the turbulent horizontal wind components, σ_u and σ_v are their standard distributions, τ_{L_u} and τ_{L_v} are the Lagrangian time scales of the auto-correlations of the horizontal wind components, and dU and dV are increments.

During operator splitting, each of the above two equations were split into a pair of equations. For the component u these have the form

$$du = -u\frac{dt}{\tau_{L_u}}, \tag{9}$$

$$du = \left(\frac{2}{\tau_{L_u}}\right)^{1/2} \sigma_u du, \tag{10}$$

and we have similar equations for v. On the base of this decomposition, we prepared the computer code of all the four splitting schemes, presented in Section 3. In this manner, we obtained five different model versions, including

the model with no splitting. The verification of these model versions with measurement data is presented in the next section. Further numerical investigations of the solutions obtained by different splitting methods can be found in *Kocsis* (2008).

4. Comparison of the model results with measurements

For the verification of the model versions measurement data collected during the European Tracer Experiment (ETEX) were used (*Nodop et al.*, 1998). In this section we present the ETEX project and the results of our comparisons.

4.1. The ETEX measurement program

The major aim of the ETEX project was a long-range experiment, in the framework of which a chosen air pollutant was emitted into the air under controled circumstances. In the autumn of 1994, two experiments were made (*Dop et al.*, 1998), during which perfluorocarbon (PMCH) particles were emitted into the air and monitored. This compound is appropriate for long-range atmospheric experiments, since it is non-toxic, not soluble in water, chemically inert, and does not harm the environment. Its background concentration is low and homogeneously distributed. The emission took place in France, near Monterfil and Treffandel (N 48° 3'33", W 2° 0'30"), 90 meters above sea level, from a 8-meter high chimney on October 23, 1994. Here the dominant wind direction is western/southwestern, and so the particles can be followed over a distance of as long as 2000 km. (A similar experiment was made on November 14, 1994, see *Nodop et al.*, 1998.)

On October 23, 1994, at 16:00 UTC, 340 kg of PMCH was emitted into the air during 12 hours, and then the concentration of this compound was measured throughout Europe, at 168 land measurement stations (including those in Hungary) and three aircrafts.

On the next day, the air mass over the area was still unstable, however, the winds weakened, since the cyclone moved forward to the north. On October 25, the wind direction changed to southerly at some places, and then again blew to southwest. On October 26, due to an anticyclone over the Black Sea, the southerly winds prevented the particles from spreading to the east (*Gryning et al.*, 1998).

Fig. 1 shows the spreading of the pollutant plume as time went by. 24 hours after the emission the plume reached Belgium, the Netherlands, and Germany. The plume decoupled, which is perhaps only a consequence of the visualization and the fact that the measurement network is sparse in the area (*Fig. 1a*). 12 hours later the plume had left France, and spread over the Benelux, Germany, and the Czech Republic (*Fig. 1b*). Some time later the position of the plume

shows rotation in the northern-southern direction (*Fig. 1c*). 60 hours after the emission the plume began to separate into two parts: one with a center over Slovakia and one over the Northern Sea (*Fig. 1d*) (*ETEX*, 1998).

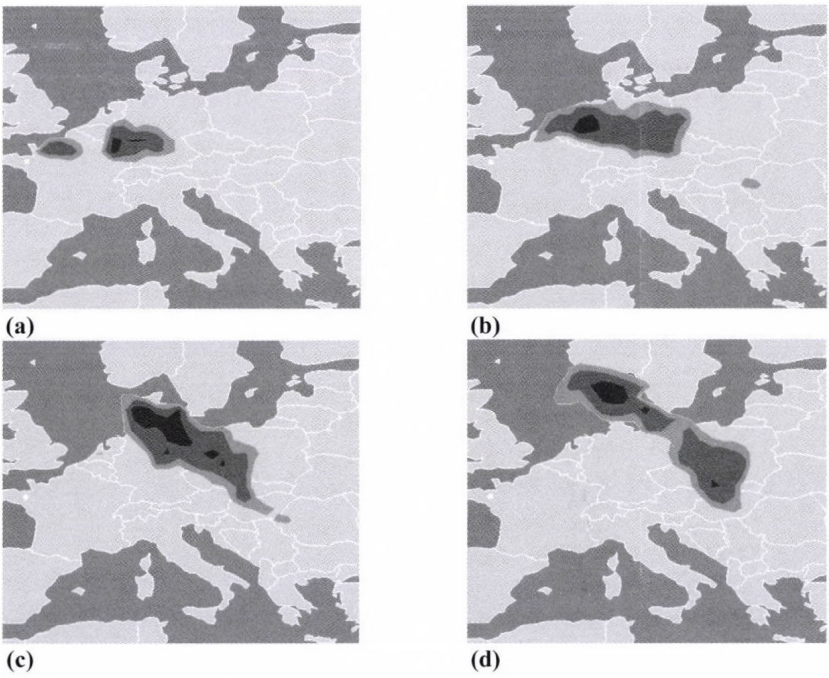

Fig. 1. The extension of the plume 24 (a), 36 (b), 48 (c), 60 (d) hours after the emission. Light grey: 0.01 ng/m^3, dark grey: 0.05 ng/m^3, black: 0.1 ng/m^3 (*ETEX*, 1998).

4.2. The results of the comparisons

Model versions obtained without splitting and with four different splitting schemes were run with the emission parameters specified by the ETEX experiment, and the 168 land stations were used as receptor points. Simulations were made by using the ECMWF analysis fields. The time integration steps were 900 seconds for the unsplit model, and 1800 seconds for the model versions with splitting. Our investigations were carried out for the beginning 54-hour period of the pollution transport. Comparisons were made by means of maps and several statistical indicators.

The maps shown in *Figs. 2* and *3* indicate the differences between the measurements and the five model versions. The left columns show the areas of overestimation, while the right columns indicate the areas of underestimation of the measurement data by the model versions. On the white areas the model results were exact.

24 hours after the emission, each model version overestimates the amount of pollutant over the central part of Germany (*Fig. 2*), on the area where the highest concentrations were measured (see *Fig. 1*). The only exception is the Marchuk-Strang splitting, which predicted higher concentrations for Luxemburg (*Fig. 2e*).

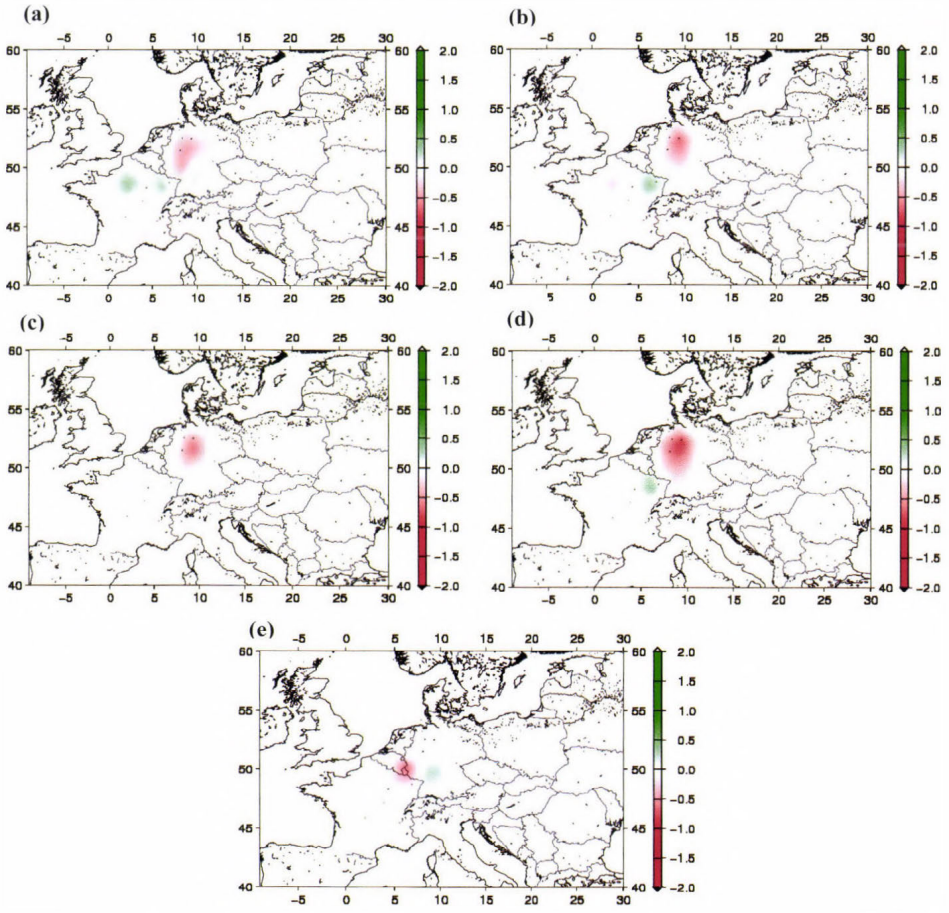

Fig. 2. Areas of underestimation (green) and overestimation (red) for the five different model versions 24 hours after the emission. (a) original, (b) sequential, (c) additive, (d) modified additive, (e) Marchuk-Strang. The tone of the colors shows the difference between the measured and modeled concentrations in ng/m^3.

54 hours after, the emission, all the model versions underestimate the concentration values in the same zone where the pollutant plume is located (*Fig. 3*). This underestimation is the smallest for the modified additive splitting (*Fig. 3d*). At some places we can find overestimation as well, namely, for the original unsplit model and for the modified additive splitting over the Baltic Sea (*Fig.*

3a, *3d*), while for the other splitting methods over the Benelux (*Fig. 3b*, *3c*, *3e*). The differences between the model results and the measurements are the largest for the Marchuk-Strang splitting, which overestimates the concentrations over huge areas of Western Europe.

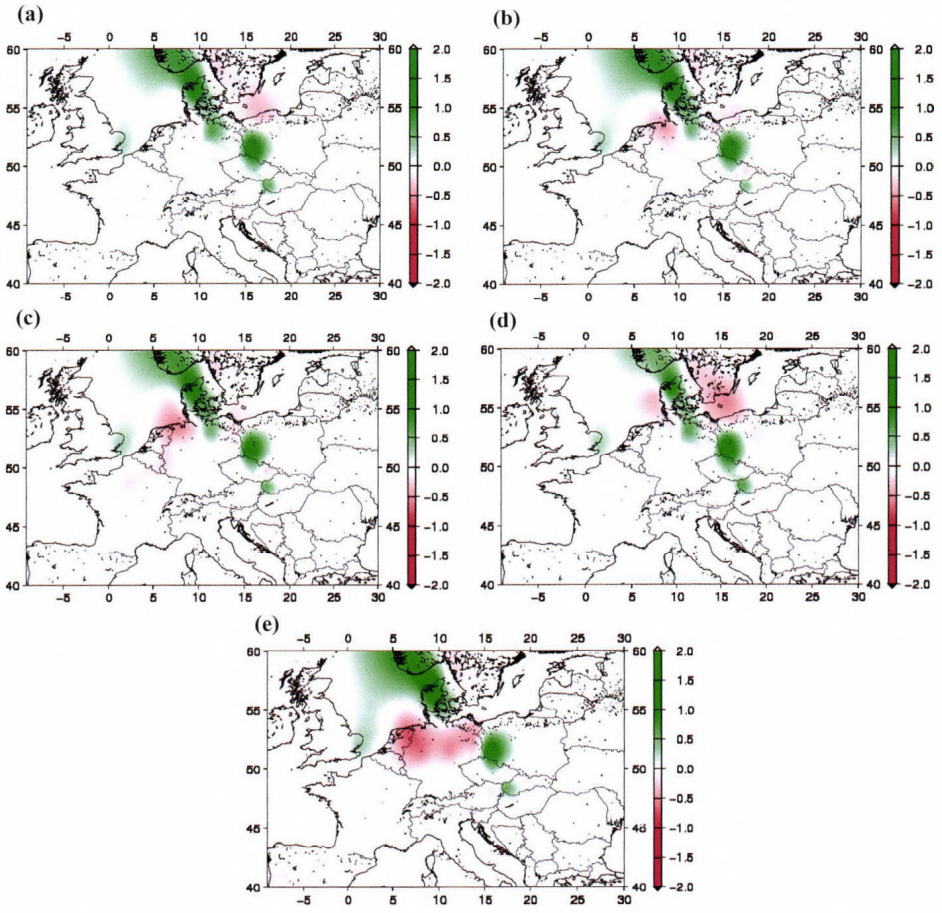

Fig. 3. The areas of underestimation (green) and overestimation (red) for the five different model versions 54 hours after the emission. (a) original, (b) sequential, (c) additive, (d) modified additive, (e) Marchuk-Strang. The tone of the colors shows the difference between the measured and modeled concentrations in ng/m^3.

In addition to the presented maps, we used several statistical indicators for the comparison of the different model versions. These indicators can be classified into two groups. The first group of indicators is used for characterizing the measure of the overestimation and underestimation, and includes, e.g., the bias

$$B_j = \frac{1}{N_j} \sum_{i=1}^{N_j} (P_{ji} - M_{ji}) \tag{11}$$

and the geometric mean error

$$MG_j = \exp\left(\frac{1}{N_j} \sum_{i=1}^{N_j} \ln P_{ji} - \frac{1}{N_j} \sum_{i=1}^{N_j} \ln M_{ji} \right). \tag{12}$$

In these formulas P_{ii}, M_{ji}, and N_j denote, respectively, the ith predicted value, the ith measurement value, and the number of measurements at time t_j. Indicators from the second group, such as the normalized mean square error

$$NMSE_j = \frac{1}{N_j} \sum_{i=1}^{N_j} \frac{(P_{ji} - M_{ji})^2}{\overline{P_j} \cdot \overline{M_j}} \quad \text{with} \quad \overline{P}_j = \frac{1}{N_j} \sum_{i=1}^{N_j} P_{ji}, \quad \overline{M_j} = \frac{1}{N_j} \sum_{i=1}^{N_j} M_{ji}, \tag{13}$$

and the geometric mean variance

$$VG_j = \exp\left[\frac{1}{N_j} \sum_{1=i}^{N_j} (\ln P_{ji} - \ln M_{ji}) \right], \tag{14}$$

measure the deviation of the model results from the measurements. If the above indicators are to be used for a time period with measurements at $t_1, t_2, \ldots, t_K$, then we will use the global quantities

$$MG = \frac{1}{K} \sum_{j=1}^{K} MG_j, \qquad NMSE = \frac{1}{K} \sum_{j=1}^{K} NMSE_j, \qquad VG = \frac{1}{K} \sum_{j=1}^{K} VG_j. \tag{15}$$

The values of B and MG in *Table 1* show that all model versions overestimate the pollution, since $B > 0$ and $MG > 1$. The largest value of B was obtained for the Marchuk-Strang splitting, while the largest values of MG for the additive and sequential splittings. In terms of B the winner is the modified additive splitting, while in terms of MG it is the original unsplit version. From the values of B one can see that we have underestimation only for the original model.

The indicators do not inform us about the exact measure of over- and underestimation, since those can compensate each other due to the summation.

That is why the values of *NMSE* and *VG* should also be examined. According to the *NMSE* values, the modified additive and sequential splittings produced the best results, and the Marchuk-Strang splitting gave the biggest error. Note that overestimating models are characterized by a smaller *NMSE*, while underestimating ones by a larger *NMSE* (*Stohl et al.*, 1998). As opposed to the *NMSE*, the *VG* index is biggest for the sequential and additive splittings, and smallest for the unsplit model.

Table 1. Statistical indicators for the different model versions for the whole studied period

	Splitting method				
	No splitting	**Sequential**	**Marchuk-Strang**	**Additive**	**Modified additive**
B	-0.262	0.177	0.664	0.300	0.149
MG	4.93	10.40	6.02	10.02	7.71
NMSE	2.743	2.440	3.311	2.660	2.336
VG	0.816	1.135	1.086	1.122	0.990

Certainly, the above indices show temporal changes. To examine these changes, we fixed the time, averaged in space, and so obtained a value for each index at each time step. *Fig. 4* reveals that at the beginning of the studied period, each model version performs similarly, they all underestimate the concentrations, and then the splitting solutions start to overestimate the concentrations in a certain time period. The largest errors are obtained for the Marchuk-Strang splitting, which is probably due to the weaker stability properties of this method.

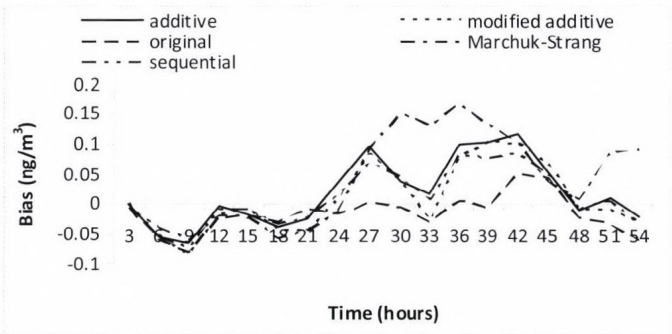

Fig. 4. Temporal changes of index *B* for the different model versions.

Fig. 5 shows the temporal changes of index *MG*. After a period of very small errors, the overestimation becomes dominant, however, the differences between the model versions are not so significant as for index *B*. At the end of the period, the values start to decrease, and the original model version and the modified additive splitting begin to underestimate the concentrations.

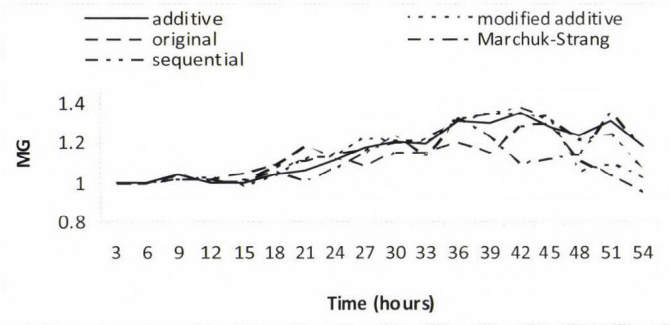

Fig. 5. Temporal changes of index *MG* for the different model versions.

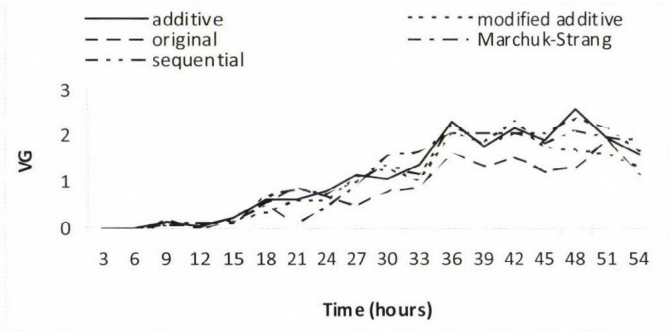

Fig. 6. Temporal changes of index *VG* for the different model versions.

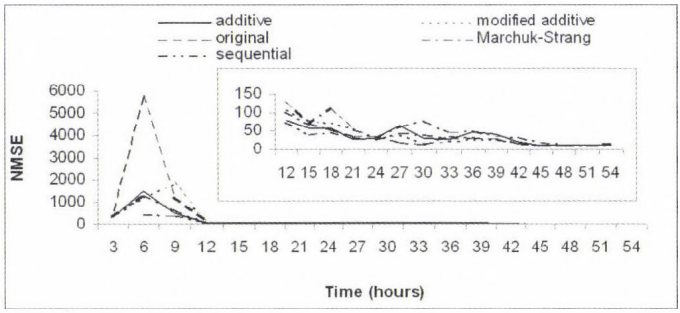

Fig. 7. Temporal changes of the index *NMSE* for the different model versions.

Fig. 6 shows the changes of index *VG* in time. The differences between the model versions are not significant. The best results are obtained for the original model version. In the case of the *NMSE*, see *Fig. 7*, the starting period is characterized by a big jump, which can be observed in each model version, and is especially significant in the unsplit case. The reason for this is that the

concentration values differ from zero only in small areas, which results in division by a small value. There may also be errors in the vertical extension of the modeled plume (*Stohl* and *Wotawa*, 1997). The *NMSE* decreases at the end of the period for all model versions.

5. Conclusions

Four different operator splitting methods were introduced for the calculation of the trajectories in the Lagrangian FLEXPART model, namely, the additive, modified additive, sequential, and Marchuk-Strang splittings. The different model versions obtained in this way were verified with measurement data collected during the ETEX project. The main results of the examination can be summarized as follows:

- The different model versions tend to overestimate the measurements. According to the studied statistical indicators, the best results were obtained for the unsplit model and for the modified additive splitting, while the worst results for the Marchuk-Strang splitting. Therefore, the Marchuk-Strang splitting, which usually provides better accuracy than the other studied splitting methods, is not recommended to use in this model.
- The running time was reduced in all model versions where operator splitting was applied, except for the Marchuk-Strang splitting. The largest reduction was obtained for the modified additive splitting (by about 10%).

Acknowledgements—This work was supported by Hungarian National Research Founds (OTKA) No. F61016. *Ágnes Havasi* is a grantee of the Bolyai János Scholarship.

References

Carvalho, J.C., Vilhena, M.T., and *Thompson, M.,* 2007: An iterative Langevin solution for turbulent dispersion in the atmosphere. *J. Comput. Appl. Math. 206*, 534-548.

ECMWF, 1995: *User Guide to ECMWF Products 2.1*, Meteorological Bulletin M3.2, Reading, UK.

ETEX, 1998: *The European Tracer Experiment* (eds.: *F. Girardi, G. Graziani, D. van Velzen, S. Galmarini, S. Mosca, R. Bianconi, S. Bellasio, W. Klug,* and *G. Fraser*). European Communities, Italy, p. 107.

Faragó, I., 2006: Application of the operator splitting method for real-life problems. *Időjárás 110*, 379-395.

Faragó, I., Thomsen, P.G., and *Zlatev, Z.,* 2008: On the additive splitting procedures and their computer realization. *Appl. Math. Model. 32*, 1552-1569.

Gryning, S., Batchvarova, E., Schneiter, D., Bessemoulin, P., and *Berger, H.,* 1998: Meteorological conditions at the realize site during the two tracer experiments. *Atmos. Environ. 32*, 4123-4137.

Havasi, Á., 2007: Wave analysis of different splitting methods in the linearized shallow water equations. *IJCSE* 3, No. 4, 264-270.

Havasi, Á., Bartholy, J., and *Faragó, I.*, 2001: Splitting method and its application in air pollution modeling. *Időjárás 105*, 39-58.

Kocsis, Zs., 2008*: Numerical Investigation of the Transport of Air Pollutants* (diploma work; in Hungarian). Eötvös Loránd University, Budapest, Hungary.

Lanser, D., Blom, J., and *Verwer, J.*, 2001: Time integration of the shallow water equations in spherical geometry. *J. Comput. Phys. 171*, 1, 373-393.

Marchuk, G. I., 1968: Some application of splitting-up methods to the solution of mathematical physics problem. *Aplik. Mat. 13*, 103-132.

Nodop, K., Connolly, R., and *Girardi, F.*, 1998: The field campaigns of the European Tracer Experiment (ETEX): overview and results. *Atmos. Environ. 32*, 4095-4108.

Stohl, A., and *Wotawa, G.*, 1997: Validation of the Lagrangian particle dispersion model FLEXPART using ETEX data. In *ETEX Symposium on Long-range Atmospheric Transport, Model Verification and Emergency Response* (ed.: *K. Nodop*).Vienna, Austria, 13-16 May 1997, 167-170.

Stohl, A., Hittenberger, M., and *Wotawa, G.*, 1998: Validation of the Lagrangian particle dispersion model FLEXPART against large-scale tracer experiment data. *Atmos. Environ. 32*, 4245-4264.

Strang, G., 1968: On the construction and comparison of difference schemes. *SIAM J. Numer. Anal. 5*, 506–517.

van Dop, H., Addis, R., Fraser, G., Girardi, F., Graziani, G., Inoue, Y., Kelly, N., Klug, W., Kulmala, A., Nodop, K., and *Pretel, J.*, 1998: ETEX: European Tracer Experiment; observations, dispersion modeling and emergency response. *Atmos. Environ. 32*, 4089-4094.

Zlatev, Z., 1995: *Computer Treatment of Large Air Pollution Models*. Kluwer Academic Publishers, Dordrecht-Boston-London.

IDŐJÁRÁS

Quarterly Journal of the Hungarian Meteorological Service
Vol. 113, No. 3, July–September 2009, pp. 203–219

Estimation of the biospheric carbon dioxide balance of Hungary using the BIOME-BGC model

Zoltán Barcza[1*], László Haszpra[2], Zoltán Somogyi[3], Dóra Hidy[4], Katalin Lovas[5], Galina Churkina[6], and László Horváth[2]

[1]*Department of Meteorology, Eötvös Loránd University,*
P.O. Box 32, H-1518 Budapest, Hungary; E-mail: bzoli@elte.hu
[2]*Hungarian Meteorological Service,*
P.O. Box 39, H-1675 Budapest, Hungary; E-mails: haszpra.l@met.hu, horvath.l@met.hu
[3]*Forest Research Institute,*
Frankel L. u. 42-44, H-1027 Budapest, Hungary; E-mail: somogyiz@erti.hu
[4]*Institute of Botany and Ecophysiology, Szent István University,*
Páter K. u. 1, H-2103 Gödöllő, Hungary; E-mail: dori.hidy@gmail.com
[5]*Hungarian Meteorological Service,*
P.O. Box 38, H-1525 Budapest, Hungary; E-mail: lovas.k@met.hu
[6]*Max Planck Institute for Biogeochemistry,*
Hans-Knöll-Str. 10, D-07745 Jena, Germany; E-mail: churkina@bgc-jena.mpg.de

(Manuscript received in final form February 19, 2009)

Abstract—Here we estimate the biospheric carbon dioxide balance of Hungary using the adapted BIOME-BGC process oriented ecological system model. The model was calibrated using the Hungarian measurements of biosphere-atmosphere carbon dioxide exchange. After calibration, the model was run for the four major land cover types such as croplands, grasslands, deciduous and coniferous forests for the period of 2002–2007. Our calculations suggest that all Hungarian ecological systems together formed a net carbon dioxide source during the time period studied. Since agricultural fields cover more than 50% of the total area of Hungary, the net carbon dioxide flux is dominated by the carbon balance of croplands. The average net release of CO_2 is 8.7 Mt per year with significant interannual variation: the highest net emission was 21.6 Mt CO_2 in 2003, while the lowest was 1.2 Mt CO_2 in 2006. Due to the model limitations, simulated CO_2 release from croplands is most likely overestimated, thus, the present results provide an upper limit for the potential range of the carbon balance of Hungary. The model results highlight the strong dependence of the biospheric carbon dioxide balance on the weather conditions. The results are compared with the carbon budget estimations previously published for Hungary as well as with those reported to the United Nations Framework Convention on Climate Change.

Key-words: biospheric carbon balance, net ecosystem exchange, ecosystem model, upscaling, eddy covariance measurements, plant functional types, BIOME-BGC model, model calibration

* Corresponding author

1. Introduction

Atmospheric carbon compounds, especially carbon dioxide and methane, play a crucial role in the formation of Earth's climate through the greenhouse effect (*Jansen et al.*, 2007). Their atmospheric amount partly depends on the activity of the biosphere, which is partly climate controlled, but also considerably affected by human activities. Because of this strong coupling between the biogeochemical cycle of carbon and the climate, the understanding of the global carbon cycle, including its interactions and feedbacks is a prerequisite to any reliable climate prediction (*Cox et al.*, 2000; *Friedlingstein et al.*, 2006; *Denman et al.*, 2007).

During most of the Holocene, the biosphere was in approximate steady state with the atmosphere: on average, the biosphere absorbed approximately as much carbon dioxide from the atmosphere through photosynthesis as it released by respiration and by the decomposition of the dead organic material produced. However, in the 1980s, the measurements revealed that the biosphere was tending to be a net carbon dioxide sink. This net uptake partly balances the anthropogenic CO_2 emission (*Cao et al.*, 2002). Currently, less than half of the anthropogenic emission (fossil fuel burning, cement industry, deforestation, etc.) remains in the atmosphere increasing the greenhouse effect. Some 50–60% of the anthropogenic emission is taken up by the oceans and the terrestrial biosphere (*Denman et al.*, 2007). However, it is poorly known where and why the biospheric carbon dioxide uptake has increased. In a similar manner, we do not know how the biosphere will behave in the future.

The climate related behavior of the biosphere has been extensively studied all over the world. At present the European efforts are coordinated by the CarboEurope Integrated Project (IP) (http://www.carboeurope.org) financed by the 6th R+D Framework Programme of the European Commission. The primary aim of the project is to determine and constrain the European carbon dioxide budget with an accuracy of as high as possible on the basis of direct field measurements and application of ecosystem models. In addition to the present authors, other Hungarian scientists also participate in the project.

Most models used in CarboEurope-IP are of coarse spatial resolution, and more importantly they only use general parameterization for specific plant functional types uniform in the entire European region (*Janssens et al.*, 2003, 2005; *Vetter et al.*, 2007; *Gervois et al.*, 2008). To achieve a higher accuracy in the carbon dioxide budget estimation, the special features of smaller geographical regions should also be taken into account.

Information on the emissions and removals by certain elements of the biosphere is also collected annually for an increasing number of countries by the United Nations Framework Convention on Climate Change (UNFCCC) in the so-called national greenhouse gas inventory reports. In these reports, internationally approved methodology by the IPCC (*IPCC*, 1997, 2003, 2006) or peer-reviewed national methodologies must be applied. However, reports under

the UNFCCC and, especially, its Kyoto Protocol may include only partial estimates for the terrestrial biospheric emissions and removals, while it is the *total* carbon dioxide budget that affects the CO_2 concentration of the air.

Hungary has also submitted her annual reports for almost two decades. However, although these reports take account of the vast majority of emissions and removals, not the whole budget is covered. The verification of these estimates is also necessary. In this verification, alternative methodologies and data sets should be used.

The present work is an attempt for the estimation of the *total* biospheric carbon dioxide balance of Hungary. For this purpose, the BIOME-BGC process oriented ecological system model (version 4.1.1) was adapted to the Hungarian conditions. The model results are compared with those CarboEurope results that can be related to Hungary, with the national land use dependent inventory data reported to UNFCCC, and with the Hungarian anthropogenic emission.

2. The BIOME-BGC model and its adaptation

BIOME-BGC was developed for the description of biosphere-atmosphere exchange of carbon dioxide, water, and nitrogen (*Running* and *Coughlan*, 1988; *Running* and *Gower*, 1991; *Running* and *Hunt*, 1993; *White et al.*, 2000; *Churkina et al.*, 2003; *Hidy et al.*, 2007). BIOME-BGC can simulate the biogeochemical cycles in evergreen and deciduous forests, shrubs, and grasses. The different ecological systems need different parameter values, thus, the model should be adapted to the systems studied (*White et al.*, 2000). The model also needs meteorological data, geographical and soil parameter values as input data, because these parameters convey the environmental constraints and conditions to the ecological systems. In order to use BIOME-BGC for the simulation of the carbon balance of large areas, the internal model parameters (ecophysiological parameters) are held constant, while the spatially varying soil and geographical parameters, and the temporally varying meteorological data are supplied to the model to reflect regional differences in the functionality of the different ecological systems. This assumption is only feasible if the spatial variability of the ecophysiological parameters is expected to be low. In case of Hungary, due to the relatively uniform climate, this assumption seems reasonable.

For the determination of the biospheric carbon dioxide balance, the area of Hungary was covered by a grid of $1/6 \times 1/6$ degree spatial resolution. The fraction of the different plant functional types and the characteristic soil type and weather condition were determined for each grid cell.

The determination of the land cover type is based on the CORINE CLC50 database (http://www.fomi.hu/corine/clc50_index.html). CLC50 was compiled based on satellite images taken between 1998 and 1999. It means that the spatial distribution of the different land use types is subject to uncertainty due to

continuous land use change activities (reforestation, afforestation, land abandonment, etc.). Our modeling approach does not take into account the changes in land use during 2000–2007. CLC50 distinguishes among 78 land cover types. BIOME-BGC, similarly to the other models of the same kind, cannot distinguish among so many different land cover types because of the necessary simplifications and generalizations in the models (mostly caused by our insufficient knowledge and computing capacity). Therefore, the 78 different land cover types were aggregated into four basic, essentially different, categories: grasslands, agricultural fields, deciduous and coniferous forests (*Fig. 1*). The four general categories cover 81.83% of the country's area (agricultural fields: 52.95%, grasslands: 10.42%, deciduous forests: 16.72%, coniferous forests: 1.74%). The rest of the country's territory is covered by artificial land cover types (roads, built-up areas) and open water surfaces (lakes, rivers). Those areas are not handled by the model, therefore, in the present study they are considered as carbon neutral surfaces in biological sense. It does not mean that those areas are not important in the carbon cycle (e.g., anthropogenic emission can take place in the built-up areas, waters can take up or release carbon, etc.).

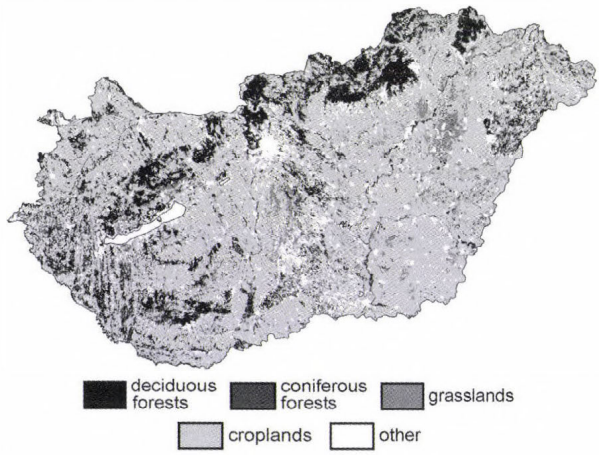

Fig. 1. Aggregated basic land cover types of Hungary used for the BIOME-BGC simulations. The map is based on the CORINE CLC50 land cover classification. Note that coniferous forests are hardly visible due to their small fraction and scattered geographical distribution.

BIOME-BGC and other process oriented biogeochemical models simulate the carbon dioxide exchange between the biosphere and atmosphere. The horizontal carbon transport (export or import of products, harvest, manure, or other carbon related materials from/to the territory studied) modifies the calculated geographical distribution of the balance. This type of geographical redistribution can be taken into account by means of additional calculations if

needed (e.g., *Ciais et al.*, 2007). The results presented here are the carbon dioxide balance formed exclusively by the local biogeochemical processes (photosynthesis, respiration, chemical decomposition) and do not involve any horizontal transport. For the geographical distribution of the full carbon budget, the anthropogenic influence should be taken into account as part of the anthropogenic activity (burning of local/imported biomass, consumption of local/imported agricultural products, export/import of decomposable biospheric product/organic material, etc.). It should be noted that the model can only simulate the effects of the anthropogenic interventions (e.g., deforestation, afforestation, reforestation, irrigation, harvesting, herbage, other types of land management) on the carbon dioxide exchange in a rather limited way. Therefore, the model results are rather uncertain on recently disturbed, converted, or non-typically used lands.

Usually, the consistent biogeochemical data set required by a model is not available because of the lack of certain measurements, sampling and analytical errors, limited representativeness of the measurements, etc. Inconsistency in the input data causes transients in the beginning of the model runs not reflecting any real process, or phenomenon. The spin-up phase of the model run is used for the elimination of these transients. The only purpose of this phase is to transform the original, inconsistent input data into a consistent, steady state data set to be used for the actual simulation.

In the spin-up phase, the processes of a long (usually several decades long) period is simulated during which the soil-vegetation system reaches a steady state. This is one of the reasons why the model is unable to produce realistic carbon dioxide exchange data on recently and significantly disturbed lands.

For the spin-up the 1901–2000 period was used for which the basic meteorological data were available from the CRU TS 1.2 database (Climatic Research Unit [CRU], University of East Anglia) (*New et al.*, 2002). This database contains monthly average temperature, diurnal temperature range, and precipitation amount data on the same grid we use. For the preparation of the daily meteorological data (daily maximum and minimum temperature, daily precipitation) required by the model, a statistical weather generator (C2W) was used (*Bürger*, 1997). The missing daily meteorological parameters (average daytime temperature, average daytime vapor pressure deficit, average daytime global radiation) were generated by the MTCLIM model (*Thornton et al.,* 2000).

In the normal phase of the carbon dioxide exchange modeling (2002–2007), the grid-interpolated measurements of the Hungarian meteorological network were used. The interpolated data fields were produced by the Hungarian Meteorological Service applying the MISH method (http://www. cosis.net/ abstracts/ EGU05/07310/EGU05-J-07310.pdf).

Using the default, generalized parameter set of BIOME-BGC, the model approximates the carbon dioxide exchange of the different ecological systems with moderate accuracy. However, significantly better results can be achieved if

the model is adapted to the real Hungarian conditions, that is the model is "calibrated". In the case of croplands and grasslands, the calibration was performed using Hungarian measurements (*Barcza et al.*, 2003; *Haszpra et al.*, 2005; *Nagy et al.*, 2007), while for deciduous and coniferous forests – in the lack of Hungarian measurements – the parameters were taken from the literature (*Pietsch et al.*, 2005).

In case of grasslands, measurements from three Hungarian monitoring sites (Bugac, Hegyhátsál, Szurdokpüspöki) were used. At all sites the biosphere-atmosphere exchange of carbon dioxide is directly measured using eddy covariance technique (*Barcza et al.*, 2003; *Haszpra et al.*, 2005; *Nagy et al.*, 2007). The calibration procedure of BIOME-BGC is published in the paper of *Hidy et al.* (2007).

The carbon exchange of crops is inherently affected by management practices (sowing, harvest, fertilization, etc.) that strongly influence the carbon, water, and nitrogen cycling through the ecosystem. Harvest causes a sudden drop in the standing biomass and alters the different carbon pools (aboveground biomass, litter), which in turn affects the carbon balance and the physiological response of the ecosystem to the environmental conditions. The current version of BIOME-BGC is unable to simulate disturbance and cropland management. However, considering larger regions where both winter and summer crops are present, the annual cycle of net ecosystem exchange (NEE) becomes more or less balanced in time (i.e., there is no sudden decrease in the NEE caused by harvest), as it is obvious from the large scale eddy covariance data measured over a mixed agricultural area in Hungary (*Haszpra et al.*, 2005; *Figs. 5* and *8*). The main cause of the balanced behavior is the conjoint presence of winter crops (e.g., winter wheat, harvested around June-July) and summer ones (e.g. corn, harvested around October–November). The measurement data suggest that the overall carbon balance can be approximated with the carbon dynamics of a perennial herbaceous ecosystem. In this sense, croplands can be handled as semi-natural grasslands without any sharp decrease in the standing biomass (thus, no modification in the model logic is needed for the simulation). This is the reason why BIOME-BGC can be used to simulate agricultural NEE with reasonable accuracy and handles crops as a kind of "super grass" (i.e., fertilized grass, see *Vetter et al.*, 2007) using the existing internal grass parameterization. This logic makes it imperative to use accurate measurement data for the calibration of the model to simulate super grass NEE in order to provide estimates that are comparable with the measured real cropland NEE. In Hungary the dominant land cover type is agriculture, thus, the success or failure of the present modeling activity strongly depends on the quality and proper use of the training data set.

The drawback of this grassland approach is the likely overestimation of NEE (higher CO_2 release) for the dormant season. The cause of this likely bias comes directly from cropland management: as part of the biomass is removed

via harvest, it cannot decompose in the field and respire back to the atmosphere. In the model the biomass removal is not handled, thus, respiration is overestimated. As a consequence, the cropland NEE data presented here might be considered as an upper limit for cropland carbon balance.

The only monitoring project producing CO_2 net ecosystem exchange data for mixed agricultural fields in Hungary is carried out at Hegyhátsál (*Haszpra et al.*, 2001, 2005). The eddy covariance system installed at 82 m elevation above the ground has been providing regional scale NEE data since 1997. As the mosaic type mixed agricultural activity (including a mixture of winter and summer crops) can be considered typical in a large part of Hungary, the data measured here can be used for the calibration of BIOME-BGC (using the grass submodel) for the general Hungarian conditions. Calibration of the BIOME-BGC model was performed with the measured daily eddy covariance data using Monte Carlo Maximum Likelihood (MCML) approach (*Hollinger* and *Richardson*, 2005). The calibration was accomplished using nine years of measurement data (1997–1999, 2001–2006; *Haszpra et al.*, 2005). Modeled gross photosynthesis (gross primary production, GPP) explained about 80% of the measured GPP variance ($R^2 = 0.8$), while modeled total ecosystem respiration (Reco) explained about 72% of the total variance ($R^2 = 0.72$).

There are no Hungarian measurements available for deciduous and coniferous forests, therefore, the model calibration cannot be performed as it was implemented for grasslands and croplands. We used the data of *Pietsch et al.* (2005) recommended for BIOME-BGC. Their parameter sets were determined on the basis of measurements in oak (*Quercus robur/petraea*) and Scotch pine (*Pinus sylvestris*) forests. The measurements were carried out in low elevation regions of Austria and Czech Republic close to Hungary, where the climatic conditions are similar to those in Hungary.

Although oak is the dominant species among the Hungarian deciduous trees, significant areas are covered by Black locust (*Robinia pseudoacacia*) and other species. Thus, the generalized application of the oak parameter set may be considered as an oversimplification to characterize all Hungarian deciduous forests, but the parameterization cannot be refined without measurements on other species yet.

A better parameterization could be achieved using Hungarian forest inventory data (see, e.g., *Somogyi*, 2007), however, the calibration methodology for BIOME-BGC is not developed yet.

In summary, the main simplifications of our modeling approach are as follows: (a) BIOME-BGC is applied mainly to disturbed ecosystems, though the model logic is not prepared yet for the precise description of managed ecosystems; (b) the ecophysiological parameters for the different plant functional types are held constant during the simulation; (c) agricultural ecosystems are handled as "super grass", which means that harvest is not simulated but the annual course of NEE is well represented; (d) only a very limited number of tree species are

simulated (oak and pine) in the lack of information about the spatial distribution of tree species and also in the lack of ecophysiological parameters for some of the other relevant tree species; (e) BIOME-BGC cannot simulate the effect of pests and diseases, and the long-term consequences of extreme weather events are not accounted for either; (f) the CLC50 database might be outdated due to land use change activities that are occurring in Hungary, which causes uncertainty in the simulation. Future research is essentially needed to address the above mentioned limitations of our modeling methodology.

3. Results

Using the input data and parameter sets presented above, the total Hungarian net biosphere-atmosphere CO_2 exchange has been calculated using daily time steps for 2002–2007 by means of BIOME-BGC. In the atmosphere-oriented studies like the present one, the net biospheric carbon uptake is denoted by negative sign, because the amount is a loss from the point of view of the atmosphere. Data are given in carbon amount throughout the paper (1 g C = 3.67 g CO_2, or 1 g CO_2 = 0.27 g C).

Fig. 2 shows the 6-year mean annual cycle of NEE for the different plant functional types averaged for all grid points. It can be seen in the figure, that the model captured the seasonal variation of the carbon exchange of the biosphere in all cases. On average, each plant functional type acts as a net carbon sink during the growing season (except for coniferous forests during July and August). Cropland NEE is balanced in time according to the modeling philosophy (super grass), that is in accordance with the measurement data (*Haszpra et al.*, 2005). Grassland carbon uptake decreases in time during the growing season because of its higher sensitivity to drought. These results are in accordance with the field evidence (*Barcza et al.*, 2003; *Nagy et al.*, 2007). During the dormant season, the ecosystems are net sources of CO_2, although for croplands it might be somewhat overestimated by the model (see above). Ecosystem respiration is the highest for deciduous forests probably due to decomposition of the high amount of organic matter. Respiration of coniferous forests is relatively low during the dormant season.

The daily data were aggregated for each year, for each grid cell, and for the entire area of Hungary taking into account the spatial extent of the different plant functional types in each individual grid cell. The annual sums of NEE for the different land cover types are presented in *Table 1* and also in *Fig. 3*. The data suggest that croplands are usually sources of carbon dioxide, grasslands are net sources or net sinks, while forest areas are usually net sinks. The balance shows that biosphere is a net source in Hungary. It seems that, on country level, the forests and croplands are the largest sinks and sources, respectively, but the contribution of grasslands must not be neglected, either.

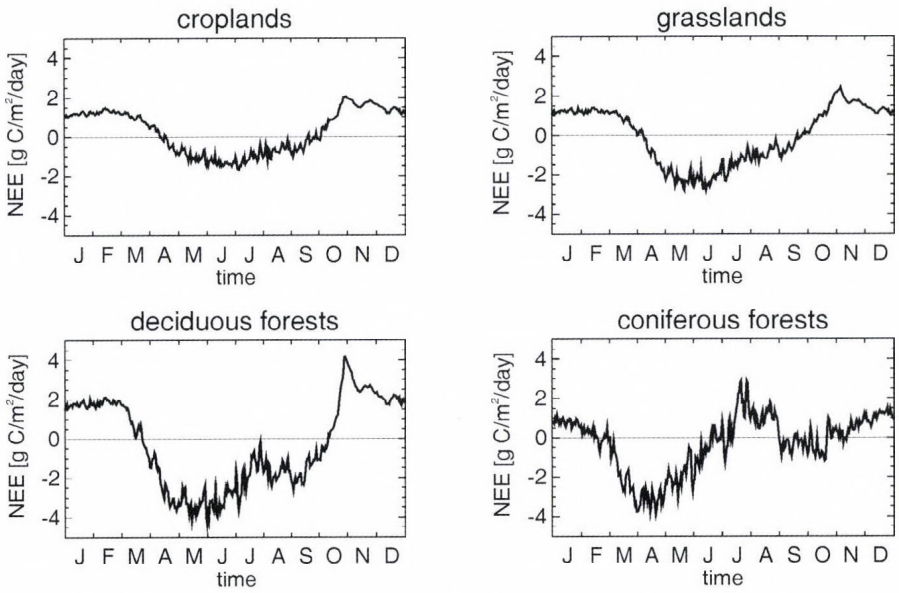

Fig. 2. Six-year mean annual cycle of modeled net ecosystem exchange of the different plant functional types averaged for all grid points. Negative NEE indicates carbon uptake by the vegetation.

Table 1. Biospheric carbon dioxide balance of Hungary estimated by the BIOME-BGC model for the time period of 2002–2007 (Mt C/year). Negative values indicate carbon uptake by the vegetation

	2002	**2003**	**2004**	**2005**	**2006**	**2007**
Croplands	5.12	4.06	4.92	5.55	4.85	3.86
Grasslands	-0.08	0.80	-0.60	-0.55	-0.94	0.32
Deciduous forests	-2.05	0.96	-3.09	-3.49	-3.40	-1.02
Evergreen coniferous forests	-0.18	0.08	-0.32	-0.25	-0.18	-0.12
Total	**2.81**	**5.90**	**0.91**	**1.26**	**0.33**	**3.04**

Our aim was not only to determine the average NEE but also to get information on the range of interannual variability (*Fig. 3*). The climate fluctuations significantly influence the activity of the biosphere and, thus, also its carbon balance. The climate variation in the study period (2002–2007) offered a unique possibility to study the effect of these fluctuations. 2003 was an extremely hot and dry year, which ended a long, increasingly warm and dry period followed by cooler and wetter years.

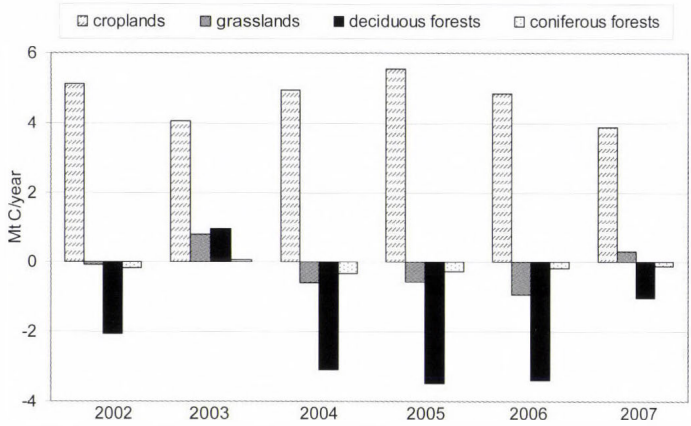

Fig. 3. Biospheric carbon dioxide exchange of the different land cover types for the entire country between 2002 and 2007 (Mt C/year) calculated using BIOME-BGC. Negative values indicate carbon uptake by the vegetation.

exchange data of the four basic land cover types for 2003 and 2004 (for two years with contrasting weather conditions, *Figs. 4* and *5*) show that agricultural fields were net carbon dioxide sources in both years, whereas grasslands were net sources in 2003, but net sinks in 2004 under the more favorable environmental conditions. These results are in accordance with the measurements presented in *Nagy et al.* (2007). In 2003, all ecological systems lost significant amount of organic material due to the extremely hot and dry weather.

The forests, storing a high amount of carbon, reacted more sensitively to the significant climate deviation than the agricultural fields and grasslands (*Figs. 4* and *5*). Except for the higher, cooler and wetter regions of the northern mountainous part of Hungary, both deciduous and coniferous forests were net carbon dioxide sources in 2003. In a significant area of the country the emissions exceeded 300 g C/m^2/year. However, in 2004, which was significantly cooler, and wetter than 2003, they became sinks at a similar rate.

Fig. 6 shows the annual mean biospheric carbon dioxide balance of Hungary for the entire study period (2002–2007). The figure was created from the BIOME-specific simulated NEE data taking into account the spatial extent of the specific land cover types for each grid cell. The figure shows that CO_2 uptake is generally associated with the forested areas (cf., *Fig. 1*). During 2003, almost the entire country became a net carbon dioxide source, only the mountainous regions in Northern Hungary and some other areas in Western Hungary acted as net sinks. It is interesting to see that in 2007, the western part of Hungary became an almost homogeneous net source, similarly to 2003.

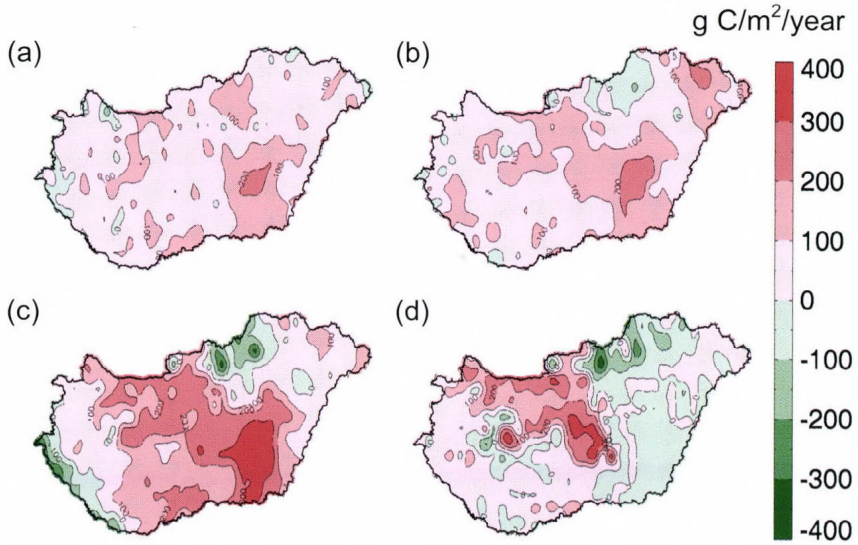

Fig. 4. Net carbon dioxide exchange of the different land cover types in 2003 (g C/m^2/year) estimated by the BIOME-BGC model. Negative values indicate carbon uptake by the vegetation. (a) croplands, (b) grasslands, (c) deciduous forests, (d) coniferous forests. Note that the numbers are only applicable where the specific plant functional types are present (see Fig. 1).

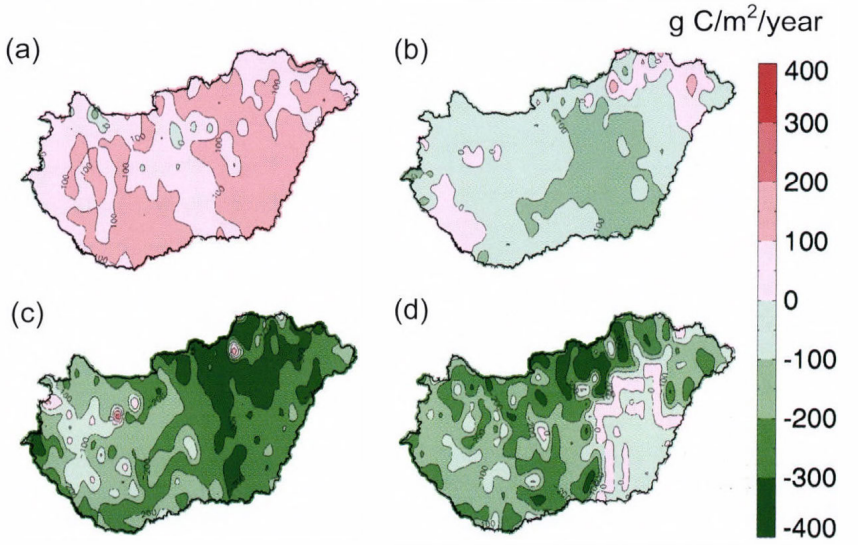

Fig. 5. Net carbon dioxide exchange of the different land cover types in 2004 (g C/m^2/year) estimated by the BIOME-BGC model. Negative values indicate carbon uptake by the vegetation. (a) croplands, (b) grasslands, (c) deciduous forests, (d) coniferous forests. Note that the numbers are only applicable where the specific plant functional types are present (see Fig. 1).

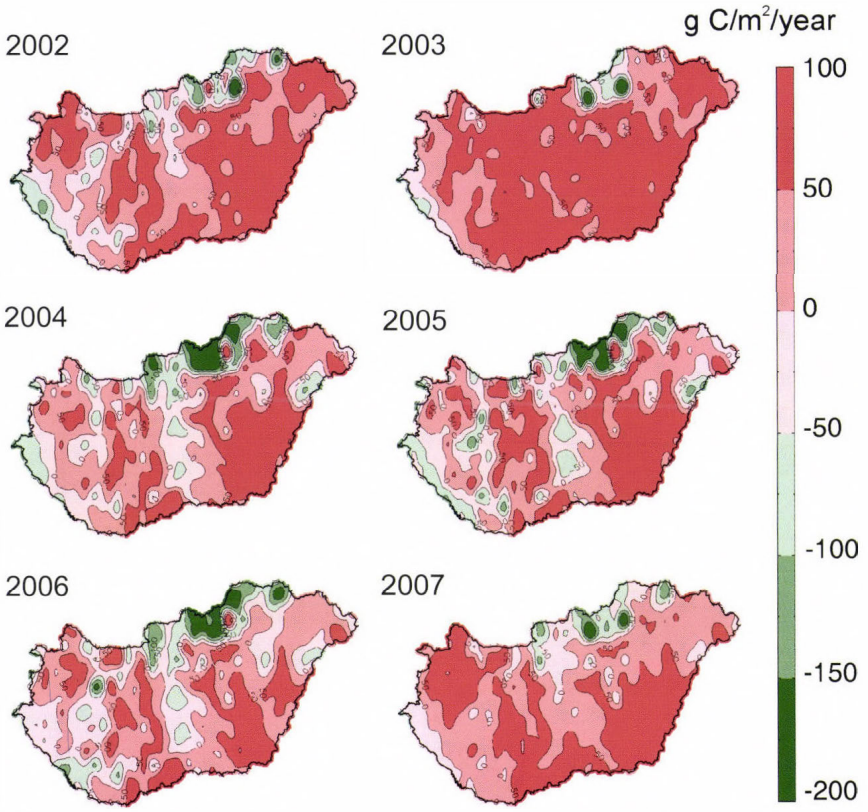

Fig. 6. Mean biospheric carbon dioxide balance of Hungary for the entire study period (2002–2007) estimated by the BIOME-BGC model (g C/m^2/year). The simulated, BIOME-specific NEE data were weighted for each grid cell. Negative values indicate carbon uptake by the vegetation.

4. Discussion

The model estimates in this study show that the net carbon dioxide balance of Hungary is positive, i.e., that the soil-vegetation system is a net carbon dioxide source on national level (*Table 1*). Its main cause is the significant net release from the agricultural fields. Any change in the ratio of the agricultural and forest areas would modify the biospheric carbon dioxide balance.

The model estimates were compared with the data reported by Hungary to the UNFCCC (*HMS*, 2008; see also *UNFCCC*, 2006). Under the UNFCCC, Hungary reported emissions of –0.76, –5.44, 0.24, –0.85, and –0.01 kt C/year for 2002, 2003, 2004, 2005, and 2006, respectively, for croplands and grasslands together, which are much lower emission estimates than those calculated by BIOME-BGC. On the other hand, Hungary reported net removals of 0.86, 1.31,

1.11, 1.58, and 1.27 Mt C/year for forests, which are considerably lower than those estimated by BIOME-BGC. At the same time, it is known that BIOME-BGC may tend to overestimate the annual net CO_2 release of croplands, but quantification of this likely overestimation needs further research. Some of the differences are due to known discrepancies in methodology. The IPCC deals with the estimation of greenhouse gas emissions and removals from human activities and takes into account yearly changes in land use instead of using one land use database. Accordingly, carbon stock changes on *managed land* in the relevant carbon pools are reported under the IPCC methodology that exludes reporting on unmanaged land, which is only required when unmanaged land is subject to land use conversion. As regards forests, Hungary reported under the UNFCCC the change only in biomass carbon pool, while soil and dead organic matter carbon pools have not been reported yet due to lack of appropriate databases. In cropland and grassland categories the changes in soil carbon pool are reported which are influenced by changes of the way land was used (abandonment of croplands and pastures, afforestation of croplands and grasslands, and tillage practices). In accordance with the IPCC methodology, the change in biomass in cropland category is estimated only for perennial woody crops. (The results of the sequestration of perennial woody biomass were not taken into account in the comparison.) For annual crops, the increase in biomass stocks in a single year is assumed to be equal to biomass losses from harvest and mortality in the same year. Thus, there is no net accumulation of biomass carbon stocks on cropland by the IPCC methodology under default assumptions. In grassland, where management practices are static, biomass carbon stocks are in an approximate steady-state, so the change in biomass carbon pool is neglected as well. Even though there are differences between the methodology of the IPCC and the model approach, this comparison clearly suggests that further studies are needed to identify the possible causes of the major differences. Due to the simplified methodology and limited data bases of both approaches, both the BIOME-BGC and the IPCC-based inventory approach should be analyzed and developed to harmonize estimates.

Fig. 7 shows the national biospheric carbon dioxide balance calculated by us and *Janssens et al.* (2005). Janssens and his coworkers (*Janssens et al.*, 2005) used a completely different approach: they estimated carbon budget based on changes in the carbon stocks, which means that they did not estimate biospheric NEE but the stock change. Of course NEE is related to the C stock change both in forests and croplands. In spite of the different methodology, their results are close to ours, though they only gave an overall value for the period studied. 2003 cannot be considered a typical year, therefore, its inclusion or exclusion significantly influences the 2002–2007 average.

It can be seen in *Fig. 7* that the significant net CO_2 release of the agricultural fields is remarkable in both cases. Because of the high share of the agricultural fields in the national net carbon dioxide balance and the related uncertainty in

the model performance, the study of the agricultural carbon cycle could be an important target of the Hungarian research.

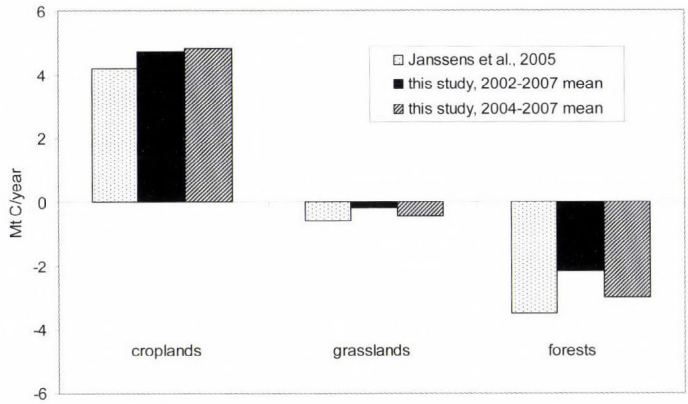

Fig. 7. Biospheric carbon dioxide balance of Hungary based on the country specific run of BIOME-BGC (present study), and on the data provided by *Janssens et al.* (2005). Negative values indicate carbon uptake by the vegetation. 2003 can not be considered a typical year (see text), thus, its inclusion or exclusion influences the average balance.

In order to illustrate the order of magnitude of our model results, it is interesting to mention that in the 2002–2005 period, the mean total anthropogenic carbon dioxide emission of Hungary, excluding emissions and removals from land use, land-use change, and forestry, was 60.75 million tons CO_2 (16.57 Mt C) (*HMS*, 2008). According to the model calculations presented, the biosphere in Hungary adds 8.7 million tons of CO_2 to this amount every year on average (2002–2007 mean) with significant interannual variation: the highest net emission was calculated for 2003 (21.6 Mt CO_2), while the lowest for 2006 (1.2 Mt CO_2).

Although forests sequester a significant amount of carbon dioxide, their CO_2 uptake may decrease or disappear with the warming climate, as it was experienced in 2003. According to the model results, the prevailing weather dramatically and rapidly influences the carbon dioxide exchange, i.e., the CO_2 uptake of the biosphere. This finding is supported by the measurements at Hegyhátsál where the net CO_2 exchange of the mixed agricultural lands changed significantly, from +69 g C/m^2/year (source) to –107 g C/m^2/year (sink) from 2003 to 2004 (*Haszpra et al.*, 2005).

Grasslands and forests are usually net carbon dioxide sinks. However, the uptake does not necessarily mean long term carbon storage. A large portion of the carbon dioxide taken up by croplands and grasslands may quickly return to the atmosphere through the consumption of the biomass by humans or animals. The total amount of carbon dioxide taken up by the forests is not stored in the

forests forever either: the carbon content of the forest vegetation also returns into the atmosphere sooner (from firewood or due to disturbances) or later (from harvested wood products like furniture, buildings, other construction materials). The above mentioned processes must be taken into account in order to provide a full carbon budget of the biosphere. The extension of the present study with the quantitative estimate of horizontal carbon transport may provide a useful tool for constraining the total carbon budget of Hungary.

Acknowledgements—Biome-BGC version 4.1.1 was provided by the Numerical Terradynamic Simulation Group (NTSG) at the University of Montana. NTSG assumes no responsibility for the proper use of Biome-BGC by others. Use of the TV-tower and transmitter building at Hegyhátsál is kindly provided by Antenna Hungária Corporation. During the years, the measurements were/are supported by the U.S.-Hungarian Scientific and Technological Joint Fund (J. F. No. 162 and 504), the Agency of Industrial Science and Technology (Japan), the Bilateral Japanese-Hungarian Intergovernmental S&T Cooperation, the Hungarian National Scientific Research Fund (OTKA T7282, T23811, N31783, T42941), the Hungarian Ministry of Economy and Transport (GVOP-3.2.1.-2004-04-0107/3.0, GVOP-AKF-3.1.1.-2004-05-0358/3.0), the INTERREG IIIB CADSES program (5D038), furthermore, the EC's 5th and 6th R&D Framework Programme (EVK2-CT-1999-00013, EVK2-CT-2002-00163, GOCE-CT-2003-505572, GOCE-037005). The copyright owner of the CLC50 database is the Institute of Geodesy, Cartography and Remote Sensing, Budapest (FÖMI). The authors highly appreciate the help and advice of *T. Szentimrei*, *R. Hodossyné Rétfalvi*, *B. Birszki* (Hungarian Meteorological Service, Budapest, Hungary), *J. Szabó*, *L. Pásztor* (Research Institute for Soil Sciences and Agricultural Chemistry, Budapest, Hungary), *K. Trusilova*, *E. Tomelleri*, *M. Jung* (Max Planck Institute for Biogeochemistry, Jena, Germany), *Z. Nagy*, *K. Pintér*, *Z. Tuba* (Szent István University, Gödöllő, Hungary), *A. Kern* (Hungarian Academy of Sciences, Budapest, Hungary).

References

Barcza, Z., Haszpra, L., Kondo, H., Saigusa, N., Yamamoto, S., and *Bartholy, J.*, 2003: Carbon exchange of grass in Hungary. *Tellus 55B*, 187-196.

Bürger, G., 1997: On the disaggregation of climatological means and anomalies. *Climate Res. 8*, 183-194.

Cao, M., Prince, S. D., and *Shugart, H. H.*, 2002: Increasing terrestrial carbon uptake from the 1980s to the 1990s with changes in climate and atmospheric CO_2. *Global Biogeochem. Cy. 16*, 1069, doi:10.1029/2001GB001553.

Churkina, G., Tenhunen, J., Thornton, P., Falge, E.M., Elbers, J.A., Erhard, M., Grunwald, T., Kowalski, A.S., and *Sprinz, D.*, 2003: Analyzing the ecosystem carbon dynamics of four European coniferous forests using a biogeochemistry model. *Ecosystems 6*, 168–184.

Ciais, P., Bousquet, P., Freibauer, A., and *Naegler, T.*, 2007: Horizontal displacement of carbon associated with agriculture and its impacts on atmospheric CO_2. *Global Biogeochem. Cy. 21*, GB2014, doi:10.1029/2006GB002741.

Cox, P.M., Betts, R.A., Jones, C.D., Spall, S.A., and *Totterdell, I.J.*, 2000: Acceleration of global warming due to carbon-cycle feedbacks in a coupled climate model. *Nature 408*, 184-187.

Denman, K.L., Brasseur, G., Chidthaisong, A., Ciais, P., Cox, P.M., Dickinson, R.E., Hauglustaine, D., Heinze, C., Holland, E., Jacob, D., Lohmann, U., Ramachandran, S., da Silva Dias, P.L., Wofsy, S.C., and *Zhang, X.*, 2007: Couplings Between Changes in the Climate System and Biogeochemistry. In *Climate Change 2007: The Physical Science Basis.* Contribution of Working Group I to the Fourth Assessment Report of the Intergovernmental Panel on Climate Change [(*Solomon, S., D. Qin, M. Manning, Z. Chen, M. Marquis, K.B. Averyt, M. Tignor* and *H.L. Miller* (eds.)]. Cambridge University Press, Cambridge, United Kingdom and New York, NY, USA.

Friedlingstein, P., Cox, P., Betts, R., Bopp, L., von Bloh, W., Brovkin, V., Cadule, P., Doney, S., Eby, M., Fung, I., Bala, G., John, J., Jones, C., Joos, F., Kato, T., Kawamiya, M., Knorr, W., Lindsay, K., Matthews, H.D., Raddatz, T., Rayner, P., Reick, C., Roeckner, E., Schnitzler, K.-G., Schnur, R., Strassmann, K., Weaver, A.J., Yoshikawa, C., and *Zeng, N.,* 2006: Climate-carbon cycle feedback analysis: results from the C4MIP model intercomparison. *J. Climate 19*, 3337-3353.

Gervois, S., Ciais, P., de Noblet-Ducoudré, N., Brisson, N., Vuichard, N., and *Viovy, N.*, 2008: Carbon and water balance of European croplands throughout the 20th century. *Global Biogeochem. Cy. 22*, GB2022, doi:10.1029/2007GB003018

Haszpra, L., Barcza, Z., Bakwin, P.S., Berger, B.W., Davis, K.J., and *Weidinger, T.*, 2001: Measuring system for the long-term monitoring of biosphere/atmosphere exchange of carbon dioxide. *J. Geophys. Res. 106D*, 3057-3070.

Haszpra, L., Barcza, Z., Davis, K. J., and *Tarczay, K.*, 2005: Long-term tall tower carbon dioxide flux monitoring over an area of mixed vegetation. *Agr. Forest Meteorol. 132*, 58-77.

Hidy, D., Barcza, Z., Haszpra, L., Churkina, G., and *Trusilova, K.*, 2007: Parameter estimation for grassland carbon cycle using nonlinear inversion of Biome-BGC. *Cereal Res. Commun. 2*, 453-456.

HMS, 2008: *National Inventory Report for 1985-2006 Hungary*. Hungarian Meteorological Service, Budapest, Hungary. http://unfccc.int/national_reports/annex_i_ghg_inventories/national_inventories_submissions/items/4303.php

Hollinger, D.Y. and *Richardson, A.D.,* 2005: Uncertainty in eddy covariance measurements and its application to physiological models. *Tree Physiol. 25*, 873-885.

IPCC, 1997: Revised 1996 IPCC Guidelines for National Greenhouse Inventories [*Houghton, J.T., Meira Filho, L.G., Lim, B., Tréanton, K., Mamaty, I., Bonduki, Y., Griggs, D.J. and Callander, B.A.* (eds.)]. IPCC/OECD/IEA, Paris, France.

IPCC, 2003: Good Practice Guidance for Land Use, land-Use Change and Forestry [*Penman J., Gytarsky M., Hiraishi T., Krug, T., Kruger D., Pipatti, R., Buendia, L., Miwa, K., Ngara, T., Tanabe, K., Wagner, F.* (eds.)]. IPCC/IGES, Hayama, Japan.

IPCC, 2006: IPCC Guidelines for National Greenhouse Gas Inventories, Prepared by the National Greenhouse Gas Inventories Programme [*Eggleston H.S., Buendia L., Miwa K., Ngara T. and Tanabe K.* (eds.)]. Published: IGES, Japan.

Jansen, E., Overpeck, J., Briffa, K.R., Duplessy, J.-C., Joos, F., Masson-Delmotte, V., Olago, D., Otto-Bliesner, B., Peltier, W.R., Rahmstorf, S., Ramesh, R., Raynaud, D., Rind, D., Solomina, O., Villalba, R., and *Zhang, D.*, 2007: Palaeoclimate. In *Climate Change 2007: The Physical Science Basis.* Contribution of Working Group I to the Fourth Assessment Report of the Intergovernmental Panel on Climate Change [*Solomon, S., Qin, D., Manning, M., Chen, Z., Marquis, M., Averyt, K. B., Tignor, M.* and *Miller, H.L.* (eds.)]. Cambridge University Press, Cambridge, United Kingdom and New York, NY, USA. 433-497.

Janssens, I.A., Freibauer, A., Ciais, P., Smith, P., Nabuurs, G.-J., Folberth, G., Schlamadinger, B., Hutjes, R.W.A., Ceulemans, R., Schulze, E.-D., Valentini, R., and *Dolman, A.J.*, 2003: Europe's terrestrial biosphere absorbs 7 to 12% of European anthropogenic CO_2 emissions. *Science 300*, 1538–1542.

Janssens, I.A., Freibauer, A., Schlamadinger, B., Ceulemans, R., Ciais, P., Dolman, A.J., Heimann, H., Nabuurs, G.-J., Smith, P., Valentini, R., and *Schulze, E.-D.*, 2005: The carbon budget of terrestrial ecosystems at country-scale - a European case study. *Biogeosciences 2*, 15-26.

Nagy, Z., Pintér, K., Czóbel, Sz., Balogh, J., Horváth, L., Fóti, Sz., Barcza, Z., Weidinger, T., Csintalan, Zs., Dinh , N.Q., Grosz, B., and *Tuba, Z.*, 2007: The carbon budget of semi-arid grassland in a wet and a dry year in Hungary. *Agr. Ecosyst. Environ. 121/1-2*, 21-29. doi: 10.1016/j.agee.2006.12.003

New, M., Lister, D., Hulme, M., and *Makin, I.*, 2002: A high-resolution data set of surface climate over global land areas. *Climate Res. 21*, 1-25.

Pietsch, S.A., Hasenauer, H., and *Thornton, P.E.*, 2005: BGC-model parameters for tree species growing in central European forests. *Forest Ecol. Manag. 211*, 264-295.

Running, S.W. and *Coughlan, J.C.*, 1988: A general model of forest ecosystem processes for regional applications I. Hydrological balance, canopy gas exchange and primary production processes. *Ecol. Model. 42*, 125-154.

Running, S.W. and *Gower, S.T.*, 1991: Forest-BGC, A general model of forest ecosystem processes for regional applications II. Dynamic carbon allocation and nitrogen budgets. *Tree Physiol. 9*, 147-160.

Running, S.W. and *Hunt, E.R.J.*, 1993: Generalization of a forest ecosystem process model for other biomes, Biome-BGC, and an application for global-scale models. In *Scaling Physiological Processes: Leaf to Globe* (eds.: *J.R. Ehleringer, C.B.* Field). San Diego (CA): Academic Press, 141-158.

Somogyi, Z., 2007: A Kyotoi Jegyzőkönyv és az erdők (in Hungarian). *Erdészeti Lapok 142*, 152-154.

Thornton, P.E., Hasenauer, H., and *White, M.A.*, 2000: Simultaneous estimation of daily solar radiation and humidity from observed temperature and precipitation: an application over complex terrain in Austria. *Agr. Forest Meteorol. 104*, 255–271.

UNFCCC (United Nations Framework Convention on Climate Change), 2006: National greenhouse gas inventory data for the period 1990–2004 and status of reporting. *Report on national greenhouse gas inventory data from Parties included in Annex I to the Convention for the period 1990–2004.* FCCC/SBI/2006/26. http://unfccc.int/documentation/documents/advanced_search/items/3594.php?rec=j&priref=600004015#beg

Vetter, M. Churkina, G., Jung, M., Reichstein, M., Zaehle, S., Bondeau, A., Chen, Y., Ciais, P., Feser, F., Freibauer, A., Geyer, R., Jones, C., Papale, D., Tenhunen, J., Tomelleri, E., Trusilova, K., Viovy, N., and *Heimann, M.*, 2007: Analyzing the causes and spatial pattern of the European 2003 carbon flux anomaly in Europe using seven models. *Biogeosciences Discussions 4*, 1201-1240.

White, M.A., Thornton, P.E., Running, S.W., and *Nemani, R.R.*, 2000: Parameterization and sensitivity analysis of the Biome-BGC terrestrial ecosystem model: net primary production controls. *Earth Interactions 4*, 1-85.

IDŐJÁRÁS

Quarterly Journal of the Hungarian Meteorological Service
Vol. 113, No. 3, July–September 2009, pp. 221–231

Seasonal and spatial distribution of physiologically equivalent temperature (PET) index in Hungary

Ágnes Gulyás[1]* and **Andreas Matzarakis**[2]

[1]*Department of Climatology and Landscape Ecology, University of Szeged, P.O. Box 653, H-6701 Szeged, Hungary; E-mail: agulyas@geo.u-szeged.hu*

[2]*Meteorological Institute, Albert-Ludwigs-University of Freiburg, Werthmannstr 10, D-79085 Freiburg im Breisgau, Germany E-mail: andreas.matzarakis@meteo.uni-freiburg.de*

(Manuscript received in final form January 23, 2009)

Abstract—The aim of this study is to present a thermal human bioclimate analysis of Hungary by means of mapping, useing multiple linear regressions. The present study links geographical information with climatological data in order to generate a spatial distribution of PET values of a region. The distribution of average PET values of seasons are drawn at 1 km resolution. Meteorological data used to draw the maps was made with the help of data collation program at the Climatic Research Unit (University of East Anglia, Norwich, UK). The calculation of PET is performed with the aid of the RayMan model, which calculates the measures of the thermal human bioclimate. The calculated PET values show that the difference between the highest and lowest temperature areas is between 7–11 °C. This means two comfort level differences generally. The winter is an exception, when the whole country can be rated to the same physiological stress level.

Key-words: physiologically equivalent temperature, thermal comfort, mapping, Hungary

1. Introduction

Assessing the climatic capabilities of a certain area, bioclimatic aspects have higher and higher significance. In case of densely populated (urban) areas or extensively visited places (popular tourist destination, health resort), the effect of the climate on the inhabitants is an important question. A bioclimatic assessment is a complex task. The effect of the climate on the human body cannot be described by a single meteorological parameter. The air temperature, air humidity, wind, and radiation fluxes never act solely, but form a complex, so-called thermal factor. This complex factor induces certain physiological

* Corresponding author

responses on the human body. Several models and indices were created in the last decades to describe this mechanism and quantify thermo-physiological phenomenon occurring in the human body (*VDI*, 1998).

The recent models, based on the human energy balance, opened new dimensions. These models take into account the heat fluxes (sensible- and latent heat loss, thermal radiation) between the body and the environment as a basis, with several additional empirical factors. Thus the coupling of meteorological parameters and the characteristics of the body give more detailed picture. The output data of the models are different bioclimatological indices, which quantify the extent of the heat stress (*Fanger*, 1972; *Jendritzky et al.*, 1990; *Höppe*, 1993, 1999; *VDI*, 1998; *Matzarakis et al.*, 1999; *Spagnolo* and *de Dear*, 2003).

Assessments can be performed at different spatial and temporal levels, according to the purpose of the study (*Jendritzky et al.*, 1990; *Matzarakis et al.*, 1999; *Koch et al.*, 2005; *Zaninovic et al.*, 2006). Microscale (~1 cm–1 km) studies can be used to examine very small microclimatic phenomena, like, for example, bioclimatic properties of a building, street, or park (*Matzarakis*, 2001; *Mayer* and *Matzarakis*, 1998a,b; *Picot*, 2004; *Gulyás et al.*, 2006; *Knez* and *Thorsson*, 2006). The data produced by such researches, which provides, for instance, quantitative information about optimal street forms in order to regulate the climate comfort, can be applied by architects and urban designers (*Ali-Toudert* and *Mayer*, 2006; *Lin et al.*, 2006). Applied studies at local- and meso-climatic scales (~100 m–200 km) can provide data for urban planning or regional planning (e.g., tourism) (*Matzarakis et al.*, 2004; *Brandenburg* and *Matzarakis*, 2007). Mainly topographical methods are used in case of bioclimatic analysis of larger areas on the macroscale (>200 km). The fast development of geoinformatical methods opens new possibilities also in these studies. Nowadays, analysis of bioclimatic maps is an integral part of regional planning processes in countries with developed tourism infrastructure and industry (*Matzarakis et al.*, 2004; *Lin* and *Matzarakis*, 2008).

The aim of this study is to present a bioclimatic analysis of Hungary by means of bioclimatical mapping with the aid of geo-statistical methods. The present study links geographical information (*Hastings et al.*, 1999) with climatological data (*New et al.*, 1999, 2000, 2002) in order to generate a spatial distribution of the bioclimatological index PET in a region. The determination of PET is performed with the aid of the RayMan Model, which calculates the thermal indices mentioned above (*Matzarakis et al.*, 2000, 2007).

2. Study area

Although the original study was done for a larger area, this paper focuses on the description of bioclimatic properties in Hungary (*Fig. 1*).

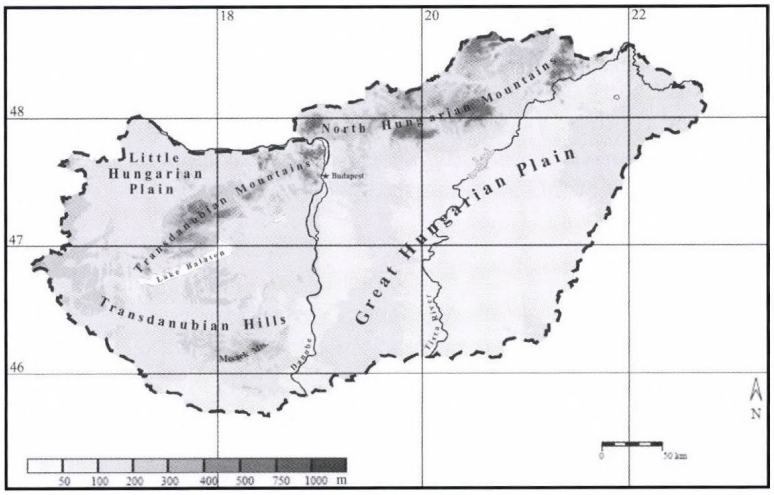

Fig. 1. Geographical location and topography of Hungary (the numbers are northern latitudes and eastern longitudes in degrees).

Hungary is situated in the Carpathian Basin almost in the central part of Europe, between the latitudes 45°48'N and 48°35'N and longitudes 16°05'E and 22°58'E, with an area of 93,030 km^2. As *Fig. 1* shows, it has three basic relief types: the low-lying regions (under 200 m above sea level) of the Great Hungarian Plain in the east, center, and southeast, and of the Little Hungarian Plain in the northwest, which together cover for two-thirds of Hungary's territory. There are the North Hungarian Mountains, the Transdanubian Mountains, and the hilly regions of Transdanubian Hills in the west and southwest.

The main characteristics of Hungary's climate and the frequent fluctuations in climatic factors are greatly due to the central position in Europe. Namely, Hungary is situated at the 'crossroads' of the East-European continental, the West-European oceanic, and subtropical Mediterranean climatic zones (*Pécsi* and *Sárfalvi*, 1964).

Using Köppen's classification, Hungary belongs to the climatic region *Cf*, which is characterized by a temperate warm climate with a rather uniform annual distribution of precipitation. Due to the relatively small spatial extension of the country and small vertical differences, the climate is quite uniform (*Justyák*, 2002).

Its annual mean temperature is 10.4 °C (in Budapest/Lőrinc). The spatial distribution of the temperature is mainly affected by the relief because of the small country size. The annual mean temperature decreases below 8 °C only in the North Hungarian Mountains, the highest peaks of the Transdanubian Mountains and close to the western border of the country. It has highest value on the southern side of the Great Hungarian Plain (just above 11 °C) (*Fig. 2*). The

coldest month is January (–1.6 °C), the warmest is July (20.8 °C). Because of the small country area the radiation conditions are affected mainly by the clouds. The sunny hours are between 1700–2100 per year; this value is highest in the Great Hungarian Plain and lowest in the mountains. The yearly global radiation sum is the highest in southeast Hungary (above 5000 MJ m^{-2}), and lowest in the North Hungarian Mountains and near the western borders (below 4300 MJ m^{-2}) (*OMSZ*, 2003).

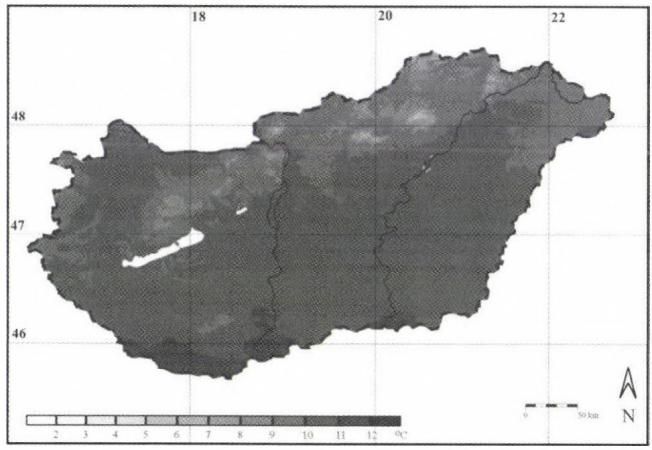

Fig. 2. The spatial pattern of the annual mean temperature in Hungary for the period 1961–1990.

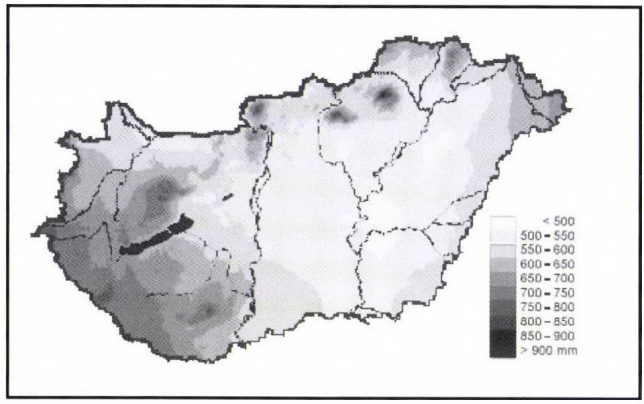

Fig. 3. Annual mean precipitation for the period 1965–1994 (*Szalai et al.*, 2005).

The annual mean precipitation is 612 mm, with high fluctuations between years. The temporal and spatial distribution of the precipitation is variable

(*Fig. 3*). Southwestern Transdanubia (with Mediterranean effect) and the higher mountain regions get considerably higher precipitation than the middle of the Great Hungarian Plain (800–1000 mm and 500–550 mm, respectively). Most of the precipitation falls in spring and summer (*WMO*, 1996). Homogenized datasets show that the climate of Hungary is getting warmer and drier in the last 100 years. This warming is similar to the global tendencies but with a higher extent (especially the summer temperatures and spring precipitation decline) (*Szalai et al.*, 2005).

3. Methods

Lots of thermal indices are used in bioclimatic studies to characterize the bioclimatic conditions of the surroundings on the human body. In this study one of the most widely used bioclimatic thermal indices, the PET is applied. PET evaluates the thermal conditions in a physiologically significant manner (*Höppe*, 1999; *Matzarakis et al.*, 1999). Meteorological parameters influencing the human energy balance, such as air temperature, air humidity, wind speed, and short- and long wave radiation (mostly the mean radiant temperature – T_{mrt} – is used to describe the radiation conditions, like the most important meteorological input parameter for the human energy balance during sunny weather in the hinterland), are represented in the PET values. PET also considers the heat transfer resistance of clothing and the internal heat production. The primary idea in the development of PET was the transfer of the actual thermal bioclimate to an equivalent fictitious indoor environment in which the same thermal sensation can be expected (*Mayer*, 1993). It is defined as the air temperature at which the human energy budget for the assumed indoor conditions is balanced by the same skin temperature and sweat rate as under the actual complex outdoor conditions to be assessed. The assumed indoor conditions are: $T_{mrt} = T_a$, $v = 0.1$ m^{-1}, $VP = 12.0$ hPa, where the T_{mrt} is the mean radiant temperature, T_a is the air temperature, v is the wind speed and VP is the vapor pressure.

PET has a widely known unit (°C) as an indicator of thermal stress and thermal comfort (*Table 1*). This makes the results easily understandable and comprehensible for potential users (according to its definition, PET values around 20 °C can be characterized as comfortable). This is especially the case for planners, decision-makers, and even the public who might be not familiar with modern human-biometeorological terminology (e.g., *Mayer* and *Höppe*, 1987; *Höppe*, 1999).

PET enables various users to compare the integral effects of complex thermal conditions outside with their own experience indoors. *Table 2* shows differences between PET values, calculated in typical summer and winter surroundings.

Table 1. PET for different levels of thermal sensation and physiological stress on human beings (during standard conditions where the heat transfer resistance of clothing is 0.9 clo and the internal heat production is 80 W) (*Matzarakis* and *Mayer*, 1996)

PET (°C)	Thermal sensation	Physiological stress level
	Very cold	Extreme cold stress
4	.....	.....
	Cold	Strong cold stress
8	.....	.....
	Cool	Moderate cold stress
13	.....	.....
	Slightly cool	Slight cold stress
18	.....	.....
	Comfortable	No thermal stress
23	.....	.....
	Slightly warm	Slight heat stress
29	.....	.....
	Warm	Moderate heat stress
35	.....	.....
	Hot	Strong heat stress
41	.....	.....
	Very hot	Extreme heat stress

Table 2. Examples of PET values under different environmental conditions

Character of the environment	T_a (°C)	T_{mrt} (°C)	v (m s^{-1})	VP (hPa)	PET (°C)
Typical indoor	21	21	0.1	12	21
Winter, sunny	-5	40	0.5	2	10
Winter, shaded	-5	-5	5.0	2	-13
Summer, sunny	30	60	1.0	21	43
Summer, shaded	30	30	1.0	21	29

One of the recently developed radiation and bioclimate models, the RayMan, is well-suited to calculate radiation fluxes (*Matzarakis*, 2002), and thus, all our calculations for T_{mrt} and PET were performed using this model. The RayMan model, developed according to the Guideline 3787 of the German Engineering Society (*VDI*, 1998), calculates the radiation flux in easy and complex environments on the basis of various parameters, such as air temperature, air humidity, degree of cloud cover, time of day and year, albedo of the surrounding surfaces, and their solid-angle proportions. The main advantage of RayMan is that it facilitates the reliable determination of the microclimatological modifications of different urban environments, since the model considers the radiation modification effects of the complex surface structure (buildings, trees) very precisely. Beside the meteorological parameters, the model requires input data on surface morphological conditions of the study area and on personal parameters.

The climate data used for this analysis were provided by the data collation program at the Climatic Research Unit (University of East Anglia, Norwich, UK) (*New et al.*, 1999, 2000, 2002). The required data for the thermal bioclimate analysis – air temperature, relative humidity, sunshine, and wind speed – are available at monthly resolution for the climate period 1961 to 1990 for the specific area. The calculated PET grid values have been used as dependent variables. They have been recalculated into a higher spatial resolution (1 km) by the use of geostatistical methods – multiple linear regression – (independent variables were latitude, longitude, and elevation). The multiple regression of the three factors can be applied to construct maps (*Matzarakis* and *Mayer*, 1997). For this purpose the digital elevation data of the GLOBE data set was used (*Hastings et al.*, 1999).

4. Results

Fig. 4 show the spatial seasonal distribution of the PET in Hungary, with spatial resolution of 1 km. Like climatic parameters, the bioclimatic parameters also show homogeneous distribution, because the majority of the country is a plain with less than 200 m elevation above the sea level. The highest PET values can be observed throughout the whole year in the south (S, SE, SW) part of the country (except for the winter). The mountains show lover PET values, especially the North Hungarian Mountains, where the lowest seasonal values can be calculated. Generally, the differences are not too high, the difference between the highest and lowest values is around 7–10 °C, thus, there is no considerable difference between the thermal sensation categories. (Obviously, this is true for the average values, which hide the extremities.)

The difference between the highest and lowest PET values is ~7 °C in *spring* (March, April, May) (*Fig. 4a*). The highest PET value (11 °C) is calculated on the southern part of the Great Hungarian Plain (except for the Duna-Tisza Interfluve) and of Transdanubian Hills. The decrease of the PET value at higher elevations is more pronounced in the North Hungarian Mountains than in other mountains. This difference means two categories in the physiological stress level, according to the average spring PET values. Thus, the warmest areas can be classified to the moderate cold stress level, while the coldest to the extreme cold stress, while the majority of the area of the country belongs to the strong cold stress level zone.

In *summer* (June, July, August) the spatial distribution of the PET values is similar to the spring situation (*Fig. 4b*). The range of PET distribution is a little higher between the highest and lowest values: ~10.5 °C. There are a two categories difference (from the slight cold stress to the slight heat stress) on the area in summer, showing 14–24.5 °C end values. These averaged values cover the extremities which are typical in the Carpathian Basin. The higher PET values (~24.5 °C) around Lake Balaton have not only touristic importance.

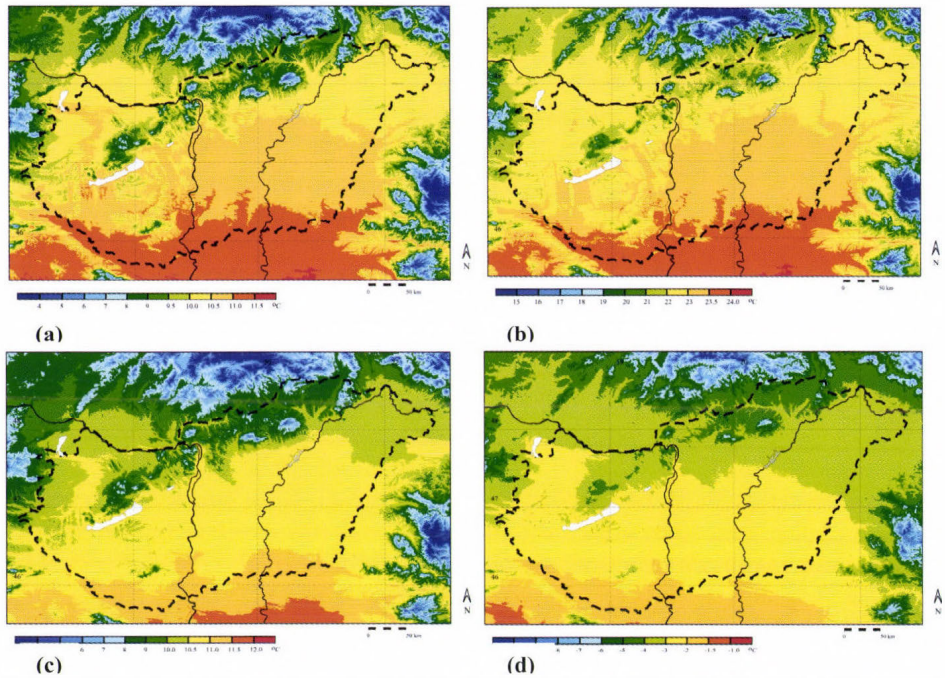

Fig. 4. Spatial distribution of PET in Hungary for (a) spring, (b) summer, (c) autumn, and (d) winter for the period 1961–1990.

The difference between the highest and lowest PET values is smaller again in *autumn* (September, October, November), it is around 7 °C (*Fig. 4c*). The values and their spatial distribution is similar to the situation in spring: 4–11 °C PET values, from the extreme cold stress to the moderate cold stress. The highest values restricted to the southern parts of the Great Hungarian Plain, the valley of Danube, and the south part of the Transdanubia. The tendency of the decrease in the southwest – northeast direction is clear on the region east of Tisza River. The pattern is more detailed in Transdanubia, due to the more diverse relief. The positive anomaly at the Lake Balaton can clearly be identified.

The bioclimatic situation of the *winter* (December, January, February) is the most homogeneous amongst the seasons (*Fig. 4d*), despite the higher difference between the lowest and highest PET values (9 °C). The lowest values can be observed at the highest peaks of the North Hungarian Mountains, covering small areas. The distribution on the Great Hungarian Plain also changed. The highest values can be observed only on the southern part of Transdanubia, possibly due to the Mediterranean effect (the Mediterranean cyclones have the strongest effect reducing continentality on this area during winter). The PET value on the Great Hungarian Plain decreases gradually from southwest towards northeast. The Transdanubian Mountains cannot be clearly

separate from their surroundings in bioclimatic aspect. This is especially true in case of the Mecsek Mountains. (It has to be noted, however, that the deficiency of the interpolation and the not calculated exposition data together might cause this phenomenon.) There is no pronounced positive anomaly around the Lake Balaton in winter. These geographical distributions do not mean different categories at the physiological stress level. The whole area of the country can be categorized to the extreme cold stress, with different intensities.

5. Conclusions

- The main novelty of our study is the first publication of maps, based on the output of a modern bioclimatic index, which refers to the human energy balance. Moreover, these calculations were performed for the whole area of Hungary with a resolution of 1 km.
- Seasonal pattern with this resolution shows characteristic spatial structure, with high similarities between the spring-summer and autumn-winter season-pairs.
- Taken the whole area of the country into consideration, there are generally two comfort level differences between the highest and lowest averaged PET values. In summer it means that the thermal sensation on some areas shows cold stress, while on others it shows heat stress. Exception is the winter, when the whole area belongs to the same physiological stress level.
- The bioclimatic situation shows homogeneous distribution due to the relatively small latitudinal and longitudinal extent and low altitudes. The Transdanubian Mountains are not separated distinctly from their surroundings in a bioclimatological sense, especially in winter, when the Mediterranean cyclones reduce continentality on this area.
- The pattern of the Great Hungarian Plain shows a southwest-northeast gradient, that can be ascribed to the increasing continental effect.
- The surroundings of the Lake Balaton, which has touristic importance, show higher PET values than the neighbouring areas, throughout the whole year. This bioclimatological difference does not stand out characteristically, only in winter.

Finally, as we earlier mentioned, the analysis has been performed with no direct data from observations by climate networks. The application of the CRU database has certain limitations on the area of Hungary. The present method includes geographical latitude, longitude, and elevation, but not the aspect ratio, exposition, and land use, which could produce inappropriate results with the existing dataset. Climate modeling offers, in our opinion, diverse opportunities

and possibilities of data in order to perform seasonal or monthly climate analysis. Due to the lack of available data sets, our results have not been compared to measured data, but we hope we will have opportunity to perform this analysis in the near future. Based on the existing data sets, several analyses for sensitive areas and sectors, i.e., agriculture, tourism, health, and regional planning can be performed, especially concerning expected climate change conditions.

Acknowledgements—The work of Ágnes Gulyás was supported by the Baden-Württembergisches Landesstipendium. Thanks to *János Unger* for proofreading and editing the manuscript.

References

Ali-Toudert, F. and *Mayer, H.*, 2006: Numerical study on the effects of aspect ratio and orientation of an urban street canyon on outdoor thermal comfort in hot and dry climate. *Build. Environ. 41*, 94-108.

Brandenburg, C. and *Matzarakis, A.*, 2007: Das thermische Empfinden von Touristen in der Region Neusiedlersee, *Ber. Meteor. Inst. Univ. Freiburg Nr. 16*, 67-72.

Fanger, P.O., 1972: *Thermal Comfort*. New York Mc Graw–Hill.

Gulyás, Á., Unger, J., Matzarakis, A., 2006: Assessment of the microclimatic and thermal comfort conditions in a complex urban environment: modelling and measurements. *Build. Environ. 41*, 1713-1722.

Hastings, D.A., Dunbar, P.K., Elphingstone, G.M., Bootz, M., Murakami, H., Maruyama, H., Masaharu, H., Holland, P., Payne, J., Bryant, N.A., Logan, T., Muller, J.-P., Schreier, G., MacDonald, J.S. (eds.) 1999: *The Global Land One-kilometer Base Elevation (GLOBE) Digital Elevation Model, Version 1.0*. National Oceanic and Atmospheric Administration, National Geophysical Data Center, 325 Broadway, Boulder, Colorado 80303, U.S.A. Digital data base on the World Wide Web (http://www.ngdc.noaa.gov/mgg/topo/globe.html)

Höppe, P., 1993: Heat balance modelling. *Experientia 49*, 741-745.

Höppe, P., 1999: The physiological equivalent temperature – a universal index for the biometeorological assessment of the thermal environment. *Int. J. Biometeorol. 43*, 71-75.

Jendritzky, G., Menz, H., Schirmer, H., Schmidt-Kessen, W., 1990: Methodik zur raumbezogene Bewertung der thermischen Komponente im Bioklima des Menschen (Fortgeschriebenes Klima-Michel-Modell). *Beitr. Akad. Raumforsch. Landesplan.* No. 114.

Justyák, J., 2002: *Climate of Hungary* (in Hungarian). Kossuth Egyetemi Kiadó, Debrecen, Hungary.

Knez, I. and *Thorsson, S.*, 2006: Influences of culture and environmental attitude on thermal, emotional and perceptual evaluations of a public square. *Int. J. Biometeorol. 50*, 258-268.

Koch, E., Marktl, W., Matzarakis, A., Nefzger, H., Rudel, E., Schunder-Tatzber, S., Zygmuntowski, M., 2005: Klimatherapie in Österreich. *Broschüre zu den Potentialen der Klimatherapie in Österreich. Bundesministerium für Wirtschaft und Arbeit.*

Lin, T.-P. and *Matzarakis, A.*, 2008: Tourism climate and thermal comfort in Sun Moon Lake, Taiwan. *Int. J. Biometeorol. 52*, 281-290.

Lin, T.-P., Matzarakis, A., Huang, J.-J., 2006: Thermal comfort and passive design strategy of bus shelters. *PLEA2006 - The 23 Conference on Passive and Low Energy Architecture*. Geneva, Switzerland.

Matzarakis, A., 2001: Die thermische Komponente des Stadtklimas. *Ber. Meteorol. Inst. Univ. Freiburg* Nr. 6.

Matzarakis, A., 2002: Validation of modeled mean radiant temperature within urban structures. *AMS Symposium on Urban Environment*, Norfolk, UK, 7.3.

Matzarakis, A. and *Mayer, H.*, 1996: Another kind of environmental stress: Thermal stress. *NEWSLETTERS* No. 18, WHO Collaborating Centre for Air Quality Management and Air Pollution Control, 7-10.

Matzarakis, A. and *Mayer, H.*, 1997: Heat stress in Greece. *Int. J. Biometeorol. 41,* 34-39.

Matzarakis, A., Mayer, H., Iziomon, M., 1999: Applications of a universal thermal index: physiological equivalent temperature. *Int. J. Biometeorol. 43*, 76-84.

Matzarakis, A., Rutz, F., Mayer, H., 2000: Estimation and calculation of the mean radiant temperature within urban structures. In *Biometeorology and Urban Climatology at the Turn of the Millenium* (eds.: *R.J. De Dear, J.D. Kalma, T.R. Oke, A. Auliciems*). Selected Papers from the Conference ICB-ICUC'99, WCASP-50, WMO/TD No. 1026. Sydney 2000, 273-278.

Matzarakis, A., de Freitas, C., Scott, D. (eds.), 2004: Advances in tourism climatology. *Ber. Meteorol. Inst. Univ. Freiburg Nr. 12,* 6-9.

Matzarakis, A., Rutz, F., Mayer, H., 2007: *Modeling radiation fluxes in simple and complex environments – Application of the RayMan model. Int. J. Biometeorol. 51,* 323–334.

Mayer, H. and *Höppe, P.*, 1987: Thermal comfort of man in different urban environments. *Theor. Appl. Climatol. 38,* 43-49.

Mayer, H., 1993: Urban bioclimatology. *Experientia 49,* 957-963.

Mayer, H. and *Matzarakis, A.*, 1998a: The urban heat island seen from the angle of human-biometeorology. *Proc. Int. Symposium on Monitoring and Management of Urban Heat Island.* Fujisawa, Japan, 84-95.

Mayer, H. and *Matzarakis, A.*, 1998b: Human-biometeorological assessment of urban microclimates' thermal component. *Proc. Int. Symposium on Monitoring and Management of Urban Heat Island.* Fujisawa, Japan, 155-168.

New, M., Hulme, M., Jones, P., 1999: Representing twentieth century space-time climate variability. Part I: Development of a 1961–90 mean monthly terrestrial climatology. *J. Climate 12,* 829-856.

New, M., Hulme, M., Jones, P., 2000: Representing twentiethcentury space-time climate variability. Part II: Development of 1901-1996 monthly grids of terrestrial surface climate. *J. Climate 13,* 2217-2238.

New, M., Lister, D., Hulme, M., Makin, I., 2002: A high-resolution data set of surface climate over global land areas. *Climate Res. 21*, 1-25.

OMSZ, 2003: *Climate Atlas of Hungary* (in Hungarian). Országos Meteorológiai Szolgálat, Budapest, Hungary.

Pécsi, M. and *Sárfalvi, B.*, 1964: *The Geography of Hungary. Corvina Press. 8°. XII.*, Budapest, 299 p.

Picot, X., 2004: Thermal comfort in urban spaces: impact of vegetation growth. Case study: Piazza della Scienza, Milan. *Italy Energy and Buildings 36*, 329–334.

Spagnolo, J. and *de Dear, R.*, 2003: A field study of thermal comfort in outdoor and semi-outdoor environments in subtropical Sydney Australia. *Build. Environ. 38*, 721-738.

Szalai, S., Bihari, Z., Lakatos, M., Szentimrey, T., 2005: Some Characteristics of the Climate of Hungary since 1901. Országos Meteorológiai Szolgálat, Budapest, Hungary. http://www.met.hu/pages/climate/Some_characteristics_of_the_climate_of_Hungary_since_1901.pdf.

VDI, 1998: Methods for the human-biometeorological assessment of climate and air hygiene for urban and regional planning. Part I: Climate. *VDI Guidline 3787.* Beuth, Berlin.

WMO, 1996: *Climatological Normals (CLINO) for the Period 1961-1990.* WMO/OMM–No. 847, Geneva.

Zaninovic, K., Matzarakis, A., Cegnar, T., 2006: Thermal comfort trends and variability in the Croatian and Slovenian mountains. *Meteorol. Z. 15*, 243-251.

IDŐJÁRÁS

Quarterly Journal of the Hungarian Meteorological Service
Vol. 113, No. 3, July–September 2009, pp. 233–243

Reconciling the sequential probability ratio test with calibration

Alexander Jann

Central Institute for Meteorology and Geodynamics,
Hohe Warte 38, A-1190 Vienna, Austria; E-mail: Alexander.Jann@zamg.ac.at

(Manuscript received in final form June 10, 2009)

Abstract—A common strategy of meteorological calibration is to continuously screen the observational series for (occasional) abrupt changes and – once an alarm has been triggered – to assess how large that change is in order to correct for it. Starting with the analysis of a sequential probability ratio test strategy once proposed in radar meteorology, it is shown that an important enhancement is to combine this change-detection procedure with a dedicated change-point positioning procedure such that the individual capabilities of both methods are exploited. An additional crucial aspect is that – even with a good change-point location – initial estimates of the new state of the system may be quite imprecise, particularly in a real-time application because of small sample sizes. A subsequent rejection of the new calibration coefficient, hence, is not necessarily a sign of another change in the system – it might rather be due to a poor first guess which requires an update. By employing certain cautionary measures in this respect, finally a calibration approach based on comparatively simple statistical analysis principles is obtained, which should be attractive to meteorologists (as well as to practitioners in other disciplines) as it is sound, responsive, and easy to implement.

Key-words: real-time calibration, change-detection, change-point location, parameter estimation, sequential analysis

1. Introduction

Detection of changes in a system is a fundamental problem arising in many scientific disciplines as well as in engineering. There are applications where it suffices to know that a significant change has occurred and to stop the procedure then (e.g., to repair a damaged device). In other instances, however, it is impossible or at least impractical to do so, and it is demanded to estimate the parameters which statistically describe the new state in order to perform a sort of calibration by computational means. Meteorology repeatedly encounters the latter situation. Here are some selected relevant examples:

- In order to account for temporal changes in the sensor characteristics, meteorological satellite operators face a need of calibrating their instruments, for example by using targets on earth with known radiation characteristics (the so-called vicarious calibration). The updating rules apparently have been rather simple in the past, such as to replace the calibration coefficient by a mean of recent instantaneous values if the new value deviates by more than 1% from the former operational value (*van de Berg et al.*, 1995).

- In radar meteorology, much work has been devoted over decades to calibrate weather radars with raingages. The simplest models derived a single gage-to-radar adjustment factor, acknowledging that such a factor varies in time (in this case as the result of a complex mixture of technical and meteorological influences), and rules are needed how to update the calibration factor. One relevant analysis is by *Smith* and *Cain* (1983) who argued that one has to insist on the statistical significance of a suspected change in the series. Otherwise, new adjustment factors arbitrarily computed from time to time would reflect little more than fluctuations in random noise and very likely do more harm than good. Though a rule as the above-mentioned one for vicarious calibration tries, to some degree, to avoid overly often re-calibration, it still may be considered a bit too heuristic and not enough statistics-driven in the light of this analysis.

- The sequential probability ratio test (SPRT) strategy proposed by *Smith* and *Cain* (1983) was picked up later (*Jann*, 1996) in an effort to detect abrupt shifts in the height assigned to a satellite-derived quantity (in order not to mix information from different levels). The implementation was unsuccessful, however, and though some theoretical explanations for this failure were given, back then it could not be demonstrated how to eliminate the shortcomings of the concept.

- Many contributions on the change-detection and change-estimation subjects are also provided by climatologists who have to catch signals in their time series being caused by changes in instruments, etc., in order not to mistake them for a real response of the climate system. Though – unlike the first two applications – this one is not a real-time problem per se, this author recently found it rewarding to handle the statistical problem in a quasi-realtime fashion (*Jann*, 2006).

Benefitting from the experience gained in the last-quoted study, we are ultimately – more than a decade after first touching the subject – in the position to present hereafter a viable implementation of the SPRT for calibration

purposes. The ambition behind the investigations documented here was to enhance a technique which we consider attractive for practical purposes because of its simple and transparent nature. It is not expected, however, that the found solution will nowadays have notable impact in the meteorological branch for which the Smith&Cain procedure was originally devised, as the simple segmentation model – with adjustment factors for a radar device held constant in-between breakpoints – appears to have fallen out of favor in this discipline and was superseded by more complex statistical approaches of blending precipitation data from different sources. Nevertheless, there are enough other types of meteorological data requiring straightforward quality control tools, so it appears worthwhile to describe in this note, how – through the addition of simple algorithmic components – we managed to augment the SPRT to better serve the needs of real-time calibration.

2. *Statistical techniques and their implementations*

2.1. The sequential probability ratio test

The principle of the sequential probability ratio test, employed by *Smith* and *Cain* (1983) for their detection of substantial changes in gage-to-radar rainfall amount ratios, is to sample values x_i of a normally distributed variable until the cumulative sum $\sum_i x_i$ confirms or opposes the null hypothesis of retaining an assumed value μ^* for the current population mean. Under the assumption of independently distributed observations x_i, the test decides between the null hypothesis H_0: $\mu-\mu^*=0$ and the two-sided alternative hypothesis H_1: $\mu-\mu^*=\pm\delta\sigma$, where μ is the (true) population mean, σ is the corresponding standard deviation, and δ is a tolerance parameter describing which deviation one is willing to admit. The SPRT test statistic writes

$$Y=\exp(-n\delta^2/2)\cosh\left((\delta/\sigma)\sum_i\left(x_i-\mu^*\right)\right). \tag{1}$$

Given prescribed values of type I and type II errors (α and β, respectively), it is checked whether the test statistic satisfies $Y\geq(1-\beta)/\alpha$, in which case H_0 is rejected. Alternatively, if the test statistic falls below $\beta/(1-\alpha)$ for some i, H_0 is accepted. This is basically how far the original implementation of the SPRT (*Wald*, 1947) goes, detecting that at some (unknown) point in the past, the actual mean started to deviate substantially from its supposed value.

2.2. *A first attempt to exploit the sequential probability ratio test in meteorological calibration*

How to proceed in case of a rejection of H_0, as, e.g., in those mentioned practical meteorological applications, where there is need for a new estimate μ^* in order to continue? *Smith* and *Cain* (1983) proposed to simply average the values between the preceding decision of the sequential test and the current rejection decision (in case of an acceptance of H_0, the value μ^* was retained, and another SPRT check of this hypothesis commenced with the next observation). It would have been instructive to assess the performance of this approach using a simulated example like that of *Fig. 1a*!

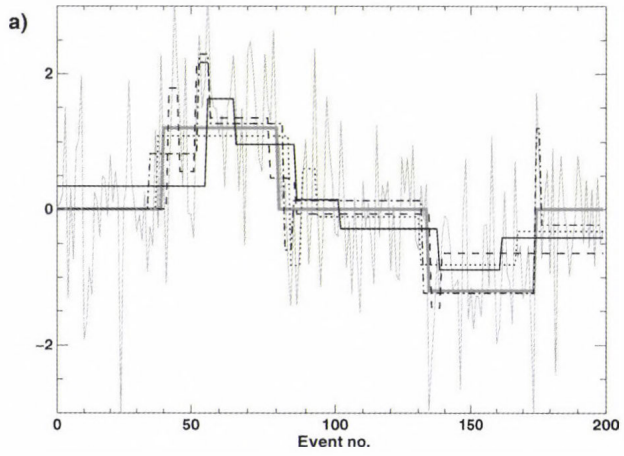

Fig. 1a. Light gray lines show a simulated 200-element time series sampled from a normally distributed population with standard deviation $\sigma=1$. Artificial shifts were applied according to an assumed course of the population mean, which is shown by the bold gray line. Black lines show population means as estimated by *Smith* and *Cain*'s (1983) sequential procedure with initial null hypothesis $\mu^*=0$ (for: $\delta=0.3$ (solid line), $\delta=0.5$ (dotted line), $\delta=0.7$ (dashed line), $\delta=0.9$ (dash-dotted line)).

As in the original report, let the initial null hypothesis be $\mu^*=0$, and $\alpha=\beta=0.1$. Take the curve for $\delta=0.3$: the first SPRT decision is to reject the null hypothesis $\mu^*=0$ at event No. 55; the average of the first 56 elements is 0.342, which is from a mixture of two populations and suits neither. Not surprisingly, this value is rejected ten events later, and from this small number of observations (though in principle 25 members of the second population have already been sampled), a new value of 1.633 is derived, being far off the specified actual value of 1.2. Many more examples of the following phenomena are observable in *Fig. 1a*:

1. quick rejections of unsuitable mean estimates (potentially leading to other highly noise-contaminated estimates which may then again cause rejections; thus, a chain of numerous poor estimates may be obtained even in cases where the mean remains perfectly stable for a long time after a jump),
2. "too late" decisions yielding mean estimates mixing many elements of two different populations with distinct mean.

Some more examples can be found in the original report by *Smith* and *Cain* (1983), where results likewise varied uncontrollably in dependence on δ. The fundamental reason for not being anywhere close to the truth (which is known by design in *Fig. 1*) is not difficult to find: parameter *estimation* tasks are delegated to the sequential probability ratio test, while it is merely a *decision* procedure (note how it does the latter job very well and repeatedly rejects the computed inadequate mean estimates). The two instructions to carry over when attempting to improve the scheme are: (1) once the SPRT indicates that a change has occurred, try to locate that change precisely; (2) yet even if this is done properly, be prepared that the first estimate μ^* could be highly noise-contaminated. Consequently, in the next section, we attempt to resolve the identified shortcomings by combining the detection procedure with a subsequent change-point positioning procedure plus a few cautionary measures on handling the derived mean estimates μ^*, i.e., a mechanism to possibly adapt such a poor hypothesis μ^* later, when more observations from the same population become available.

2.3. The proposed procedure combining change-point detection by the SPRT with separate change-point positioning and parameter estimation

It was argued above that there are two possible reasons why a hypothesis $\mu = \mu^*$ is rejected: one is an actual shift in the series, the other is a poor estimate of the mean, either by mixing populations or by having available too few observations. Therefore, for the case of two subsequent rejections of working hypotheses, the possible scenarios are

1. two actual shifts, or
2. one actual shift with a poor initial estimate of μ (which, using additional data, shall be tuned/updated; if it proves to be appropriate, the additional information shall also allow to shift the change point to a better position).

Consequently, one needs a change-point positioning procedure which evaluates both one-shift and two-shift configurations and is able to select the appropriate model. One candidate is the Schwarz criterion (*Schwarz*, 1978).

(Actually, a variant proposed by *Zurbenko et al.* (1996) is used, which resembles the Caussinus-Lyazrhi rule (*Caussinus* and *Lyazrhi*, 1997) in terms of penalizing the number of change points. See also the comparison results in *Caussinus* and *Mestre* (2004), supporting the choice made here).

$$(n/2)\ln s_a^2 + \nu \ln n \rightarrow \min! \tag{2}$$

where n is the sample size; s_a^2 is the variance of the adjusted series (i.e., for each supposed population the derived sample mean is subtracted from its members); ν designates the number of indicated change points. With this, all components are now assembled to formulate rules how decisions from the SPRT shall be handled in the calibration setting:

1. After an acceptance of the supposed mean, the last-detected shift has apparently been positioned adequately; it consequently may be fixed. As there are now more observations from the population available and one should in general benefit from this, if the hypothesized mean μ^* is recomputed from the larger sample, this is the action to be taken.

2. In case of a rejection after an acceptance, the partial series from the last change point onwards has to be investigated. We expect exactly one change point, so Eq. (2) is evaluated only for such configurations, i.e., ν=1.

3. In case of another rejection after a rejection, the partial series from the last but one change point onwards has to be investigated. Because of the options listed above, the (modified) Schwarz criterion, Eq. (2), has to be investigated for all configurations with 1 or 2 change points.

4. At the very beginning, the procedure is initiated with an arbitrarily assumed hypothesis concerning μ, which easily may be inadequate. So, if the first decision of the SPRT is a rejection of that hypothesis, there is possibly no jump at all in the series investigated so far. Hence, the configurations with 0 or 1 change points have to be examined in this situation.

3. Results

For illustrating the mechanims, the same example as above is taken (*Fig. 1b*). It is a clear-cut one, i.e., the sample consists of simulated data satisfying the basic assumptions of the tests, without outliers, violent short-term fluctuations, or other peculiarities in the series, which could adversely affect the performance of the SPRT or the Schwarz test. As there is no point in probing and discussing the robustness of the basic tests in light of the existing literature about them, the focus here is on the proper combined implementation.

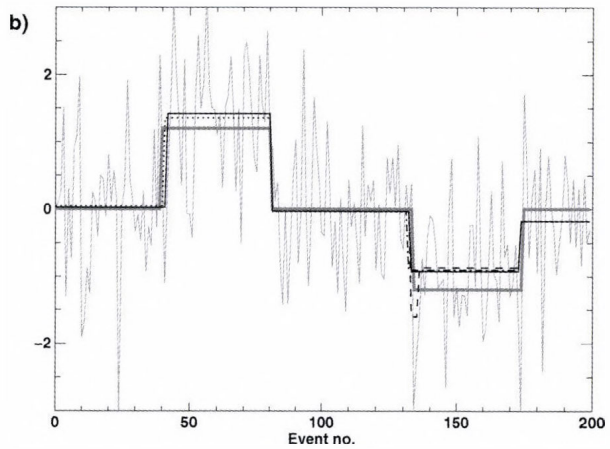

Fig. 1b. Courses of population means, as derived from the SPRT+Schwarz test combination with initial SPRT null hypothesis $\mu^* = 0$ (solid line: for $\delta = 0.3$, dotted line: $\delta = 0.5$, dashed line: $\delta = 0.7$, dash-dotted line: $\delta = 0.9$).

A hypothesis μ^* derived from elements M to N will be denoted as $\mu^*(M-N)$ hereafter. If change-points are fixed and a mean estimate is no longer subject to statistical inference, the asterisk is dropped: $\mu(M-N)$. The term "change-point" shall designate the position *after* which a change in the population mean is taking place. The prescribed values of the test series in *Fig. 1* (i.e., "the truth") are: $\sigma = 1$ (assumed to be known in advance, i.e., before starting the SPRT); $\mu(0-39) = \mu(81-133) = \mu(175-199) = 0$; $\mu(40-80) = 1.2$; $\mu(134-174) = -1.2$.

We start with the results for $\delta = 0.3$:

- Decision No. 1 of the SPRT: Rejection of the null hypothesis $\mu = 0$ at event No. 55; the Schwarz test applied to the series of the first 56 elements proposes to position a change-point at No. 41; $\mu^*(0-41) = 0.023$, and the new working hypothesis is taken from $\mu^*(42-55) = 1.297$.
- Decision No. 2 of the SPRT: Rejection of $\mu^* = 1.297$ at event No. 96; now the Schwarz test has to investigate all elements sampled so far and find out whether there are actually two change-points. It does in fact indicate a two-shift solution, confirming the change-point at No. 41 (which is definitively fixed $\rightarrow \mu(0-41) = 0.023$), and hypothesizing a new one at No. 80. The resulting new working hypothesis is $\mu^*(81-96) = -0.049$, the updated value for the mean of the preceding population $\mu^*(42-80) = 1.422$.

- Decision No. 3 of the SPRT: Rejection of $\mu^* = -0.049$ at event 152. The Schwarz test investigates elements 42 to 152 and proposes a two-step configuration with jumps at No. 132 and, again, at No. 80 (the population mean estimate for elements 42 to 80 is, therefore, definitively accepted as 1.422). The preliminary assumption is that $\mu^*(81-132) = -0.033$; the SPRT continues with $\mu^*(133-152) = -1.032$.
- Decision No. 4 of the SPRT: Rejection of $\mu^* = -1.032$ at event 185. The Schwarz test investigates elements 81 to 185 and once more votes for a two-step configuration with jumps at No. 132 and at No. 173: $\mu(81-132) = -0.033$; the preliminary assumption is that $\mu^*(133-173) = -0.924$; continuation of the SPRT with the new hypothesis $\mu^*(174-185) = -0.185$.
- No further SPRT decision is made until the end of the series. However, a final Schwarz test is performed for elements 133 to 199 to see if the final change-point shall possibly be readjusted on the basis of the latest information that has become available. The position of the break does not alter, however. Assuming that this indicates that elements 174 to 199 are from the very same population, the mean estimate changes slightly from –0.185 to –0.172.

The results for $\delta = 0.5$ should also be briefly considered here in order to illustrate how different the points of time of the SPRT decisions (and consequently the preliminary mean estimates) are and how stable the outcome after combination with the change-point positioning procedure nevertheless eventually is:

- Decision No. 1 of the SPRT: preference of null hypothesis over alternate hypothesis at event No. 18; $\mu^*(0-18) = -0.038$ used as new null hypothesis.
- Decision No. 2 of the SPRT: preference of null hypothesis over alternate hypothesis at event No. 36; $\mu^*(0-36) = -0.047$ used as new null hypothesis.
- Decision No. 3 of the SPRT: rejection of $\mu^* = -0.047$ at No. 44. The Schwarz test positions the change-point at no. 40; $\mu^*(0-40) = 0.051$; $\mu^*(41-44) = 1.003$.
- Decision No. 4 of the SPRT: preference of null hypothesis $\mu^* = 1.003$ over alternate hypothesis at event No. 87; $\mu(0-40) = 0.051$; $\mu^*(41-87) = 1.112$.
- Decision No. 5 of the SPRT: rejection of $\mu^* = 1.112$ at event no. 96, change point at position 80 suggested; $\mu^*(41-80) = 1.359$, new working hypothesis: $\mu^*(81-96) = -0.049$.

- Decision No. 6 of the SPRT: preference of null hypothesis $\mu^* = -0.049$ over alternate hypothesis at event No. 115; update: $\mu^*(81-115) = -0.039$.
- Decision No. 7 of the SPRT: rejection of $\mu^* = -0.039$ at no. 146, with a new change-point indicated at No. 132; $\mu^*(81-132) = -0.033$; $\mu^*(133-146) = -1.111$.
- Decision No. 8 of the SPRT: rejection of $\mu^* = -1.111$ at event No. 181, with the Schwarz test for elements 81 to 181 indicating two change-points at Nos. 132 and 173, $\mu^*(133-173) = -0.924$; $\mu^*(174-181) = -0.076$.
- No further SPRT decision observed. The final Schwarz test at the end of the series adjusts the last change-point by one position to No. 174.

Also the diagram for $\delta = 0.9$ in *Fig. 1b*) shows hardly any differences. For $\delta = 0.7$, 4 elements are pooled together in a separate population around event no. 132; though substantially deviating from the designed course of the population mean, there is little to discuss about this glitch here since it merely reflects the normal uncertainty inherent in statistical procedures (particularly when they are run with such high error probabilities as here). The important thing to note is that this questionable decision has only local impact as the analysis remains stable with mean estimates quickly returning to almost the same levels as for the other values of δ.

It is of course somewhat optimistic in the above experiment to assume that the process is known good enough to prescribe the right value of σ. *Smith* and *Cain* (1983) ran the SPRT using the standard deviation of the series under investigation. This choice, to some degree, has its point in retrospective experiments, since it is the optimum estimate for σ if there are no changes in the series, which in a heuristic sense gives this value the highest probability of being "correct". For the series in *Fig. 1b*, this standard deviation amounts to 1.19, and the SPRT/Schwarz combination was re-run with this value to assess the robustness against the inevitable uncertainties in a practical setting about the exact value of σ. Though SPRT decisions of course occurred at somewhat different times, the final results exhibited unspectacular deviations: only one shift of a change-point by one position was registered (namely, for the run with $\delta = 0.5$, the change-point at no. 40 moved to position 41, and the solution became identical to the one with $\delta = 0.3$ shown in *Fig. 1b*).

4. Discussion

For certain applications, there are very good reasons to select a sequential analysis procedure, since this area of mathematics strives for methods with the

quickest possible reaction time to jumps in the series (already the inventor of the SPRT, *Wald* (1947), gave impressive numbers on this criterion). As one can see from a review like that of *Lai* (2001), also parameter estimation of the distribution after a change-point in a sequential framework has been the subject of mathematical research for long. However, the practical usage of many of the more sophisticated concepts has been fairly limited, and though apparently more and more procedures addressing the practitioners' requirements have surfaced in recent years, reality in meteorology (and elsewhere) indicates that so far they failed to supersede established simple procedures. Part of the cause appears to be a certain ambition to have change-point detection, change-point location, and parameter estimation altogether in a closed sequential framework, whereby one then arrives at relatively complex schemes. We found it supportive for our own approach towards the problem to identify precursors that separated change-point detection and change-point location for no other reason than being able to master the otherwise excessive computational demands. The first appearance of this approach apparently was due to *von Brandt* (1983), with the change-point positioning step based on a simplified version of the underlying sequential framework. The present paper takes the liberty to go a step further as the change-point location has no sequential background at all.

In fact, we presented a concept that allows to successfully employ a sequential analysis change-*detection* procedure like the SPRT in calibration problems, provided the change-point *location* is handled by another technique being tailored to this task and consulted in case of need. Though in principle the latter component alone would suffice to solve the problem, there are noteworthy practical advantages motivating the combination with the sequential change-detection. With an unknown number of change points in the series, expressions like the Schwarz criterion may quickly become impractical for longer series due to the combinatorial explosion of the number of configurations to check. A sequential analysis procedure in this case can be used to alert when the presence of a recent change is likely. Note that in the implementation presented above, the Schwarz criterion computations are constrained to $\nu \leq 2$, which keeps the number of possible combinations rather low and generally should be compatible with a real-time procedure. Of course, the number of detectable change-points in the whole series is still unlimited.

References

Caussinus, H. and *Lyazrhi, F.*, 1997: Choosing a linear model with a random number of change-points and outliers. *Ann. Inst. Stat. Math. 49*, 761-775.

Caussinus, H. and *Mestre, O.*, 2004: Detection and correction of artificial shifts in climate series. *Appl. Statist. 53*, 405-425.

Jann, A., 1996: Use of METEOSAT upper tropospheric humidity fields in synoptic practice. In *Proc. of the 1996 Meteorological Satellite Data Users' Conference*, September 16-20, 1996. Vienna, Austria, 265-272.

Jann, A., 2006: Genetic algorithms: Towards their use in the homogenization of climatological records. *Croatian Meteorological Journal 41*, 3-19.

Lai, T.L., 2001: Sequential analysis: some classical problems and new challenges (with discussion). *Stat. Sinica 11*, 303-408.

Schwarz, G., 1978: Estimating the dimension of a model. *The Annals of Statistics 6*, 461-464.

Smith, P.L. and *Cain, D.E.*, 1983: Use of sequential analysis methods in adjusting radar rainfall estimates on the basis of raingage data. *Report 83-2. Institute of Atmospheric Sciences, South Dakota School of Mines and Technology*, Rapid City, SD.

van de Berg, L., *Schmetz, J.* and *Whitlock, J.*, 1995: On the calibration of the Meteosat water vapour channel. *J. Geophys. Res. 100(D10)*, 21069-21076.

von Brandt, A., 1983: Detecting and estimating parameter jumps using ladder algorithms and likelihood ratio test. In *Proc. IEEE International Conference on ICASSP '83.* Boston, MA, 1017-1020.

Wald, A., 1947: *Sequential Analysis*. Wiley, New York.

Zurbenko, I., Porter, P.S., Rao, S.T., Ku, J.Y., Gui R., and *Eskridge, R.E.*, 1996: Detecting discontinuities in time series of upper-air data: Development and demonstration of an adaptive filter technique. *J. Climate 9*, 3548-3560.

GUIDE FOR AUTHORS OF *IDŐJÁRÁS*

The purpose of the journal is to publish papers in any field of meteorology and atmosphere related scientific areas. These may be

- research papers on new results of scientific investigations,
- critical review articles summarizing the current state of art of a certain topic,
- short contributions dealing with a particular question.

Some issues contain "News" and "Book review", therefore, such contributions are also welcome. The papers must be in American English and should be checked by a native speaker if necessary.

Authors are requested to send their manuscripts to

Editor-in Chief of IDŐJÁRÁS
P.O. Box 39, H-1675 Budapest, Hungary
E-mail: antal.e@met.hu

including all illustrations. MS Word format is preferred in electronic submission. Papers will then be reviewed normally by two independent referees, who remain unidentified for the author(s). The Editor-in-Chief will inform the author(s) whether or not the paper is acceptable for publication, and what modifications, if any, are necessary.

Please, follow the order given below when typing manuscripts.

Title page: should consist of the title, the name(s) of the author(s), their affiliation(s) including full postal and e-mail address(es). In case of more than one author, the corresponding author must be identified.

Abstract: should contain the purpose, the applied data and methods as well as the basic conclusion(s) of the paper.

Key-words: must be included (from 5 to 10) to help to classify the topic.

Text: has to be typed in single spacing on an A4 size paper using 14 pt Times New Roman font if possible. Use of S.I. units are expected, and the use of negative exponent is preferred to fractional sign. Mathematical formulae are expected to be as simple as possible and numbered in parentheses at the right margin.

All publications cited in the text should be presented in the *list of references*, arranged in alphabetical order. For an article: name(s) of author(s) in Italics, year, title of article, name of journal, volume, number (the latter two in Italics) and pages. E.g., *Nathan, K.K.,* 1986: A note on the relationship between photosynthetically active radiation and cloud amount. *Időjárás 90,* 10-13. For a book: name(s) of author(s), year, title of the book (all in Italics except the year), publisher and place of publication. E.g., *Junge, C.E.,* 1963: *Air Chemistry and Radioactivity.* Academic Press, New York and London. Reference in the text should contain the name(s) of the author(s) in Italics and year of publication. E.g., in the case of one author: *Miller* (1989); in the case of two authors: *Gamov* and *Cleveland* (1973); and if there are more than two authors: *Smith et al.* (1990). If the name of the author cannot be fitted into the text: *(Miller,* 1989); etc. When referring papers published in the same year by the same author, letters a, b, c, etc. should follow the year of publication.

Tables should be marked by Arabic numbers and printed in separate sheets with their numbers and legends given below them. Avoid too lengthy or complicated tables, or tables duplicating results given in other form in the manuscript (e.g., graphs).

Figures should also be marked with Arabic numbers and printed in black and white or color (under special arrangement) in separate sheets with their numbers and captions given below them. JPG, TIF, GIF, BMP, PNG or EPS formats should be used for electronic artwork submission.

Reprints: authors receive 30 reprints free of charge. Additional reprints may be ordered at the authors' expense when sending back the proofs to the Editorial Office.

More information for authors is available: antal.e@met.hu

Published by the Hungarian Meteorological Service

Budapest, Hungary

INDEX 26 361

HU ISSN 0324-6329